INFORMATION TO USERS

This material was produced from a microfilm copy of the original document. While the most advanced technological means to photograph and reproduce this document have been used, the quality is heavily dependent upon the quality of the original submitted.

The following explanation of techniques is provided to help you understand markings or patterns which may appear on this reproduction.

1. The sign or "target" for pages apparently lacking from the document photographed is "Missing Page(s)". If it was possible to obtain the missing page(s) or section, they are spliced into the film along with adjacent pages. This may have necessitated cutting thru an image and duplicating adjacent pages to insure you complete continuity.

2. When an image on the film is obliterated with a large round black mark, it is an indication that the photographer suspected that the copy may have moved during exposure and thus cause a blurred image. You will find a good image of the page in the adjacent frame.

3. When a map, drawing or chart, etc., was part of the material being photographed the photographer followed a definite method in "sectioning" the material. It is customary to begin photoing at the upper left hand corner of a large sheet and to continue photoing from left to right in equal sections with a small overlap. If necessary, sectioning is continued again — beginning below the first row and continuing on until complete.

4. The majority of users indicate that the textual content is of greatest value, however, a somewhat higher quality reproduction could be made from "photographs" if essential to the understanding of the dissertation. Silver prints of "photographs" may be ordered at additional charge by writing the Order Department, giving the catalog number, title, author and specific pages you wish reproduced.

5. PLEASE NOTE: Some pages may have indistinct print. Filmed as received.

Xerox University Microfilms

300 North Zeeb Road
Ann Arbor, Michigan 48106

75-20,314

CHEN, Tsing-Chang, 1942-
ON THE KINETIC ENERGY OF THE DIVERGENT AND NONDIVERGENT FLOW IN THE ATMOSPHERE.

The University of Michigan, Ph.D., 1975
Geophysics

Xerox University Microfilms, Ann Arbor, Michigan 48106

THIS DISSERTATION HAS BEEN MICROFILMED EXACTLY AS RECEIVED.

ON THE KINETIC ENERGY OF THE DIVERGENT AND NONDIVERGENT FLOW IN THE ATMOSPHERE

by

Tsing-Chang Chen

A dissertation submitted in partial fulfillment
of the requirements for the degree of
Doctor of Philosophy
(Atmospheric Science)
in The University of Michigan
1975

Doctoral Committee:

Professor Aksel C. Wiin-Nielsen, Co-Chairman
Associate Professor William R. Kuhn, Co-Chairman
Professor Ferdinand Baer
Associate Professor S. Roland Drayson
Professor Chia-Shun Yih

ACKNOWLEDGMENTS

I wish to thank Professors A.C. Wiin-Nielsen, W.R. Kuhn, F. Baer, S.R. Drayson, and C.S. Yih for serving as members of the Doctoral committee.

In particular, I would like to express my sincere gratitude to Professor A.C. Wiin-Nielsen for suggesting this study, his sustained guidance, encouragement, and availability throughout its course. It is also a pleasure to acknowledge his contribution to my education through excellent teaching as well as advice.

Thanks are due to Professor W.R. Kuhn for his constructive critism and his willingness to serve as co-chairman of my committee.

The computations reported in Chapter III are based upon the history data of the NCAR general circulation model under a joint research project between NCAR and University of Michigan. I am grateful to Mrs. Gloria Williamson for preparing the condensed tape of the GCM data. Stimulating conversation to Dr. Warren Washington of NCAR is appreciated. Particular thanks go to Dr. James Pfaendtner who programmed the substantial calculations of Chapter III.

To Mr. William Burrows, I appreciate his generosity for providing the observational data which made the computations of Chapter IV possible. Mr. James Sterken provided help in programming the calculation of this chapter.

I would also like to thank my fellow students for many helpful conversation, especially Mr. Joseph Tribbia and Jordan Alpert.

Many thanks go to Judith Tucker, Debra Lurkins, and Janet Siantz, the secretaries of the Department of Atmospheric and Oceanic Science, for their excellent typing.

The use of computer facilities of the National Center for Atmospheric Research, sponsored by the National Science Fundation, and the sponsorship of this study from National Science Fundation are appreciated.

Finally, I thank my parents for giving me intellectual ambition, and my wife and children for their patience and understanding through the long struggle of my graduate study.

TABLE OF CONTENTS

	Page
ACKNOWLEDGMENTS	ii
LIST OF TABLES	vi
LIST OF FIGURES	viii
LIST OF APPENDICES	xi
LIST OF SYMBOLS	xii
CHAPTER	
I. INTRODUCTION	1
1.1. Review of Historical Development	1
1.2. Purpose and Outline of the Study	8
II. THE THEORETICAL BACKGROUND	11
2.1. Energy Relations	11
2.2. Simplified Models	19
2.3. Discussion	24
III. THE NCAR GENERAL CIRCULATION MODEL	27
3.1. A Brief Description of the NCAR General Circulation Model and Data	27
3.2. Energy Relations in the z-Coordinate System	30
3.3. The Scheme of Separating the Horizontal Wind Vector into its Divergent and Nondivergent Parts	35
3.3.1. Computation of Vorticity and Divergence	36
3.3.2. Separation of the Horizontal Wind Vector Into Its Divergent and Nondivergent Parts	38
3.4. Procedure for the Numerical Integration	43
3.5. Kinetic Energies of Divergent Flow and Nondivergent Flow	45
3.6. Energy Conversions	49

TABLE OF CONTENTS (concluded)

		Page
IV.	THE OBSERVATIONAL STUDY	76
	4.1. Data	76
	4.2. The Calculation of Energy and Energy Conversions	78
	4.3. Kinetic Energies of Divergent Flow and Nondivergent Flow	83
	4.4. Energy Conversions	90
V.	CONCLUSION	104
	5.1. Concluding Remarks	104
	5.2. Suggestions for Future Study	107
APPENDIX		111
REFERENCES		139

LIST OF TABLES

Table		Page
1	The value of k at different latitudes.	37
2	Mean value of the kinetic energy quantities K, K_2, and K_3, and the ratios, $K_2/(K_2+K_3)$ and $K_3/(K_2+K_3)$ from day 71 to 100 of the NCAR GCM. Unit for K, K_2, and K_3: 10^8erg cm^{-2} (10^5 joule m^{-2}).	45
3	Yearly mean value and monthly mean values for January and July of K from Wiin-Nielsen (1967). Unit: 10^8erg cm^{-2} (10^5 joule m^{-2}).	46
4	Yearly mean value and monthly mean value for January and July of K from Peixoto and Oort (1974). Unit: 10^8erg cm^{-2} (10^5 joule m^{-2}).	47
5	Mean value and standard deviation of various terms in (3.13) and (3.10) for day 71 to 100 of the NCAR GCM. Unit: 10^3erg cm^{-2} sec^{-1} (watts m^{-2}).	50
6	Oort and Peixoto's (1974) energy conversion from potential energy to kinetic energy. Unit: watts m^{-2} (10^3ergs cm^{-2} sec^{-1}).	54
7	Comparison between $C(K_3,K_2)$ and various terms of (3.20)	55
8	Mean value of various energy conversions of Northern Hemisphere (N.H.) and Southern Hemisphere (S.H.) for day 71 to 100 of the NCAR GCM. Unit: 10^3ergs cm^{-2} sec^{-1} (watts m^{-2}).	56
9	Comparison between $C(K_3,K_2)$ and various terms of (3.20), and residence time of K_3, and K_2 for both hemispheres.	57
10	Mean value of the kinetic energy quantities, K, K_2, and K_3 over the period of August 1 to 15, 1970. Unit: 10^5 joule m^{-2} (10^8ergs cm^{-2}).	83

LIST OF TABLES (concluded)

Table		Page
11	Mean value and standard deviation of $C(K_3,K_2)A1$, $C(K_3,K_2)A2$, $C(K_3,K_2)B$ for the period of August 1 to 15, 1970. Unit: watts m^{-2} (10^3ergs cm^{-2} sec^{-1}).	91
D1	Divergence field at 7.5 km level of the NCAR GCM calculated from $\vec{V}$ field for time step 41040. Unit: $10^{-6}sec^{-1}$.	133
D2	Vorticity field at 7.5 km level of the NCAR GCM calculated from $\vec{V}$ field for time step 41040. Unit: $10^{-5}sec^{-1}$.	134
D3	Divergence field at 7.5 km level of the NCAR GCM calculated from $\vec{V}$ field for time step 41040. Unit: $10^{-8}sec^{-1}$.	135
D4	Vorticity field at 7.5 km level of the NCAR GCM calculated from $\vec{V}_2$ field for time step 41040. Unit: $10^{-5}sec^{-1}$.	136
D5	Divergence field at 7.5 km level of the NCAR GCM calculated from $\vec{V}_3$ field for time step 41040. Unit: $10^{-6}sec^{-1}$.	137
D6	Vorticity field at 7.5 km level of the NCAR GCM calculated from $\vec{V}_3$ field for time step 41040. Unit: $10^{-8}sec^{-1}$.	138

LIST OF FIGURES

Figure		Page
1	Schematic energy diagram showing the different forms of energy, enercy conversions, and energy dissipation included in this study.	19
2	Six-layer NCAR general circulation model with orography (after Kasahara and Washington, 1971).	28
3	Horizontal grid system of the NCAR GCM. The horizontal grids of the NCAR GCM are arranged in spherical surfaces. The picture shown above illustrates the arrangement of grid points. i and j represent the indices of grid points in longitudinal and latitudinal circles, respectively.	42
4	Contributions to K_2 and K_3 from different latitude bands. Unit: 10^8ergs cm^{-2} (10^5 joules m^{-2}).	62
5	Latitude-height distribution of 30-day (day 71 - 100) mean of zonally averaged K_2. Unit: 10^2ergs cm^{-3} (10 joule m^{-3}).	63
6	Latitude-height distribution of 30-day (day 71 - 100) mean of zonally averaged K_3. Unit: 10^2ergs cm^{-3} (10^{-1} joule cm^{-3}).	64
7	Contributions to $C(P,K_3)$ from different latitude bands. Unit: 10^3ergs cm^{-2} sec^{-1} (watts m^{-2}).	65
8	Contributions to (a) $C(K_3,K_2)$, (b) $C(K_3,K_2)A1$, (c) $C(K_3,K_2)A2$, and (d) $C(K_3,K_2)B$ from different latitude bands. Unit: 10^3ergs cm^{-2} sec^{-1} (watts m^{-2}).	66
9	Contributions to (a) $D(K_2)$ and (b) $D(K_3)$ from different latitude bands. Unit: 10^3ergs cm^{-2} sec^{-1} (watts m^{-2}).	68
10	Latitude-height distribution of 30-day (day 71-100) mean of zonally averaged $C(p,K_3)$. Unit: 10^{-3}erg cm^{-3} sec^{-1}.	69

LIST OF FIGURES (continued)

Figure		Page
11	Latitude-height distribution of 30-day (day 71 - 100) mean of zonally averaged $C(K_3,K_2)$. Unit: 10^{-3}erg cm^{-3} sec^{-1}.	70
12	Latitude-height distribution of 30-day (day 71 - 100) mean of zonally averaged $C(K_3,K_2)A1$. Unit: 10^{-3}erg cm^{-3} sec^{-1}.	71
13	Latitude-height distribution of 30-day (day 71 - 100) mean of zonally averaged $C(K_3,K_2)A2$. Unit: 10^{-4}erg cm^{-3} sec^{-1}.	72
14	Latitude-height distribution of 30-day (day 71 - 100) mean of zonally averaged $C(K_3,K_2)B$. Unit: 10^{-3}erg cm^{-3} sec^{-1}.	73
15	Latitude-height distribution of 30-day (day 71 - 100) mean of zonally averaged $D(K_2)$. Unit: 10^{-3}erg cm^{-3} sec^{-1}.	74
16	Latitude-height distribution of 30-day (day 71 - 100) mean of zonally averaged $D(K_3)$. Unit: 10^{-4}erg cm^{-3} sec^{-1}.	75
17	The vertical grid used in calculations. A is a physical quantity per unit mass at a given level. p_o is the surface pressure.	82
18	Vertical profile of zonally averaged K_2 and K_3 as a function of pressure. Unit: 10^3 joules m^{-2} cb^{-1}.	86
19	Contributions to K_2 and K_3 from different latitude bands. Unit: 10^5 joules m^{-2} (10^8ergs cm^{-2}).	86
20	Latitude-height distribution of zonally averaged K_2. Unit: 10^3 joules m^{-2} cb^{-1}.	87

LIST OF FIGURES (concluded)

Figure		Page
21	Latitude-height distribution of zonally averaged K_3. Unit: 10^3 joules m^{-2} cb^{-1}.	88
22	Vertical profile of (a) $C(K_3,K_2)A1$, (b) $C(K_3,K_2)A2$, (c) $C(K_3,K_2)B$, (d) $C'(K_3,K_2)$, and (e) $C(P,K_3)$ as a function of pressure. Unit: 10^{-3} joule m^{-2} cb^{-1} sec^{-1}.	95
23	Contributions to (a) $C(K_3,K_2)A1$, (b) $C(K_3,K_2)A2$, (c) $C(K_3,K_2)B$, (d) $C'(K_3,K_2)$, and (e) $C(P,K_3)$ from different latitude bands. Unit: watts m^{-2} (10^3 ergs cm^{-2} sec^{-1}).	97
24	Latitude-height distribution of zonally averaged $C(P,K_3)$. Unit: 10^{-3} watt m^{-2} cb^{-1}.	99
25	Latitude-height distribution of zonally averaged $C'(K_3,K_2)$. Unit: 10^{-3} watt m^{-2} cb^{-1}.	100
C1	A coordinate system in which the origin is located at the pole.	124
D1	Latitude-height of distribution of $\bar{u}$ for time step 41040 of the NCAR GCM. Unit: m/sec.	129
D2	Latitude-height distribution of $\bar{v}$ for time step 41040 of the NCAR GCM. Unit: m/sec.	130
D3	Latitude-height distribution of $\bar{u}_2$ for time setp 41040 of the NCAR GCM. Unit: m/sec.	131
D4	Latitude-height distribution of $\bar{v}_3$ for time step 41040 of the NCAR GCM. Unit: m/sec.	132

LIST OF APPENDICES

		page
APPENDIX A.	The Derivation of the Potential Energy Equation	111
A.1.	The Potential Energy Equation in the p-Coordinate System	111
A.2	The Potential Energy Equation in the z-Coordinate System of the NCAR GCM	115
APPENDIX B.	The Physical Interpretation of $C(K_3,K_2)$, An Example -- Cyclone	118
APPENDIX C.	The Scheme of Filling Wind Data at Poles	124
APPENDIX D.	Verification of the Direct Method of Dividing the Horizontal Wind Vector into its Divergent and Nondivergent Parts	127

LIST OF SYMBOLS

A	arbitrary physical quantity per unit volume in Chapter III
A_1	A at a given level 1
a	mean radius of the earth
b	arbitrary scalar variable
C_v	specific heat of air at constant volume
C_p	specific heat of air at constant pressure
$C(K_3,K_2)$	conversion between kinetic energies of divergent and nondivergent flow
$C(K_3,K_2)A$	$C(K_3,K_2)A1 + C(K_3,K_2)A2$
$C(K_3,K_2)A1$	$-\int_V f\vec{V}_2\cdot(\vec{k}x\vec{V}_3)\rho dV$ in Chapter III
	$-\int_s \int_o^{p_o} f\vec{V}_2\cdot(\vec{k}x\vec{V}_3)dpds$ in Chapter IV
$C(K_3,K_2)A2$	$-\int_V \zeta_2\vec{V}_2\cdot(\vec{k}x\vec{V}_3)\rho dV$ in Chapter III
	$-\int_s \int_o^{p_o} \zeta_2\vec{V}_2\cdot(\vec{k}x\vec{V}_3)dpds$ in Chapter IV
$C(K_3,K_2)B$	$-\int_V k_2\nabla\cdot(\zeta\vec{V}_3)dV$ in Chapter III
	$-\int_s \int_o^{p_o} k_2\nabla\cdot\vec{V}_3 dpds$ in Chapter IV
$C(K_3,K_2)B1$	$-\int_V k_2\vec{V}_3\cdot\nabla\rho dV$ in Chapter III

$C(K_3,K_2)C$	$-\int_V \vec{V}_2 \cdot w_3 \frac{\partial \vec{V}_3}{\partial z} \rho dV$ in Chapter III $-\int_s \int_o^{p_o} \vec{V}_2 \cdot \omega_3 \frac{\partial \vec{V}_3}{\partial p} dpds$ in Chapter IV
$C(K_3,K_2)$	$C(K_3,K_2)A + C(K_3,K_2)B$ in Chapter IV
$C(P,K_3)$	conversion between total potential energy and kinetic energy of divergent flow
$D(K_2)$	frictional dissipation of divergent flow
$D(K_3)$	frictional dissipation of nondivergent flow
E_I	internal energy of the atmosphere
E_p	potential energy of the atmosphere
DIV	divergence in equation (3.23)
E_{IZ}	internal energy of the NCAR GCM
E_{PZ}	potential energy of the NCAR GCM
$\vec{F}$	vector of frictional force
F_1	tangential force induced by the change of angular momentum of the horizontal motion
F_2	tangential force induced due to the exchange of momentum by the vertical motion
F_x	frictional force along the x-axis
F_y	frictional force along the y-axis
F_λ	frictional force along the longitudinal direction
F_ϕ	frictional force along the latitudinal direction
FNWC	Fleet Numerical Weather Center

LIST OF SYMBOLS (continued)

f	Coriolis parameter
f_o	a standard value of Coriolis parameter
G(P)	generation of total potential energy
g	acceleration of gravity
GCM	general circulation model
H	mountain height above mean sea level in the NCAR GMC
i	index of grid point along latitudinal circle in section 3.31
i	$\sqrt{-1}$ in section 4.2
i	index of vertical grids in section 4.2
$\vec{i}$	unit vector along the x-axis
j	index of grid point along longitudinal circle in section 3.1
$\vec{j}$	unit vector along the y-axis
J	jacobian
K	total kinetic energy in the atmosphere
K_2	total kinetic energy of nondivergent flow in the atmosphere
K_3	total kinetic energy of divergent flow in the atmosphere
k	kinetic energy per unit mass except in section 3.3.1 and 3.4
k	a factor of maintaining a nearly constant geographical distance between mesh points in section 3.3.1
k	index of regular levels of the NCAR GCM in section 3.4
k_2	kinetic energy of nondivergnet flow per unit volume

LIST OF SYMBOLS (continued)

k_3	kinetic energy of divergent flow per unit volume
k	vertical unit vector
L	angular momentum in Appendix B
l	index of intermediate levels of the NCAR GCM in section 3.4
M	momentum in Appendix B
m	zonal wave number
NCAR	National Center for Atmospheric
N.H.	Northern Hemisphere
NMC	National Meteorological Center
N.P.	North Pole
n	degree of surface harmonies
P	total potential energy, the sum of potential and internal energy of the atmosphere
P_n^m	normalized associated legendre function
p	pressure
p_o	surface pressure
p_s	pressure at anemometer height (~10m)
Q	adiabatic heating
q	humidity
q_s	humidity at anemometer height (~10m)
R	gas constant of dry air
r	radial distance
S.H.	Southern Hemisphere
S.P.	South Pole

LIST OF SYMBOLS (continued)

s	total area
sfc	surface
T	temperature
T_s	temperature at anemometer height (~10m)
u	component of horizontal wind in the x-axis or longitudinal direction
u_p	correction in u-component of wind field (u,v) to make divergence zero
u_R	correction in u-component of the corrected wind field (u,v) to make the vorticity of the corrected wind field equal to the vorticity of original wind field
u_s	u-component of wind field at anemometer height (~10m)
u'	new u-component of the wind field (u,v) after making u_D and v_D correction
u"	new u-component of the wind field (u',v') after making u_R and v_R correction
$\vec{V}$	horizontal wind vector
$\vec{V}_s$	horizontal wind vector at anemometer height
$\vec{V}_2$	nondivergent part of horizontal wind vector
$\vec{V}_3$	divergent part of horizontal wind vector
v	component of horizontal wind in the y-axis or latitudinal direction
v_D	correction in v-component of wind field (u,v)
v_R	correction in v-component of the corrected wind (u',v') field to make the vorticity of the corrected wind field equal to the vorticity of original wind field
v_s	v-component of wind field at anemometer height (~10m)

LIST OF SYMBOLS (continued)

v'	new v-component of the wind field (u,v) after making u_D and v_D correction
v''	new v-component of the wind field (u',v') after making u_R and v_R correction
Vort	vorticity in equation (3.24)
w	vertical velocity
w_s	vertical velocity at anemometer height (~10m)
w_3	vertical velocity of divergent field
y_n^m	surface harmonies
z	height
z_T	top of model atmosphere of the NCAR GCM
α	specific volume in Appendix A. 2 (or 72) for the south (or north) pole in Appendix C
ζ	vertical component of relative vorticity from total wind field
ζ_2	vertical component of relative vorticity of evaluated from nondivergent wind field
ζ_n^m	spherical harmonic coefficient of vorticity
θ	colatitude
Λ	an arbitrary physical quantity per unit volume in Chapter 4
Λ_1	Λ at a given level 1
λ	longitude
ρ	density
ρ_s	density at anemometer height (10m)
σ_1	orography factor at a given level, 1
Φ	geopotential

LIST OF SYMBOLS (concluded)

Φ_1	geopotential with subscript 1 denoting that this quantity is derived through hydrostatic approximation
χ	velocity potential
χ_3	velocity potential of divergent flow
ψ	stream function
ψ_2	stream function of nondivergent flow
ψ_n^m	spherical harmonic coefficient of stream function
ϕ	latitude
ω	vertical (pressure) velocity, dp/dt
ω_3	vertical (pressure) velocity of divergent flow
$(\ )^*$	complex conjugate of ( )
$\overline{(\ )}$	$\frac{1}{2\pi}\int_0^{2\pi} (\ )\,d\lambda$
∇	horizontal gradient operator
$\nabla \cdot (\ )$	horizontal divergence operator
$(\ ) \cdot (\ )$	scalar multiplication (dot product)
$(\ ) \times (\ )$	vector multiplication (cross product)

Chapter I

Introduction

1.1. Review of Historical Development

The structure and physical properties of the atmosphere are very complicated. In order to study the dynamics of the atmosphere and to make weather forecasts, numerous models of the atmosphere have been designed. In general, atmospheric models fall into two categories; balanced and unbalanced models. A detailed explanation of the distinction and function of these two general models seems equivalent to describing the history of numerical weather prediction.

Some five decades ago, Richardson (1922) tried to integrate numerically the primitive equations* using observed meteorological data that was available at that time. Instead of producing a meteorologically accurate forecast, only skepticism was generated from his "glaring error" in the calculated pressure tendencies. It was not until recently that anyone attempted to follow Richardson's approach to weather forecasting. After World War II, interest in numerical weather prediction revived because of the vast expansion of meteorological observing networks and the impact of high-speed digital computers.

---

*The Eulerian hydrodynamic equations modified by the assumption of hydrostatic equilibrium are called, in meteorology, the primitive equations.

Meanwhile, it was realized that Richardson's scheme was not the simplest one for numerical prediction. Richardson's equations govern not only the slow-moving meteorologically important motions, but also high-speed wave motions*, e.g. gravity wave, as solutions. If the initial conditions contain these high-speed oscillations, they would amplify spuriously thereby obscuring the meteorologically significant motion.

In order to avoid the aforementioned difficulty in Richardson's scheme, Rossby, in 1939, proposed that the principal mechanism governing large-scale short-period atmospheric evolution is the conservation of the vertical component of absolute vorticity. In other words, the local rate of change of the vertical component of absolute vorticity is due to the horizontal advection of this quantity itself. Indeed, Rossby's proposal is not only the essential of the so-called barotropic model, but also the forerunner of the balanced model.

One decade later, Charney (1948) introduced scale analysis to set up an approximate but consistent set of dynamic equations applicable to motions in middle and high latitudes. This new dynamic system is the so-called quasi-geostrophic system, in which the sound wave and gravity wave are eliminated by the hydrostatic and

---

*The sound wave is one of the high-speed wave motions in the atmosphere. Richardson made hydrostatic assumptions in his scheme such that the vertical component of the sound wave is filtered out.

quasi-geostrophic assumption, respectively. In 1950, Charney, Fjortoft, and von Neumann at the Institute of Advanced Studies at Prineeton presented the first successful numerical prediction based upon the quasi-geostrophic theory.

Many investigations, e.g. Phillips (1956), have shown that quasi-geostrophic models are adequate for the study of the large-scale motion in the atmosphere. However, quasi-geostrophic equations are a first approximation to the governing equations which are used to describe the atmospheric motion and are valid only when deviations from geostrophic balance are small. Experiences with operational forecasts indicate that the performance of quasi-geostrophic models for short-range prediction has not been satisfactoty, even though quasi-geostrophic baroclinic models are able to predict the development of cyclones and anticyclones. From his study of the prediction for the famous Thanksgiving storm of 1950, Phillips (1958) pointed out that the geostrophic winds always overestimate in the trough region and underestimate in the ridge region due to the neglect of curvature effects in the geostrophic equations. To alleviate this difficulty of the quasi-geostrophic models, Phillips suggested that the geostrophic wind in the horizontal advection of absolute vorticity should be replaced by the rotational wind.

To give a proper relationship between the mass and wind fields, attempts were made to improve the geostrophic formulation by using the balance equation instead of the geostrophic wind relation (Thompson, 1956; Lorenz, 1960; Charney, 1962, and others). The balance equation is formulated from the divergence equation by ignoring the time-rate-of-change of the divergence. This simplification of the divergence equation results in the removal of the gravity wave from the mechanics of the atmospheric model (Thompson, 1961).

Lorenz (1960) and Arakawa (1962) have given a procedure, based on consistency requirements and scale analysis, by which we may design a hierachy of atmospheric models. Following Lorenz and Arakawa, we find that the filtered models in the historical development of numerical prediction after World War II are the extension of Rossby's (1939) approach. The application of Rossby's approach to the prognostic equations leads naturally to use of the differentiated forms of the equations of motion to describe the dynamics of the atmosphere. The differentiated forms are the curl and divergence of the horizontal equations, namely, the vorticity and divergence equation, but the latter is replaced by the balance equation. The most complete generalization of Rossby's approach is the set consisting of the vorticity and balance equations. They are generally known as "balanced equations".

One should notice that the balance equations are of higher order than the primitive equations. Calculations with the former involve additional integrations and boundary conditions. If the balance equations are not simplified by further approximations the additional integrations become very complex. Charney (1955) proposed the possibility of using the primitive equations as Richardson first did. This has been successfully performed and routine operational weather forecasts based upon the primitive equations model have been carried out at the National Meteorological Center (Shuman and Hovermale, 1968) and several other places. Furthermore, the fundamental problem of the general circulation of the earth's atmosphere has also attracted more attention due to the advent of high-speed computers and stimulus of the development of numerical weather prediction techniques. Phillips (1956) successfully simulated the gross features of the general circulation of the atmosphere based upon quasi-geostrophic theory. To remove the quasi-geostrophic assumption, Smagorinsky (1963) performed a similar experiment using the primitive equations. Following these early attempts, more elaborate models based upon the primitive equations system were carried out by Leith (1965), Mintz (1965), Arakawa (1966), Smagorinsky, Manabe, and Holloway (1965), Kasahara and Washington (1967, 1971), Washington and Kasahara (1970).

Let us compare the philosphies of Richardson and Rossby. The major difference between them is that the latter neglects the time-rate-of-change of divergence to eliminate the high-speed gravity wave which exists in the former. It is known that the horizontal wind vector can be divided into its divergent and nondivergent parts according to Helmholtz' theorem. The divergent part of large-scale motion in the atmosphere contains only a very small fraction of the total kinetic energy in the hydrostatic atmosphere. The neglect of the time variation of divergence in the generalization of Rossby's scheme may alter the role played by the divergence. In this study we intend to investigate the role of divergence in the conversion between total potential energy and kinetic energy. It is preferable to call the atmospheric models in Richardson's and generalized Rossby's schemes unbalanced and balanced models respectively, rather than unfiltered and filtered models as is usually done.

It should be noted that ignoring the time-rate-of-change of a given variable will make this variable determined implicitly. Richardson (1922) introduced the hydrostatic assumption in his scheme so that the vertical velocity is evaluated implicitly through a diagnostic equation which is known as the Richardson equation. Furthermore, the simplification of the governing equations

would modify the energy processes as far as the energetics of the atmosphere is concerned.

In a barotropic atmosphere, the variation of the meteorological system is governed by horizontal advection in such a way that the kinetic energy of the system is conserved if the fluid is frictionless. In other works, no potential energy can be transformed to kinetic energy in a barotropic system.

Wiin-Nielsen (1968) pointed out that the averaged temperature is conserved in a quasi-geostrophic system if the system is adiabatic. Therefore, the quasi-geostrophic model may not give a realistic description of changes of the total potential energy. In order to give a proper estimate of energy conversion from total potential energy to kinetic energy, Lorenz (1956) introduced the concept of available potential energy. Numerous studies of the energetics of the atmosphere have been made following the general scheme proposed by Lorenz.

Wiin-Nielsen (1968) also investigated the modification in the energetics of the atmosphere due to the hydrostatic assumption in the primitive equations. He concluded that the constraint of the hydrostatic assumption not only reduced the vertical velocity to an implicit physical variable, but also makes the reservoir of kinetic energy of vertical motion a "catalyst" to channel the internal energy to the potential energy.

In balanced models, the time-rate-of-change of divergence is ignored so that a divergence becomes an implicit variable. Wiin-Nielsen's (1968) study may suggest that the divergent part of the motion plays a similar role in balanced models as the vertical motion in the hydrostatic-atmosphere. Wippermann (1957), based upon an extension of balanced models, similar to Lorenz (1960) and Arakawa (1962), presented the possibility of energy conversion between divergent and nondivergent flow. Wiin-Nielsen (1974) proposed the same consideration from the primitive equations. The kinetic energy of the divergent flow is small, but its behavior is puzzling. However, the difference in the energetics of the atmosphere based upon the balanced models and unbalanced models will show the role played by the divergent field of the large-scale motions in the atmosphere when the conversion between the total potential energy and kinetic energy is considered.

1.2. Purpose and outline of the study

The purposes of this study are:

1. To analyze the energy budget of the divergent part of the large-scale flow of the atmsophere.

2. To investigate how the energy transforms from the total potential energy to the kinetic energy of divergent and nondivergent flow, and especially to compare the energy conversion in different models.

3. To study the extent to which the kinetic energy of the divergent flow is catalytic.

To accomplish these goals, we derive directly from the equations of motion in a hydrostatic atmosphere the equations for the rate of change of kinetic energy of the divergent and nondivergent parts of the total flow. We also analyze the relationship between the kinetic energy of divergent and nondivergent flow and their relation to the rate of change of total potential energy in Chapter 2. A further analysis will consider the form of energy conversions in simplified models.

The use of pressure as the vertical coordinate makes the governing equations of quasi-static large-scale motion of the atmosphere simpler in many ways and more feasible in connection with aerological data (Eliassen, 1949). The numerical prediction system of balanced models is therefore formulated in the p-coordinate system. In fact, the meteorological data of current observations provides only two dimensional wind vectors.The evaluation of vertical motion usually is based upon some particular model, i.e., the so-called indirect method. In practice,the vertical velocity estimated by the indirect method may not be consistent with the horizontal wind field from meteorological observations. The computation of the energy conversion between kinetic energy of divergent and nondivergent flow requires

a three dimensional wind vector. To satisfy this requirement of wind data, the generation of wind data from a general circulation model (GCM) is called for. History data of a GCM was provided by the National Center of Atmospheric Research (NCAR). Since the NCAR GCM is formulated in the z-coordinate systen, it is required that the theory described in Chapter 2 be reformulated in the z-coordinate system. However,the slope of the isobaric surface is in general small so that the energy quantities of the z-coordinate system give acceptable approximations of corresponding quantities of the p-coordinate system.

A set of observational data of 15 days from August 1, 00Z to August 15, 12Z of 1970 is utilized to repeat the computation of energies and energy conversions of interest in this study. Results of these computations are displayed in Chapter 4.

Finally, the concluding remarks and suggestions for future work are provided in Chapter 5.

Chapter II

The Theoretical Background

2.1. Energy Relations

We shall adopt a system of notation similar to the one used by Lorenz (1960). The thermodynamic variables (density, specific volume, temperature, potential temperature) and the geopotential (due to its relation to the specific volume through the hydrostatic equation) will be denoted by a subscript 1, while its nondivergent wind, the stream function, and its vorticity will have 2 as a subscript. Finally, the subscript 3 is reserved for the divergent part of the wind, its velocity potential, its two-dimensional divergence, and its vertical velocity.

According to Helmholtz' theorem we may write

$$\vec{V} = \vec{V}_2 + \vec{V}_3 \tag{2.1}$$

where

$$\vec{V}_2 = \vec{k} \times \nabla \psi_2, \quad \vec{V}_3 = \nabla \chi_3 \tag{2.2}$$

in which $\vec{k}$ is a vertical unit vector, ψ_2 the stream-function and χ_3 the velocity potential. If $k = \frac{1}{2} \vec{V} \cdot \vec{V}$ is the kinetic energy per unit mass, we may write

$$k = k_2 + k_3 + \vec{V}_2 \cdot \vec{V}_3 \tag{2.3}$$

where

$$k_2 = \frac{1}{2}\vec{V}_2\cdot\vec{V}_2 \text{ and } k_3 = \frac{1}{2}\vec{V}_3\cdot\vec{V}_3$$

The total kinetic energy in the atmosphere is

$$K = \frac{1}{g}\int_o^{p_o}\int_s k\,ds\,dp \tag{2.4}$$

where g is the acceleration of gravity, p_o the surface pressure, s the total area of the earth, and ds the area element. We find from (2.3) that

$$K = K_2 + K_3 \tag{2.5}$$

where

$$K_2 = \frac{1}{g}\int_o^{p_o}\int_s k_2\,ds\,dp \tag{2.6}$$

and

$$K_3 = \frac{1}{g}\int_o^{p_o}\int_s k_3\,ds\,dp \tag{2.7}$$

(2.5) holds because the last term in (2.3) integrates to zero, i.e.,

$$\frac{1}{g}\int_o^{p_o}\int_s \vec{V}_2\cdot\vec{V}_3\,ds\,dp = \frac{1}{g}\int_o^{p_o}\int_s J(\psi_2,\chi_3)\,ds\,dp = 0 \tag{2.8}$$

It follows from (2.6) and (2.7) that the kinetic energy equations of divergent and nondivergent flows are

$$\frac{dK_2}{dt} = \frac{1}{g}\int_o^{p_o}\int_s \left(u_2\frac{\partial u_2}{\partial t} + v_2\frac{\partial v_2}{\partial t}\right)ds\,dp \tag{2.9}$$

and

$$\frac{dK_3}{dt} = \frac{1}{g}\int_o^{p_o}\int_s (u_3\frac{\partial u_3}{\partial t} + v_3\frac{\partial v_3}{\partial t})\,dsdp \qquad (2.10)$$

where u and v are the zonal and meridional wind components, respectively. It should be noted that the surface pressure tendency is very small so that we neglect its contribution. For later use we note the following results:

$$\frac{1}{g}\int_o^{p_o}\int_s (u_2\frac{\partial u_3}{\partial t} + v_2\frac{\partial v_3}{\partial t})\,dsdp = \frac{1}{g}\int_o^{p_o}\int_s J(\psi_2,\frac{\partial \chi_3}{\partial t})\,dsdp = 0 \qquad (2.11)$$

and

$$\frac{1}{g}\int_o^{p_o}\int_s (u_3\frac{\partial u_2}{\partial t} + v_3\frac{\partial v_3}{\partial t})\,dsdp = -\frac{1}{g}\int_o^{p_o}\int_s J(\psi_2,\frac{\partial \chi_3}{\partial t})\,dsdp = 0 \qquad (2.12)$$

Our next concern is to evaluate (2.9) and (2.10) from the equations of motion. We start from the usual equations

$$\frac{\partial u}{\partial t} + u\frac{\partial u}{\partial x} + v\frac{\partial u}{\partial y} + \omega\frac{\partial u}{\partial p} = -\frac{\partial \phi}{\partial x} + fv + F_x \qquad (2.13)$$

$$\frac{\partial v}{\partial t} + v\frac{\partial v}{\partial x} + \frac{\partial v}{\partial y} + \omega\frac{\partial v}{\partial p} = -\frac{\partial \phi}{\partial y} - fu + F_y \qquad (2.14)$$

By simple differentiation it is straightforward to show the following identities:

$$u\frac{\partial u}{\partial x} + v\frac{\partial u}{\partial y} = \frac{\partial k}{\partial x} - \zeta v \qquad (2.15)$$

where $\zeta = \partial v/\partial x - \partial u/\partial y$ is the vorticity, and

$$u\frac{\partial v}{\partial x} + v\frac{\partial v}{\partial y} = \frac{\partial k}{\partial y} + \zeta u \tag{2.16}$$

The equations (2.13) and (2.14) may be written in the form

$$\frac{\partial u}{\partial t} + \frac{\partial k}{\partial x} - (\zeta + f)v + \omega\frac{\partial u}{\partial p} + \frac{\partial \phi}{\partial x} = F_x \tag{2.17}$$

$$\frac{\partial v}{\partial t} + \frac{\partial k}{\partial y} + (\zeta + f)u + \omega\frac{\partial v}{\partial p} + \frac{\partial \phi}{\partial y} = F_y \tag{2.18}$$

The divergent and nondivergent wind components are introduced in (2.13) and (2.14). Using the system of subscripts we obtain:

$$\frac{\partial u_2}{\partial t} + \frac{\partial u_3}{\partial t} + \frac{\partial k_2}{\partial x} + \frac{\partial k_3}{\partial x} + \frac{\partial(\vec{V}_2\cdot\vec{V}_3)}{\partial x} - (\zeta_2 + f)v_2$$

$$- (\zeta_2 + f)v_3 + \omega_3\frac{\partial u_2}{\partial p} + \omega_3\frac{\partial u_3}{\partial p} + \frac{\partial \phi_1}{\partial x} = F_x \tag{2.19}$$

and

$$\frac{\partial v_2}{\partial t} + \frac{\partial v_3}{\partial t} + \frac{\partial k_2}{\partial y} + \frac{\partial k_3}{\partial y} + \frac{\partial(\vec{V}_2\cdot\vec{V}_3)}{\partial y} + (\zeta_2 + f)u_2$$

$$+ (\zeta_2 + f)u_3 + \omega_3\frac{\partial u_2}{\partial p} + \omega_3\frac{\partial u_3}{\partial p} + \frac{\partial \phi_1}{\partial y} = F_y \tag{2.20}$$

According to (2.9) we must multiply (2.19) by u_2 and (2.20) by v_2 and add the resulting equations in order to

find the rate of change of K_2. In deriving the final result we make use of (2.11) and the fact that $\vec{V}_2$ is non-divergent. Using Gauss' theorem repeatedly and the fact that the divergence of any vector integrates to zero over a closed spherical surface we find nonzero contributions from terms having indices that add to 7 and 8. The result is:

$$\frac{dK_2}{dt} = -\frac{1}{g}\int_o^{p_o}\int_s [(\zeta_2 + f)\ (u_3v_2 - u_2v_3) + \omega_3\frac{\partial k_2}{\partial p} + \omega_3\vec{V}_2\cdot\frac{\partial\vec{V}_3}{\partial p}]dsdp + \frac{1}{g}\int_o^{p_o}\int_s \vec{V}_2\cdot\vec{F}\ dsdp \tag{2.21}$$

Using the boundary conditions $\omega_3 = 0$ at $p = 0$ and $p = p_o$ and the continuity equation, we may write (2.21) in the form

$$\frac{dK_2}{dt} = -\frac{1}{g}\int_o^{p_o}\int_s [(\zeta_2 + f)\vec{V}_2\cdot(\vec{k}\times\vec{V}_3) + k_2\nabla\cdot\vec{V}_3 + \omega_3\vec{V}_2\cdot\frac{\partial\vec{V}_3}{\partial p}]dsdp + \frac{1}{g}\int_o^{p_o}\int_s \vec{V}_2\cdot\vec{F}\ dsdp \tag{2.22}$$

We may naturally obtain an equation for dK_3/dt by multiplying (2.19) and (2.20) by u_3 and v_3, respectively, adding and integrating. It is, however, more convenient to make use of (2.5) and derive the general equation for dK/dt which may be obtained from (2.17) and (2.18) in the

usual way. As is well known, e.g., Wiin-Nielsen (1973), the result is

$$\frac{dK}{dt} = - \int_o^{p_o} \int_s \vec{V}\cdot\nabla\phi ds dp + \frac{1}{g} \int_o^{p_o} \int_s \vec{V}\cdot\vec{F} ds dp \quad (2.23)$$

The first term on the right-hand side of (2.23) may be taken as the energy conversion from potential energy to kinetic energy due to the cross-contour flow (Kung, 1966). According to (2.1), the integrand of this energy conversion term may be written as,

$$- \vec{V}\cdot\nabla\phi = - \vec{V}_2\cdot\nabla\phi_1 - \vec{V}_3\cdot\nabla\phi_1 \quad (2.23)$$

These two terms on the right-hand side represent the barotropic and baroclinic processes (Pearce, 1974) respectively. Integrating the foregoing equation over the whole mass of the atmosphere by using (2.2),

$$- \frac{1}{g} \int_o^{p_o} \int_s \vec{V}\cdot\nabla\phi ds dp = - \frac{1}{g} \int_o^{p_o} \int_s J(\psi_2,\phi_1) ds dp$$

$$- \frac{1}{g} \int_o^{p_o} \int_s \vec{V}_3\cdot\nabla\phi_1 ds dp$$

$$= - \frac{1}{g} \int_o^{p_o} \int_s \vec{V}_3\cdot\nabla\phi_1 ds dp$$

The barotropic term vanishes because a Jacobian intergrates to zero over a closed domain. Physically, the barotropic process cannot cause the conversion between the potential

energy and kinetic energy over the whole atmosphere. This energy conversion is completely accomplished by the baroclinic process. Under these considerations, we shall express (2.23) in the form

$$\frac{dK}{dt} = -\frac{1}{g}\int_o^{p_o}\int_s \vec{V}_3\cdot\nabla\phi_1 dsdp + \frac{1}{g}\int_o^{p_o}\int_s \vec{V}\cdot\vec{F}\ dsdp \tag{2.24}$$

Subtracting (2.22) from (2.24) we get:

$$\frac{dK_3}{dt} = -\frac{1}{g}\int_o^{p_o}\int_s \vec{V}_3\cdot\nabla\phi_1 dsdp + \frac{1}{g}\int_o^{p_o}\int_s [(\zeta_2 + f)\vec{V}_2\cdot (\vec{k}x\vec{V}_3) + k_2\nabla\cdot\vec{V}_3 + \omega_3\vec{V}_2\cdot\frac{\partial\vec{V}_3}{\partial p}]dsdp + \frac{1}{g}\int_o^{p_o}\int_s \vec{V}_3\cdot\vec{F}\ dsdp \tag{2.25}$$

(2.22) and (2.25) indicate that the energy conversion from total potential to kinetic energy, (this energy conversion is shown in Appendix A), i.e.

$$C(P,K) = C(P,K_3) = -\frac{1}{g}\int_o^{p_o}\int_s \vec{V}_3\cdot\nabla\phi_1\ dsdp \tag{2.26}$$

goes into the kinetic energy of the divergent part of the flow. On the other hand, this form of energy may be converted into the kinetic energy of the nondivergent part of the flow. The same two equations, (2.22) and (2.25), show that the latter energy conversion can be calculated

from the formula

$$C(K_3,K_2) = -\frac{1}{g}\int_o^{p_o}\int_s [(\zeta_2 + f)\vec{V}_2\cdot(\vec{k}x\vec{V}_3) + k_2\nabla\cdot\vec{V}_3 + \omega_3\vec{V}_2\cdot\frac{\partial\vec{V}_3}{\partial p}]\, dsdp \tag{2.27}$$

In order to illustrate this energy conversion physically and qualitatively, an example of a cyclone is given in Appendix B.

The symbolic energy equations which contain the major result of this section are therefore

$$\frac{dK_3}{dt} = C(P,K_3) - C(K_3,K_2) - D(K_3) \tag{2.28}$$

$$\frac{dK_2}{dt} = C(K_3,K_2) - D(K_2) \tag{2.29}$$

where

$$D(K_3) = -\frac{1}{g}\int_o^{p_o}\int_s \vec{V}_3\cdot\vec{F}dsdp \tag{2.30}$$

and

$$D(K_2) = -\frac{1}{g}\int_o^{p_o}\int_s \vec{V}_2\cdot\vec{F}dsdp \tag{2.31}$$

(2.28) and (2.29) can be illustrated by an energy diagram

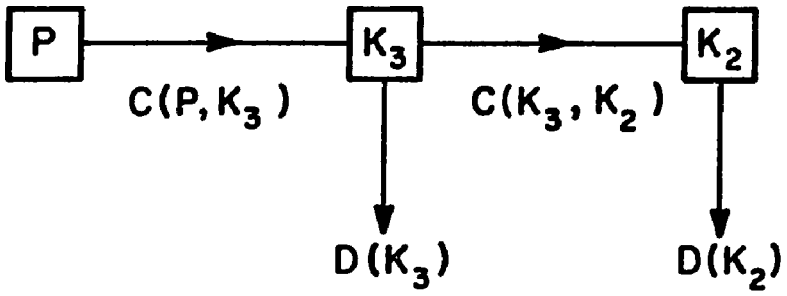


Fig. 1. Schematic energy diagram showing the different forms of energy, energy conversions, and energy dissipation included in this study.

The arrows in this diagram show the possible directions of energy conversions.

2.2. Simplified Models

It is not expected that the three parts of the integrand in (2.27) will be equally important. A check of the derivation of (2.22) and (2.25) from (2.19) and (2.20) shows that the last two terms in the integrand in (2.27) come from the vertical advection of momentum in the equations of motion or, equivalently, from the vertical advection of vorticity and the twisting term in the vorticity equation. Scale analysis (Phillips, 1963) shows that these terms are, in general, one order of magnitude smaller than the dominant terms in the basic equations. Haltiner (1971) distinguishes the most general model for which (2.27) applies, and a model in which the nondivergent wind replaces the total wind in the term expressing the vertical transport of momentum. It is easy to see from (2.19) and

(2.20) that (2.27) in the latter case reduces to

$$C(K_3,K_2) = -\frac{1}{g}\int_o^{p_o}\int_s [(\zeta_2 + f)\vec{V}_2\cdot(\vec{k}\times\vec{V}_3) + k_2\nabla\cdot\vec{V}_3]dsdp \tag{2.32}$$

A further simplification is obtained if the vertical transport of momentum or, if the model is based on the vorticity equation, the vertical transport of vorticity and the twisting term, are neglected altogether. In that case (2.32) becomes even simpler because the second term in (2.32) will vanish, i.e.

$$C(K_3,K_2) = -\frac{1}{g}\int_o^{p_o}\int_s (\zeta_2 + f)\vec{V}_2\cdot(\vec{k}\times\vec{V}_3)dsdp \tag{2.33}$$

The models mentioned above are still based on the primitive equations with or without the neglect of certain items. Alternatively, we may use the vorticity or divergence equations. The main point is that K_3 can still change in magnitude during the integration of (2.32) or (2.33). If we, on the other hand, make further simplifications and consider the so-called balance models, K_3 remains constant in an energetically consistent model which incorporates the balance equation. Several models of this kind have been given by Lorenz (1960). All of them make use of a balance equation. The most general

balance equation is obtained from (2.19) and (2.20); by neglecting friction, differentiating (2.19) with respect to x, (2.20) with respect to y, adding the resulting equations, and keeping those terms which belong to classes 1 and 2 only, we obtain

$$\nabla^2 k_2 - \nabla\cdot[(\zeta_2 + f)\nabla\psi_2] + \nabla^2\phi_1 = 0, \qquad (2.34)$$

It can be shown by elementary differentiation that (2.34) reduces to the customary balance equation

$$\nabla\cdot(f\nabla\psi_2) + 2\,\frac{\partial^2\psi_2}{\partial x^2}\,\frac{\partial^2\psi_2}{\partial y^2} - \frac{\partial^2\psi}{\partial x\partial y} = \nabla^2\phi_1 \qquad (2.35)$$

Since (2.34) is obtained from the general divergence equation by neglecting the time derivative and other terms, it follows that the kinetic energy of the divergent part of the flow will remain constant, or that

$$C(P,K_3) = C(K_3,K_2) \qquad (2.36)$$

To obtain the formulas for the two energy conversions in (2.36) we multiply (2.34) by χ_3 and integrate over the total mass of the atmosphere. The contributions from the various terms are:

$$\frac{1}{g}\int_o^{p_o}\int_s \chi_3\nabla^2\phi_1 dsdp = -\frac{1}{g}\int_o^{p_o}\int_s \nabla\chi_3\cdot\nabla\phi_1 dsdp$$

$$= -\frac{1}{g}\int_o^{p_o}\int_s \vec{V}_3\cdot\nabla\phi_1 dsdp = C(P,K_3) \tag{2.37}$$

and

$$\frac{1}{g}\int_o^{p_o}\int_s \chi_3\left[\nabla\cdot[(\zeta_2 + f)\nabla\psi_2] - \nabla^2 k_2\right] dsdp$$

$$= -\frac{1}{g}\int_o^{p_o}\int_s [(\zeta_2 + f)\vec{V}_2\cdot(\vec{k}\times\vec{V}_3) + k_2\nabla\cdot\vec{V}_3]dsdp \tag{2.38}$$

The expression (2.38) is identical to (2.32). We have therefore shown that (2.36) holds provided the vorticity equation is used in the form

$$\frac{\partial\zeta_2}{\partial t} + \nabla\cdot[(\zeta_2 + f)\vec{V}_2] + \nabla\cdot[(\zeta_2 + f)\vec{V}_3]$$

$$+ \nabla\cdot[\,\omega_3\,\frac{\partial\psi_2}{\partial p}\,] = \vec{k}\cdot\nabla\times\vec{F} \tag{2.39}$$

where the only approximation is the replacement of the total horizontal wind by its nondivergent part in the vertical advection of vorticity and the twisting term.

A simplified form of (2.35) has occasionally been used in numerical prediction models. Assume for example that (2.35) was replaced by

$$\nabla\cdot(f\nabla\psi_2) = \nabla^2\phi_1 \tag{2.40}$$

This balance implies that

$$C(P,K_3) = \frac{1}{g}\int_o^{p_o}\int_s \chi_3\nabla^2\phi_1 dsdp$$

$$= -\frac{1}{g}\int_o^{p_o}\int_s f\nabla\phi_2\cdot\nabla\chi_3 dsdp \qquad (2.41)$$

$$= \frac{1}{g}\int_o^{p_o}\int_s f\vec{V}_2\cdot(\vec{k}x\vec{V}_3)dsdp$$

The last expression must be equal to $C(K_3,K_2)$. This is accomplished by adapting the vorticity equation to the form

$$\frac{\partial\zeta_2}{\partial t} + \nabla\cdot[(\zeta_2 + f)\vec{V}_2] + \nabla\cdot[f\vec{V}_3] = \vec{k}\cdot\nabla x\vec{F} \qquad (2.42)$$

which after multiplication by $-\psi_2$ and integration leads to the equation

$$\frac{dK_2}{dt} = -\frac{1}{g}\int_o^{p_o}\int_s f\vec{V}_2\cdot(\vec{k}x\vec{V}_3)dsdp - D(K_2) \qquad (2.43)$$

An even simpler form of (2.35) is adopted in the quasi-geostrophic models where (2.35) is replaced by

$$f_o\nabla^2\psi_2 = \nabla^2\phi_1 \qquad (2.44)$$

where f_o is a standard value of the Coriolis parameter. (2.41) reduces in this case to

$$C(P,K_3) = -\frac{1}{g}\int_o^{p_o}\int_s f_o\vec{V}_2\cdot(\vec{k}x\vec{V}_3)\,ds\,dp \qquad (2.45)$$

The expression in (2.45) must again be equal to $C(K_3,K_2)$ and this is accomplished by adopting the vorticity equation in the form:

$$\frac{\partial\zeta_2}{\partial t} = \nabla\cdot[(\zeta_2 + f)\vec{V}_2] + f_o\nabla\cdot\vec{V}_3 = \vec{k}\cdot\nabla x\vec{F} \qquad (2.46)$$

It is thus seen that the balanced, energetically consistent models imply a conservation of the kinetic energy of the divergent part of the flow, while variation in K_3 can take place in more general models.

2.3. Discussion

Equation (2.27) gives the energy conversion from K_3 to K_2 in a general model based upon the so-called primitive equations. No evaluation of $C(K_3,K_2)$ from meteorological data or from a general circulation model is presently available. It is obvious that the evaluation of the various terms in (2.27) requires the knowledge of $\vec{V}_2,\vec{V}_3$ and ω_3 where the last two parameters are connected through the continuity equation:

$$\nabla\cdot\vec{V}_3 + \frac{\partial\omega_3}{\partial p} = 0 \qquad (2.47)$$

$\vec{V}_2$ and $\vec{V}_3$ can be generated by separating the horizontal wind vector into its divergent and nondivergent parts. This process can be achieved by several approaches. They will be discussed in the following chapters. ω_3 can be evaluated by the indirect methods from meteorological data, e.g. Petterssen (1956), or can be provided by the direct output of a general circulation model based upon the primitive equations.

The main purpose of such a calculation will be to compare the magnitude and the direction of $C(P,K_3)$ and $C(K_3,K_2)$ as shown in Figure 1. We expect that these two energy conversions will both be positive, i.e. the direction indicated by arrows in Figure 1 and are equal if we average them over a sufficiently long time. Strictly speaking this statement is true only when we disregard the frictional dissipation of K_3, i.e. $D(K_3)$. One would expect that $D(K_3)$ would be small, but it can be evaluated because $\vec{F}$, the horizontal force of friction, is parameterized in any general circulation model. In the same long-term average we must have

$$C(K_3,K_2) = D(K_2) \tag{2.48}$$

One should notice that one of the major characteristics of the large-scale flow in the atmosphere is that the amount of energy in the divergent flow seems to remain small at all times. This must mean that $C(P,K_3)$

and $C(K_3,K_2)$ are approximately equal at all times because if they were unequal for any reasonably long time period we would find large values of K_3. While the kinetic energy of the divergent part of the flow is an extremely important energy reservoir because all the energy converted from the total potential energy must go through K_3, it appears nevertheless that K_3 plays an almost catalytic role because it must be present all the time, but the major energy conversion appears to be almost directly from P to K_2.

We do not know a great deal about the behavior of K_3. So far we have been satisfied by noting that it is small. However, the calculation of $C(P,K_3)$ and $C(K_3,K_2)$ may as a matter of fact show the extent to which K_3 is catalytic.

Chapter III

The Study of the NCAR General Circulation Model

3.1. A Brief Description of the NCAR General Circulation Model and Data

The history data which are the output of the NCAR general circulation model are used for numerical evaluation of energies and energy conversions. A brief description of the model and the data source will make the computations more understandable.

The NCAR general circulation model is formulated in the z-coordinate system, i.e., height is the vertical coordinate (Kasahara and Washington, 1967; Washington and Kasahara, 1970; Kasahara and Washington, 1971). The dynamic framework of this model is very similar to the one proposed by Richardson (1922). The data used in this study are derived from the NCAR six-layer version which has a spherical horizontal spacing of $2\frac{1}{2}^{\circ}$ in longitude and latitude for the globe.

A vertical cross-section of the six-layer model is shown in Figure 2, where the mountainous regions are indicated by shading, above sea level, z=0 (where z denotes the height as the vertical coordinate). The height increment Δz, is chosen to be 3 km. The top is located at $z=z_T$ (= $6\Delta z$ = 18 km), which corresponds approximately to the 75 mb pressure level. Mountain heights, adopted from Berkofsky and Bertoni (1955), are a function of latitude

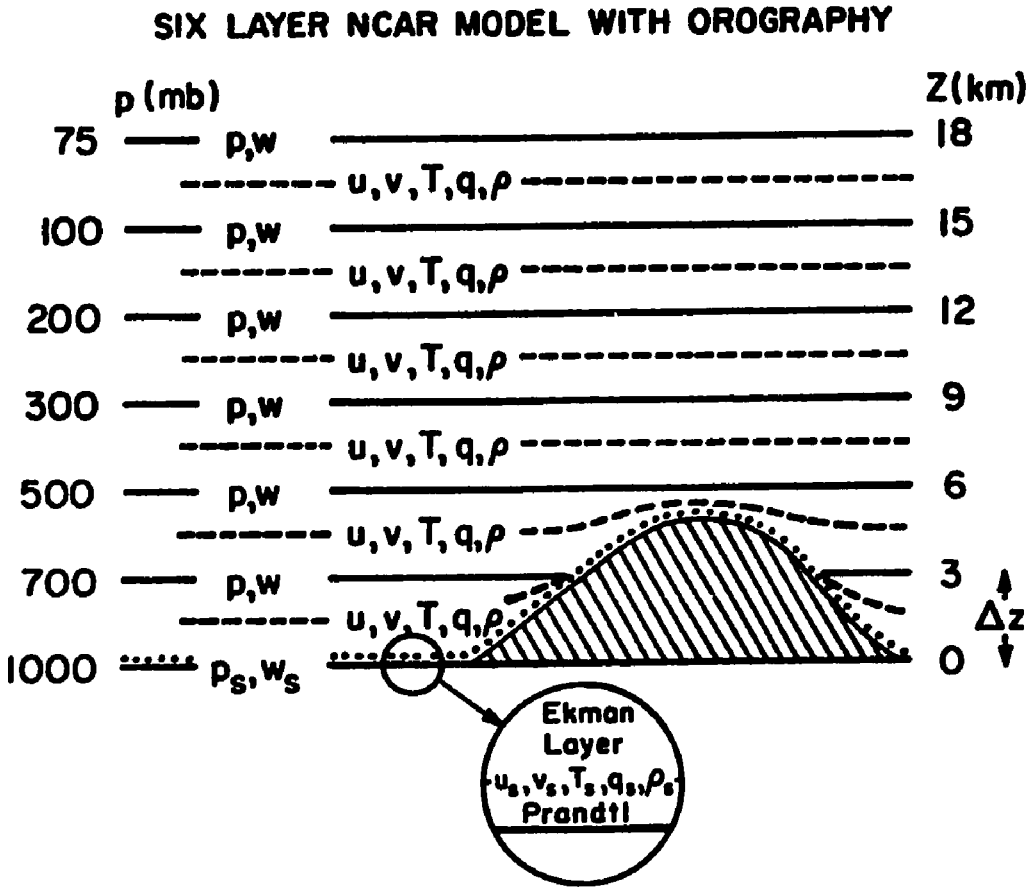


Fig. 2. Six-layer NCAR general circualtion model with orography (after Kasahara and Washington, 1971).

and longitude.

Surface pressure, p_s, is evaluated along the mountain surface. Pressure, p, and vertical velocity, w, correspond to z=3, 6, 9, 12, 15, and 18 km, and wind components, u, v, temperature, T, density ρ, and the specific humidity, q, are at intermediate levels, i.e., z = 1.5 km, 4.5 km, etc.

The surface boundary (Prandtl) layer is included in the model as shown in the inset of Figure 2. The variables u_s, v_s, T_s, q_s, and p_s,which correspond to the surface boundary, are evaluated from the lower boundary conditions.

The upper boundary condition, required for mass conservation, is

$$w = 0 \qquad \text{at} \qquad z = z_T \tag{3.1}$$

The lower boundary which is placed at the anemometer height (~ 10 m above the earth's surface), is indicated by s. At the lower boundary a kinematic condition requires that,

$$w = \vec{V}_s \cdot \nabla H = w_s \qquad \text{at} \qquad z = H \tag{3.2}$$

where $\vec{V}_s = u_s\vec{i} + v_s\vec{j}$, $\vec{i}$ and $\vec{j}$ being unit vectors in the east and north directions, respectively. Also,

$$V_s \cdot \nabla = \frac{u_s}{a \cos\phi} \frac{\partial}{\partial\lambda} + \frac{v_s}{a} \frac{\partial}{\partial\phi} \tag{3.3}$$

The data for this study consist of u, v, w, p, and ζ of the NCAR GCM at 12-hour intervals. It is kindly provided by the GCM group in the form of condensed tapes starting

from day 71 and going to 100. In addition, the longitudinal and latitudinal components of frictional force per unit volume, (known in this study as F_x and F_y) are also furnished at intermediate levels every 12 hours.

3.2. Energy Relations in the z-Coordinate System

In order to use the data fields produced by the NCAR GCM to evaluate the energy quantities depicted in Figure 1, we should reformulate the kinetic energy equations of the divergent and nondivergent flows in the z-coordinate system. The energy relations in the z-coordinate system are slightly different from those in Chapter 2. We shall follow the same reasoning as before to obtain these equations. The notation system of Chapter 2 is also adopted here.

The total kinetic energy of the model atmosphere is

$$K = \int_H^{Z_T} \int_s k\rho ds dz = K_2 + K_3 + \int_H^{Z_T} \int_s \vec{V}_2 \cdot \vec{V}_3 \rho ds dz \tag{3.4}$$

where

$$K_2 = \int_H^{Z_T} \int_s k_2 \rho ds dz \tag{3.5}$$

and

$$K_3 = \int_H^{Z_T} \int_s k_3 \rho ds dz \tag{3.6}$$

Z_T and H in the expressions above are the top and bottom of the model atmosphere respectively. Here k, k_2, and k_3 have the same definitions as (2.3).

The rate of change of K_2 and K_3 according to (3.5) and (3.6) are

$$\frac{dK_2}{dt} = \int_H^{Z_T} \int_s \frac{\partial}{\partial t}(k_2\rho)\ dsdz \tag{3.7}$$

and

$$\frac{dK_3}{dt} = \int_H^{Z_T} \int_s \frac{\partial}{\partial t}(k_3\rho)\ dsdz \tag{3.8}$$

(3.7) and (3.8) can be evaluated from the equation of motion which should be in the form of (2.17) in the Z-coordinate system,

$$\frac{\partial V}{\partial t} + \nabla k - (\zeta + f)\vec{k}X\vec{V} + w\frac{\partial V}{\partial Z} + \frac{1}{\rho}\nabla p = \frac{1}{\rho}\vec{F} \tag{3.9}$$

and the continuity equation

$$\frac{\partial \rho}{\partial t} + \nabla\cdot(\rho\vec{V}) + \frac{\partial}{\partial Z}(\rho w) = 0 \tag{3.10}$$

Introducing the divergent and nondivergent wind components in (3.6) and (3.7),

$$\begin{aligned}&\frac{\partial \vec{V}_2}{\partial t} + \frac{\partial \vec{V}_3}{\partial t} + \nabla k_2 + \nabla k_3 + \nabla(\vec{V}_2\cdot\vec{V}_3) - (\zeta_2 + f)\vec{k}X\vec{V}_2 \\ &- (\zeta_2 + f)\vec{k}X\vec{V}_3 + w_3\frac{\partial \vec{V}_2}{\partial Z} + w_3\frac{\partial \vec{V}_3}{\partial Z} + \frac{1}{\rho}\nabla p_1 = \frac{1}{\rho}\vec{F}\end{aligned} \tag{3.11}$$

and

$$\frac{\partial \rho}{\partial t} + \nabla\cdot(\rho\vec{V}_2) + \nabla\cdot(\rho\vec{V}_3) + \frac{\partial}{\partial Z}(\rho w_3) = 0 \tag{3.12}$$

In order to find the rate of change of K_2, we must multiply (3.11) by $\vec{V}_2$ and (3.12) by k_2, i.e., $\frac{1}{2}\vec{V}_2\cdot\vec{V}_2$, and add the resulting equations together. Using Gauss' theorem repeatedly as we integrate the final equation, we obtain

$$\frac{dK_2}{dt} = -\int_H^{Z_T}\int_s [(\zeta_2 + f)\vec{V}_2\cdot(\vec{k}\times\vec{V}_3) + \frac{1}{\rho}k_2\nabla\cdot(\rho\vec{V}_3) + w_3\vec{V}_2\cdot\frac{\partial V_3}{\partial z}]\rho ds dz - \int_H^{Z_T}\int_s \vec{V}_2\cdot\frac{\partial\vec{V}_3}{\partial t}\rho ds dz - \int_H^{Z_T}\int_s \vec{V}_2\cdot\nabla(k_3 + \vec{V}_2\cdot\vec{V}_3)\rho ds dz + \int_s (\rho w_3 k_2)_H ds + \int_H^{Z_T}\int_s \vec{V}_2\cdot\vec{F} ds dz \tag{3.13}$$

The boundary conditions at the top and bottom of the NCAR general circulation model, (3.2) and (3.3) have been applied in (3.13).

The general equation for dK/dt can be obtained from (3.9) and (3.10) in the usual way

$$\frac{dK}{dt} = -\int_H^{Z_T}\int_s \vec{V}\cdot\nabla p ds dz - \int_H^{Z_T}\int_s \vec{V}\cdot\vec{F} ds dp + \int_s (\rho w k)_H ds \tag{3.14}$$

According to (3.4)

$$\frac{dK}{dt} = \frac{dK_2}{dt} + \frac{dK_3}{dt} + \frac{d}{dt}\int_H^{Z_T}\int_s \vec{V}_2\cdot\vec{V}_3\rho ds dz \tag{3.15}$$

dK_3/dt can be easily formed by subtracting (3.13) from (3.15), using (3.14),

$$\frac{dK_3}{dt} = \int_H^{Z_T} \int_s [(\zeta_2 + f)V_2 \cdot (\vec{k}\times\vec{V}_3) + \frac{1}{\rho}k_2 \nabla\cdot(\rho\vec{V}_3) + w_3\vec{V}_2 \cdot \frac{\partial\vec{V}_3}{\partial z}]\rho ds dz - \frac{d}{dt}\int_H^{Z_T} \int_s \vec{V}_2\cdot\vec{V}_3\rho ds dz + \int_H^{Z_T} \int_s \vec{V}_2 \cdot \frac{\partial\vec{V}_3}{\partial t}\rho ds dz + \int_H^{Z_T} \int_s \vec{V}_2 \cdot \nabla(k_3+\vec{V}_2\cdot\vec{V}_3)\rho ds dz + \int_s [\rho w_3(k_3 + \vec{V}_2\cdot\vec{V}_3)]_H ds + \int_H^{Z_T} \int_s \vec{V}_3\cdot\nabla p_1 ds dz + \int_H^{Z_T} \int_s \vec{V}_3\cdot\vec{F} ds dz \qquad (3.16)$$

(3.13) and (3.16) are the kinetic energy equations of the divergent and nondivergent flow in the z-coordinate system. Comparing these two equations with (2.22) and (2.25) which are formulated in the p-coordinate system, we find that (3.13) and (3.16) involve some extra terms. They are caused from the nonvanishing of the integration of Jacobian terms in the surfaces of constant height due to the presence of density, ρ, in the integrands, and from the lower boundary condition of the GCM, because the upward motion, w_s, occurs due to the orography of the surface, (3.2). As we observe from meteorological observations, the slope of the isobaric surface is usually small, and we may therefore expect that terms involving

the integration of Jacobian are not significant. The vertical velocity at the surface induced by the orography (or surface friction) is so small that we may also expect the vertical flux terms at the surface to be unimportant as far as the energy conversion is concerned. In addition, the first integral on the right-hand side of (3.13) or (3.16) is similar to (2.27) except for the middle integrand which is $-\frac{1}{\rho}k_2\nabla\cdot(\rho\vec{V}_3) = -k_2\nabla\cdot\vec{V}_3 - \frac{1}{\rho}k_2\vec{V}_3\cdot\nabla\rho$. The horizontal gradient of density is usually small for large-scale motions of the atmosphere such that we express $-\frac{1}{\rho}k_2\nabla\cdot(\rho\vec{V}_3) \approx -k_2\nabla\cdot V_3$, where the right-hand side coresponds to the second integrand of (2.27). These aforementioned approximations will be discussed further in section 3.5.

From these considerations, we may anticipate that (3.13) and (3.16) are similar to (2.22) and (2.25). The symbolic presentation of (2.22) and (2.25) may be adopted to represent (3.13) and (3.16).

$$\frac{dK_3}{dt} \approx C(P,K_3) - C(K_3,K_2) - D(K_3) \tag{3.17}$$

and

$$\frac{dK_2}{dt} \approx C(K_3,K_2) - D(K_2) \tag{3.18}$$

where

$$C(P,K_3) = \int_H^{Z_T} \int_S \vec{V}_3\cdot\nabla p_1 \, ds\,dp \tag{3.19}$$

$$C(K_3,K_2) = -\int_H^{Z_T} \int_S [(\zeta_2 + f)\vec{V}_2\cdot(\vec{k}\times\vec{V}_3) + \frac{1}{\rho}k_2\nabla\cdot(\rho\vec{V}_3) + w_3\vec{V}_2\cdot\frac{\partial\vec{V}_3}{\partial z}]\,\rho\,ds\,dz \tag{3.20}$$

$$D(K_2) = -\int_H^{Z_T} \int_s \vec{V}_2 \cdot \vec{F} ds dz \tag{3.21}$$

$$D(K_3) = -\int_H^{Z_T} \int_s \vec{V}_3 \cdot \vec{F} ds dz \tag{3.22}$$

The energy conversions between the total potential energy and kinetic energy, and between the potential energy and kinetic energy of the divergent flow are formulated in Appendix A.

3.3. The Scheme of Separating the Horizontal Wind Vector into Its Divergent and Nondivergent Parts

A number of investigations have been made to compute the stream function, ψ , and velocity potential χ, from the horizontal wind field, e.g., Hawkins and Rosenthal (1965), Macuso (1967), Shukla and Saha (1974). One may, of course, obtain the divergent and nondivergent wind field through (2.2). Most previous studies in this regard used a limited region with the particular specification of boundary conditions. Swarztrauber (1974) recently proposed solving the Poisson equation numerically in the spherical coordinate system. Since the existence of mountains in the GCM causes the global surface at the lower levels of the model to become a multiply-connected domain, Swarztrauber's scheme may not be used except in the case of removing mountains by applying some kind of extrapolation scheme. Regardless of the extrapolation

scheme we employ, a certain finite difference error can be introduced. To circumvent this problem, a direct method to divide the horizontal wind into its divergent and non-divergent parts for a finite region (Endlich, 1971) is extended to the globe.

3.3.1. Computation of Vorticity and Divergence

The vorticity and divergence in the spherical coordinate system are,

$$\text{Div} = \frac{1}{a\cos\phi}\frac{\partial u}{\partial \lambda} + \frac{1}{a}\frac{\partial v}{\partial \phi} - \frac{v}{a}\tan\phi \tag{3.23}$$

$$\text{Vort} = \frac{1}{a\cos\phi}\frac{\partial v}{\partial \lambda} - \frac{1}{a}\frac{\partial u}{\partial \phi} + \frac{u}{a}\tan\phi \tag{3.24}$$

The central finite difference form of these two quantities are

$$\text{Div}(i,j) = \frac{1}{a}\left[\frac{u(i+k,j) - u(i-k,j)}{2k\cos\phi\Delta\lambda} + \frac{v(i,j+1) - v(i,j-1)}{2\Delta\phi} - v(i,j)\tan\phi(j)\right] \tag{3.25}$$

$$\text{Vort}(i,j) = \frac{1}{a}\left[\frac{v(i+k,j) - v(i-k,j)}{2k\cos\phi\Delta\lambda} + \frac{u(i,j+1) - u(i,j-1)}{2\Delta\phi} + u(i,j)\tan\phi(j)\right] \tag{3.26}$$

where $1 \le i \le 144$, $2 \le j \le 72$, $\Delta\lambda = \Delta\phi = \pi/72$, and the value of k depends on the latitude ϕ_j, the dependence being given by Table 1.

Table 1. The value of k at different latitudes

j	2	3	4	5	6	7	8	9
ϕ_j	87.5°S	85°S	82.5°S	80°S	77.5°S	75°S	77.2°S	70°S
k	6	6	4	3	2	2	1	1
j	65	66	67	68	69	70	71	72
ϕ_j	70°N	72.5°N	75°N	77.5°N	80°N	82.5°N	85°N	87.5°N
k	1	1	2	2	3	4	6	6

The reason for introducing the factor k is to maintain a nearly constant geographical distance between mesh points. Some high-latitude points are omitted so that the number of grid points along the latitudinal circle, where $|\phi_j| \geq 75^\circ$, will reduce to be one half, one third, one fourth, etc. of that along the lower latitudinal circle, $|\phi_j| \leq 75^\circ$. The conventional scheme of objective analysis (Cressman, 1959) is applied to fill data in all grid points in the region where $|\phi_j| \geq 75^\circ$. In addition, wind fields at the north and south poles are also found by a scheme which is given in Appendix C1.

It should be noticed that the following rules are used to handle the situation where mountains are blocking a grid point (i,j).

1. (i,j) blocked no Vort(i,j) and Div(i.j)evaluated
2. (i+k,j) blocked set u(i+k,j)=0 and v(i+k,j)=v(i,j)
3. (i-k,j) blocked set u(i-k,j)=0 and v(i-k,j)=v(i,j)
4. (i,j+1) blocked set u(i,j+1)=u(i,j) and v(i,j-1)=0
5. (i,j-1) blocked set u(i,j-1)=u(i,j) and v(i,j-1)=0

3.3.2. Separation of the Horizontal Wind Vector into Its Divergent and Nondivergent Parts

By definition, the nondivergent flow must have a proper value of vorticity and zero divergence, and the divergent flow should possess a proper value of divergence and zero vorticity. To find the nondivergent and divergent wind from the real wind field, a procedure similar to a relaxation process is used.

Small corrections, u_D and v_D are made to the wind field at grid points adjacent to a given grid point (i,j) so that the finite difference equation (3.25) forces zero divergence at the grid point (i,j). This adjustment can be written,

$$\frac{1}{a}\left\{\frac{[u(i+k,j) + u_D(i,j)] - [u(i-k,j) - u_D(i,j)]}{2k(\pi/72)\cos\phi(j)} + \frac{[v(i,j+1) + v_D(i,j)] - [v(i,j-1) - v_D(i,j)]}{2(\pi/72)} - v(i,j)\tan\phi(j)\right\} = 0$$

which also can be expressed as,

$$\frac{u_D(i,j)}{ak(\pi/72)\cos\phi(j)} + \frac{v_D(i,j)}{a(\pi/72)} + Div(i,j)=0 \qquad (3.27)$$

To determine the correction of wind fields, u_D and v_D, in (3.26), Endlich assumed that the first two terms of (3.27) contribute equally to the divergence. We modify his assumption be setting

$$v_D(i,j) = -\left(\frac{k}{2}\cos\phi(j)\right)a(\pi/72)Div(i,j) \qquad (3.28)$$

where $\frac{k}{2}\cos\phi(j)$ is a weighting factor which was determined experimentally to improve convergence, and letting

$$u_D = (2 - k\cos\phi(j))v_D \qquad (3.29)$$

The wind values at the grid points adjacent to (i,j) after this adjustment are,

$$\begin{aligned} u'(i+k,j) &= u(i+k,j) + u_D(i,j) \\ u'(i-k,j) &= u(i-k,j) - u_D(i,j) \\ v'(i,j+1) &= v(i,j+1) + v_D(i,j) \\ v'(i,j-1) &= v(i,j-1) - v_D(i,j) \end{aligned} \qquad (3.30)$$

where ' denotes the new values of the wind field. One should notice that this adjustment of eliminating divergence may change the vorticity. Therefore, another

correction to the wind fields, u_R and v_R, is introduced to restore the new vorticity back to its original value. Writing (3.26) to include the adjustments $u_R(i,j)$ and $v_R(i,j)$ needed to maintain the vorticity at its original value, we obtain

$$\text{Vort}(i,j)=\frac{1}{a}\left\{\frac{[v'(i+k,j)+(v_R(i,j)]-[v'(i-k,j)-v_R(i,j)]}{2k(\pi/72)\ \cos\phi(j)}\right.$$

$$-\ \frac{[u'(i,j+1)+u_R(i,j)]-[v'(i-k,j)-v_R(i,j)]}{2(\pi/72)}$$

$$\left.-\ u'(i,j)\ \tan\phi(j)\right\}$$

which can be written as,

$$\frac{v_R(i,j)}{ak(\pi/72)\ \cos\phi(j)}-\frac{u_R(i,j)}{a(\pi/72)}+[\text{Vort}'(i,j)-\text{Vort}(i,j)]=0 \qquad (3.31)$$

Following (3.28) and (3.29), we can write u_R and v_R,

$$u_R(i,j)\ =\ (\tfrac{k}{2}\cos\phi(j))a(\pi/72)\,[\text{Vort}'(i,j)-\text{Vort}(i,j)] \qquad (3.32)$$

and

$$v_R(i,j)\ =\ (k\cos\phi(j)-2)u_R \qquad (3.33)$$

The new wind fields of u and v after the second adjustments are

$$
\begin{aligned}
u''(i,j+1) &= u'(i,j+1) + u_R(i,j) \\
u''(i,j-1) &= u'(i,j-1) - u_R(i,j) \\
v''(i+k,j) &= v'(i+k,j) + v_R(i,j) \\
v''(i-k,j) &= v'(i-k,j) - v_R(i,j)
\end{aligned}
\tag{3.34}
$$

Modification of the wind fields is carried out by traversals of the grids shown in Figure 3 in the following order; first (72,1)→(72,2)→--→(72,144)→(71,1)→--→(2,2)→(2,1) which covers the entire sphere once. Notice that wind fields at the north pole are determined and then averaged to be a fixed value for the next iterations by the scheme depicted in Appendix C1. As the first traversal of iteration over the whole sphere is completed, the procedure is repeated with another set of grids in the order (2,144)→(2.143)→--→(2,1)→(3,144)→--→(72,2)→(71,1). The wind fields at the south pole are also determined by the scheme of Appendix C1. These two traversals of the sphere represent one pass of the relaxation scheme.

Throughout the pass we also accumulated the sum of the corrections of wind fields by

$$
ERR = \sum_{i,j} \frac{|u_R(i,j)| + |v_D(i,j)|}{|u(i,j)| + |v(i,j)|} \tag{3.35}
$$

as a measure of the error still to be removed from the wind. If at the end of a pass the error, ERR $\geq 1.5 \times 10^{-3}$,

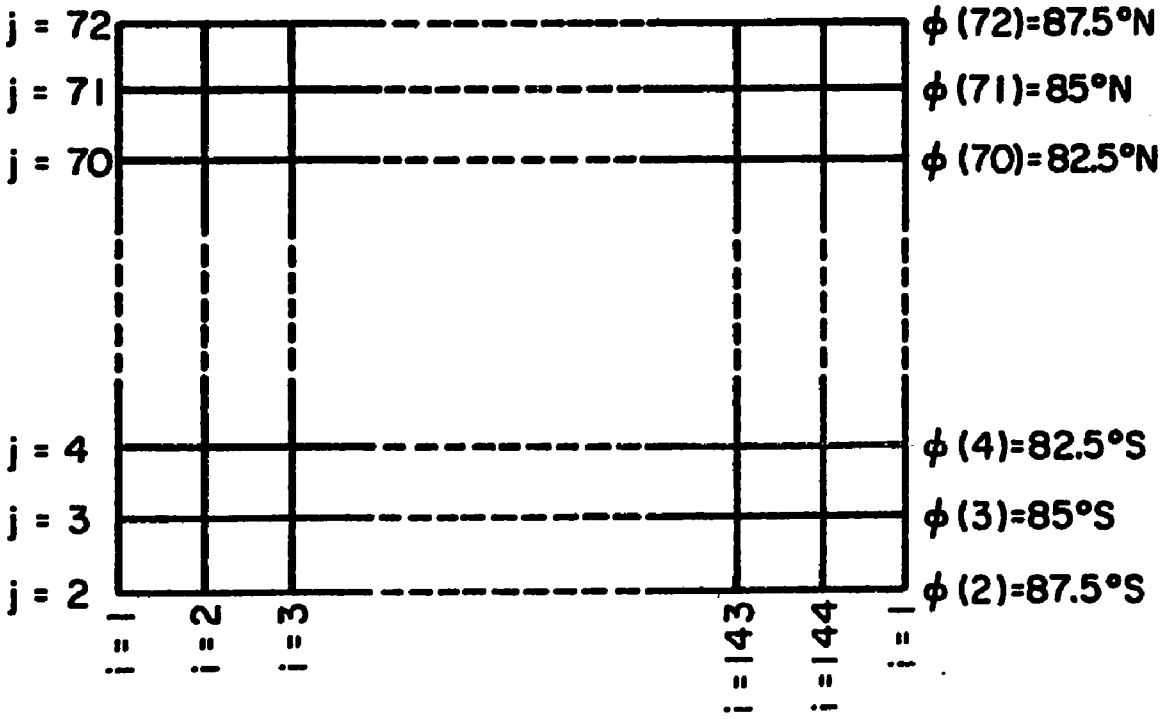


Fig. 3. Horizontal grid system of the NCAR GCM. The horizontal grids of the NCAR GCM are arranged in spherical surfaces. The picture shown above illustrates the arrangement of grid points. i and j represent the indices of grid points in longitudinal and latitudinal circles, respectively.

ERR is set back to zero and another pass through the grids is then done. One the whole it requires 40 ~ 60 passes at the 1.5 km level and about 20 passes for the upper levels to obtain convergence.

The wind fields that appear after the last pass of the relaxation process are taken as the nondivergent wind, i.e., $\vec{V}_2$. The divergent wind fields, $\vec{V}_3$, are simply obtained by the subtraction of the nondivergent wind, $\vec{V}_2$, from the total wind $\vec{V}$.

3.4. The Procedure for the Numerical Integration of Physical Quantities

Let a physical quantity per unit area have the form,

$$\Lambda = \frac{1}{4\pi a^2} \int_0^{2\pi} \int_{-\pi/2}^{\pi/2} \int_H^{Z_T} Aa^2 \cos\phi d\phi d\lambda dz \qquad (3.36)$$

where a is the earth's radius, and A is a physical quantity per unit volume. The contribution from any arbitrary level is

$$\Lambda = \frac{\Delta Z}{4\pi} \int_0^{2\pi} \int_{-\pi/2}^{\pi/2} \Lambda_\ell \sigma_\ell \cos\phi d\phi d\lambda \qquad (3.37)$$

where σ_ℓ is a factor of orography. Following Kasahara and Washington (1971), σ_ℓ is defined as

$$\sigma_\ell = \frac{Z_{k+1} - Z_k}{\Delta Z} , \quad k = \ell$$

where ΔZ = 3km, and ℓ and k denote the intermediate and regular levels respectively as shown in Figure 2, the vertical cross section of the data field. In terms of (3.37), Λ in (3.36) can be evaluated numerically,

$$\Lambda = \sum_{\ell=1}^{6} \Lambda_{\ell} \tag{3.38}$$

One should notice that pressure and vertical velocity do not exist at the intermediate levels of Figure 2. By using (3.37) to evaluate physical quantities involving horizontal pressure gradient, vertical velocity, and vertical gradient of velocity, some adjustments have to be made. Firstly, the pressure is interpolated to intermediate levels under the hydrostatic approximation in such a way that the horizontal pressure gradient at these levels can be calculated. Secondly, $\partial\vec{V}_3/\partial Z$ is simply evaluated by the central finite difference scheme so that $w_3 \frac{\partial\vec{V}_3}{\partial Z}$ can be computed at the regular levels. To compute the last integrand in (3.20) at the intermediate levels, an average of $w_3 \frac{\partial\vec{V}_3}{\partial Z}$ at two regular levels is taken. Notice that $w_3 \frac{\partial\vec{V}_3}{\partial Z}$ at the top or bottom of intermediate levels is evaluated by extrapolation from nearby intermediate levels. Finally, $\vec{V}_2$ and $\vec{V}_3$ involved in the vertical flux terms at the surface are calculated by a linear extrapolation of $\vec{V}_2$ and $\vec{V}_3$ from levels aloft.

3.5. Kinetic Energies of Divergent Flow and Nondivergent Flow

The mean values of K, K_2, and K_3 from day 71 to 100 of the NCAR GCM are shown in Table 2 for three cases; the globe, Northern Hemisphere (N.H.), and Southern Hemisphere (S.H.).

Table 2: Mean value of the kinetic energy K, K_2, and K_3, and the ratios, $K_2/(K_2 + K_3)$, and $K_3/(K_2 + K_3)$ from day 71 to 100 of the NCAR GCM. Unit for K, K_2, and K_3: 10^8erg cm^{-2} (10^5 joule m^{-2})

	Globe	N.H.	S.H.
K	14.71	19.03	10.39
K_2	14.52	18.78	10.24
K_3	0.18	0.23	0.13
$K_2/(K_2+K_3)$	98.8%	98.8%	98.7%
$K_3/(K_2+K_3)$	1.2%	1.2%	1.3%

Table 2 displays a small discrepancy between K and the sum of K_2 and K_3. According to (3.4), this discrepancy is attributed to the nonvanishing of the last term, i.e.,

$$\int_S \int_H^Z \vec{V}_2 \cdot \vec{V}_3 \rho ds dZ \neq 0.$$

(2.8) shows that $\vec{V}_3 \cdot \vec{V}_3$ is a Jacobian of ψ_2 and χ_3 in the isobaric surface, therefore $\vec{V}_2 \cdot \vec{V}_3$ integrates to zero over

a closed domain. The presence of density, ρ, in the last term of (3.4) makes the null result of (2.8) inapplicable here. One should notice that V_2 and V_3 are measured on a constant height surface in the z-coordinate system. As a matter of fact, the small value of

$$\int_S \int_H^{Z_T} \vec{V}_2 \cdot \vec{V}_3 \rho ds dz$$

is due to the fact that the slope of isobaric surfaces of large scale motion usually is small under the hydrostatic assumption such that the difference of $\vec{V}_2 \cdot \vec{V}_3$ measured at the constant height surfaces and isobaric surfaces is small.

Furthermore, it is of interest to compare the kinetic energy, K, of the NCAR GCM with observational studies. January is a winter month in the Northern Hemisphere, but it is a summer month in the Southern Hemisphere. Therefore, we may take the global mean value of K in January of the NCAR GCM to compare the yearly mean at the Northern Hemisphere from observational studies. Wiin-Nielsen (1967) used the data of NMC from February 1963 to January 1964, and obtained values of K shown in Talbe 3.

Table 3: Yearly mean value and monthly mean values for January and July of K from Wiin-Nielsen (1967) Unit: 10^8erg cm^{-2} (10^5Joule m^{-2})

yearly	January	July
18.49	28.07	9.21

Recently Peixoto and Oort (1974) used a collection of 5 years of daily upper air data covering the area of the globe north of 10^{o}S from the so-called MIT general circulation library. Their results are shown in Table 4.

Table 4: Yearly mean value and monthly mean value for January and July of K from Peixoto and Oort (1974). Unit: 10^{8}erg cm^{-2}(10^{5}Joule m^{-2}).

yearly	January	July
12.39	17.34	7.01

Wiin-Nielsen's values of K are higher than Peixoto and Oort's and ours. The reason that Wiin-Nielsen obtained higher values of K may be because of the use of the NMC data and thus the lack of contributions from the tropics to reduce his values of K. However, this comparison shows that the mean value of K of the NCAR GCM is acceptable.

In view of stronger baroclinicity in winter than in summer, the general circulation of the atmosphere must be more intense in winter. This may explain that the value of K in the Northern Hemisphere is larger than that in the Southern Hemisphere for January simulation of the GCM. Even though this comparison is not made for the same hemisphere, the observational results from Wiin-Nielsen and Peixoto and Oort for the Northern Hemisphere shown in Table 3 and 4 respectively may help us understand the difference of K in winter and summer.

The magnitude of K_2 is very close to that of K. The foregoing discussion for K therefore displays that K_2 possesses a time variation similar to K. This consideration may clarify why K_2 presents a higher value in the N.H. than in the S.H. during January.

The ratios, $K_2/(K_3+K_2)$ and $K_3/(K_3+K_2)$, are shown in Table 2 for the globe, N.H., and S.H. It is obvious that K_3 is two orders less then K_2. In other words, the kinetic energy budget of the NCAR GCM is mostly explained by K_2.

Figure 4 displays the contributions from latitude zones to K_2 and K_3. The contributions to K_2 comes mainly from the middle latitudes of both hemispheres where the strong westerlies exist. Contributions to K_3 have a larger value over the N.H.. Figures 5 and 6 shows the altitude-height contribution to K_2 and K_3, respectively, expressed in erg cm^{-3}. The largest values of K_2 appear in the upper and middle layers of the model atmosphere. A relative maximum of K_2 exists in the lower layer between $60^{o}S$ and $70^{o}S$. This is due to strong easterlies over this region. Contributions to K_3 come mainly from the lower layers over the whole globe, and the middle and upper layers in the tropics of the Northern Hemisphere where the Hadley cell circulation is particularly intense during the winter time. The value of K_3 in the lower layer of the Northern Hemisphere is larger than that in the Southern Hemisphere because of more intense activities of cyclones and anticyclones in wintertime.

3.6. Energy Conversions

The mean value and standard deviation of various terms in (3.13) and (3.16) for day 71 to 100 of the NCAR GCM are shown in Table. 5. Comparing the magnitude of terms in (3.13) and (3.16), we find that the terms which have integrands corresponding to the Jacobians in the p-coordinate system are small. Thus, the approximations made in (3.17) and (3.18) are reasonable as far as energy conversions are concerned.

A comparison among $C(P,K_3)$, $C(K_3,K_2)$, and $D(K_2)$ displayed in Table 5 shows that $C(K_3,K_2)$ is smaller than either $C(P,K_3)$ or $D(K_2)$. Even though $D(K_3)$, which is an order less than $D(K_2)$, may reduce the input of K_3 from $C(P,K_3)$, this reduction is not significant. Consequently, we might expect that K_3 grows and K_2 decays. On the contrary, the NCAR GCM is more or less stable (Kasahara and Washington, 1971; Kasahara, Sasamori and Washington, 1974). In fact, the GCM should be internally consistent such that one may expect the existence of energy balance in the GCM. Our computational results show a discrepancy among $C(P,K_3)$, $C(K_3,K_2) + D(K_3)$, and $D(K_2)$. The discrepancy can be attributed to either of two causes: errors in our numerical computation or an energy inconsistency in the GCM.

The same subroutine in our program was used to evaluate the volume integral and areal average for all energy parameters. A final test of our numerical scheme

Table 5: Mean value and standard deviation of various terms in (3.13) and (3.16) for day 71 to 100 of the NCAR GCM. Unit: 10^3erg $cm^{-2}sec^{-1}$(watts m^{-2}).

	Mean Value	Standard Deviation
$C(P,K_3)$	2.8512	0.575
$C(K_3,K_2)$	1.7444	0.447
$C(K_3,K_2)A1 = -\int_V f\vec{V}_2\cdot(\vec{K}x\vec{V}_3)\rho dV$	1.7224	0.413
$C(K_3,K_2)A2 = -\int_V \zeta_2\vec{V}_2\cdot(\vec{K}x\vec{V}_3)\rho dV$	-0.2920	0.162
$C(K_3,K_2)B = -\int_V k_2\nabla\cdot(\rho\vec{V}_3)dV$	0.2697	0.137
$C(K_3,K_2)B1 = -\int_V k_2\vec{V}_3\cdot\nabla\rho dV$	0.0111	0.014
$C(K_3,K_2)C = -\int_V \vec{V}_2\cdot w_3\frac{\partial\vec{V}_3}{\partial z}\rho dV$	0.0443	0.032
$-\int_V \vec{V}_2\cdot\frac{\partial\vec{V}_3}{\partial t}\rho dV$	-0.0030	0.004
$-\frac{d}{dt}\int_V \vec{V}_2\cdot\vec{V}_3\rho dV$	0.0049	0.027
$-\int_V \vec{V}_2\cdot\nabla(k_3+\vec{V}_2\cdot\vec{V}_3)\rho dV$	0.0163	0.007
$\int_s(\rho w_3 k_2)_H ds$	0.0052	0.009
$\int_s \rho w_3(k_3+\vec{V}_2\cdot\vec{V}_3)_H ds$	-0.001	0.003
$D(K_2)$	-2.5231	0.401
$D(K_3)$	-0.2216	0.096

to calculate the physical quantities may be accomplished by the comparison of our computational result of energy parameters with the corresponding quantities of Kasahara and Washington* (1971). The sum of $D(K_2)$ and $D(K_3)$ which is equal to the total frictional dissipation can be selected for this purpose. Since $D(K_3)$ is small, $D(K_2)$ should be a good approximation to the total frictional dissipation. Contributions from different latitude zones to $D(K_2)$ as shown in Figure 9 are similar to that of K & W's (1971) Figure 33. One should notice that the data used in this study are the output from the $2\frac{1}{2}^{o}$ grid version of the GCM and data fields are smoothed by the conventional objective analysis of the regions north of $65^{o}N$ and south of $65^{o}S$. Therefore, one cannot expect the magnitude of our sum of $D(K_3)$ and $D(K_2)$ to be exactly equal to K & W's (1971).

The hydrostatic approximation is applied in calculating $C(P,K_3)$. NCAR provided the pressure field at regular levels, therefore, we have to interpolate the pressure field to intermediate levels under the hydrostatic approximation. Extensive checking has led us to believe that the error is not in the programming or in the numerical scheme, although round-off error and finite difference error of the numerical computation may introduce some small discrepancy in the energy balance. Nevertheless, this kind of

*We will cite papers by authors Kasahara and Washington by the abbreviation (K & W).

discrepancy is not large enough to cause energy imbalance between $C(P,K_3)$ and $C(K_3,K_2) + D(K_2)$ to occur in our result. As mentioned earlier, another possibility that could cause the energy imbalance that occurred in our result is an energy inconsistency in the GCM.

The energy cycle of the NCAR GCM as shown in K & W (1971) exhibits discrepancies in energy conversions. The input and output of the whole system of the model are 4.6 watts m^{-2} and 3.9 watts m^{-2}, respectively. The excess input may explain the increasing of $\bar{K}$, the zonal kinetic energy, and $\bar{I}$, zonal internal energy (which is not shown in 6-layer version, but shown in 12-layer version of the simulation of stratosphere circualtion (Kasahara, Sasamori and Washington,(1973)). The time variation of K', the eddy kinetic energy, is small. In other words, K' is more or less constant from day 20 on. Let us compare the input and output of K' and K & W's (1971) energy diagram; an excess output of 1.12 watts m^{-2} exists. The change of K' over 30 days should be 2.9×10^6 joules m^{-2} which is larger than $K' = 4.5 \times 10^5$ joules m^{-2}. The energy conversion between $\bar{I}$ and K', i.e., the input of K', used by K & W (1971) is approximated by neglecting some small terms in the exact form of $C(\bar{I},K')$ (K & W, 1967). It seems that the neglect of small terms in $C(\bar{I},K')$ does not explain the significant discrepancy between the input and output of K'. The argument above implies the existence either of a fictitious source of K' or an internal adjustment to make

K' stable over the long-term integration. Neither the mechanism of a fictitious source of K' nor the internal adjustment of the model is clear. Wiin-Nielsen (1966), Wellck et al. (1971) and others pointed out that the numerical model usually presents weaker intensity of eddy activities. Therefore $C(\overline{I},K')$ of the GCM may be smaller than what it should be. Nevertheless, the excess output of K' in the GCM may be applicable to explain the discrepancy between $C(K_3,K_2)$ and $D(K_2)$ in our computation.

Regarding the comparison between $C(P,K_3)$ and $C(K_3,K_2) + D(K_3)$, it is very substantial in this study as discussed in Chapter 2. If the GCM is internally consistent, one may expect a quasi-balance between $C(P,K_3)$ and $C(K_3,K_2) + D(K_3)$ which does not exist in our results. In order to examine what causes the discrepancy between $C(P,K_3)$ and $C(K_3,K_2) + D(K_3)$, let us compare the latitude-height distribution of $C(P,K_3)$ and $C(K_3,K_2)$ as shown respectively in Figures 10 and 11 which will be described in detail later. The discrepancy between $C(P,K_3)$ and $C(K_3,K_2)$ mainly occurs in the lower layers of the region between $30^{o}N$ and $30^{o}S$ where the surface easterlies and the lower branch of the Hadley circulation exist. The significant $C(P,K_3)$ that occurs in the lower layers of the subtropical regions is caused by a high correlation between the divergent wind field V_3 and the horizontal pressure gradient. If this high correlation can be understood, we may be able to explain the discrepancy between $C(P,K_3)$ and $C(K_3,K_2) + D(K_3)$.

This would be a problem connected to the internal physical processes of the GCM.

The foregoing discussion indicates that we may not expect a quasi-balance in the energy cycle of this study by using the data of the GCM. However, the positive value of $C(P,K_3)$ and $C(K_3,K_2)$ confirms that the energy must be transformed from potential energy to K_3, and then from the latter to K_2 which will be dissipated by $D(K_2)$.

Wiin-Nielsen (1968) obtained 2.5 watts m^{-2} (2.5×10^3 ergs $cm^{-2}sec^{-1}$) for the yearly mean of energy conversion from potential energy to kinetic energy. Oort and Peixoto (1974) used 5 years of daily upper air data and obtained a value of 2.0 watts m^{-2} (2.0×10^3ergs $cm^{-2}sec^{-1}$) shown in Table 6.

Table 6: Oort and Peixoto's (1974) energy conversion from potential energy to kinetic energy. Unit: watts m^{-2} (10^3ergs $cm^{-2}sec^{-1}$).

yearly mean	January	July
2.0	3.3	1.0

Comparing the result presented in Table 5 and the observational studies we find that the value of $C(P,K_3)$, $C(K_3,K_2)$ and $D(K_2)$ fall in the range of real value in the atmosphere.

It is of interest to compare the contributions from various terms of (3.20) to $C(K_3,K_2)$. Table 7 shows that the Coriolis effect which is denoted by $C(K_3,K_2)Al$ explains

Table 7: Comparison between $C(K_3,K_2)$ and various terms of (3.20).

$C(K_3,K_2)A1/C(K_3,K_2)$	98.7%
$-C(K_3,K_2)A2/C(K_3,K_2)$	16.7%
$C(K_3,K_2)B/C(K_3,K_2)$	15.5%
$C(K_3,K_2)C/C(K_3,K_2)$	2.5%

most of $C(K_3,K_2)$. The contributions from the second term and the relative vorticity effect in the first term of (3.20) are apparently an order less than $C(K_3,K_2)A1$. The third term of (3.20) is two orders less than $C(K_3,K_2)A1$. Although these energy conversions are formulated in the z-coordinate system, the small slope of the isobaric surface probably implies that the expression of (3.20) gives a good estimate of the possible magnitude of the various terms in (2.27). If this conjecture is correct, the quasi-geostrophic model where f is assumed constant may be a godd approximation with regard to the energy conversion between the divergent and nondivergent flow. Furthermore, the small value of $C(K_3,K_2)C$ also indicates that the difference between $C(K_3,K_2)$ in the unbalanced and balanced models is not significant.

To elucidate the catalytic role played by K_3, one has to compare the residence time of K_3 and K_2. This can be achieved by calculating $K_3/C(K_2,K_3)$ and $K_2/C(K_3,K_2)$. From

our results, the residence time of K_3 and K_2 are 3 hours and 9.6 days respectively. K_3 is the only bridge between total potential energy and K_2. The short residence time of K_3 shows that the energy conversion from total potential energy to K_2 occurs without significant delay. In other words, K_3 appears to aid the energy conversion from total potential energy to K_2 without appreciably increasing K_3. This property of the foregoing energy conversion is implicative of a quasi-catalytic nature for K_3.

It has been shown in section 3.5 that the Northern and Southern Hemisphere possess different kinetic energy contents. We may therefore expect that the energy conversions in both hemispheres are also different. According to Krueger, et al. (1965), Wiin-Nielsen (1968), and Oort and Peixoto (1974), one may intuitively expect that energy

Table 8: Mean value of various energy conversions of Northern Hemisphere (N.H.) and Southern Hemisphere (S.H.) for day 71 to 100 of the NCAR GCM. Unit: 10^3ergs $cm^{-2}sec^{-1}$ (watts m^{-2}).

	N.H.	S.H.
$C(P,K_3)$	2.5030	3.1994
$C(K_3,K_2)$	1.5455	1.9440
$C(K_3,K_2)A1$	1.5236	1.9214
$C(K_3,K_2)A2$	-0.4426	-0.1414
$C(K_3,K_2)B$	0.4096	0.1298
$C(K_3,K_2)C$	0.0549	0.0341
$D(K_2)$	2.9580	2.0883
$D(K_3)$	0.2911	0.1521

conversions during January are larger in the Northern Hemisphere than in the Southern Hemisphere because the former is winter while the latter is summer during January. On the contrary the NCAR GCM gives higher values of $C(P,K_3)$ and $C(K_3,K_2)$ and lower value of $D(K_2)$ and $D(K_3)$ in the Southern Hemisphere for January.

It is of interest to compare the contribution to $C(K_3,K_2)$ from various terms in (3.20) and the catalytic role of K_3 for both hemispheres. This comparison can be found from Table 9.

Table 9: Comparison between $C(K_3,K_2)$ and various terms of (3.20), and residence time of K_3 and K_2 for both hemispheres.

	N.H.	S.H.
$C(K_3,K_2)A1/C(K_3,K_2)$	98.6%	98.8%
$C(K_3,K_2)A2/C(K_3,K_2)$	28.6%	7.3%
$-C(K_3,K_2)B/C(K_3,K_2)$	26.5%	6.7%
$C(K_3,K_2)C/C(K_3,K_2)$	3.6%	1.7%
$K_2/C(K_3,K_2)$	14.1 days	6.1 days
$K_3/C(K_3,K_2)$	4 hrs	2 hrs

Regardless of the magnitude of energies and energy conversions, it is surprising that $C(K_3,K_2)A2$ and $C(K_3,K_2)B$ make relatively larger contributions to $C(K_3,K_2)$ in the Northern Hemisphere than in the Southern Hemisphere. Furthermore, the residence time of K_2 and K_3 is longer in the Northern Hemisphere than in the Southern Hemisphere.

This is because the baroclinic process in the winter hemisphere is stronger than in the summer hemisphere.

Figure 7 presents the latitudinal distribution of $C(P,K_3)$. The major contribution to $C(P,K_3)$ is from the subtropics and middle latitudes. This energy conversion is due to the release of the available potential energy to kinetic energy by baroclinic processes.The baroclinic process is as a matter of fact dominant over the middle latitudes, but the results of using the data of the NCAR GCM present significant contributions to $C(P,K_3)$ from the subtropics. The latitude-height distribution of $C(P,K_3)$ is shown in Figure 10. The baroclinic process mainly occurs at the lower layers so that $C(P,K_3)$ is dominant there. It is interesting to notice that a negative value of $C(P,K_3)$ appears in some parts of the upper layers in the Northern Hemisphere of the model atmosphere which reduces the mean value of $C(P,K_3)$ in the Northern Hemisphere. The negative value of $C(P,K_3)$ means that the energy is transformed from K_3 to total potential energy.

As is well known, the baroclinicity is weak in the subtropical regions. This implies that little available energy can be released in that region. The significant contributions to $C(P,K_3)$ from the lower layers of the subtropical regions is difficult to explain in this study. As discussed earlier, the discrepancy between $C(P,K_3)$ and $C(K_3,K_2)$ is mainly attributed to the contributions to $C(P,K_3)$ from the lower layers of the subtropics. What

causes the significant baroclinicity to occur in the lower layers of the subtropics in the GCM? That is a problem of the internal physical processes of the GCM. The answer to this problem is beyond the purpose of this study.

Figure 8a shows the latitudinal distribution of $C(K_3,K_2)$. The kinetic energy conversion from divergent flow to non-divergent flow is accomplished by the baroclinic eddies which largely exist in the middle and high latitudes. The most significant contribution to $C(K_3,K_2)$ appears in the middle and high latitudes of the Northern and Southern Hemisphere in Figure 8a. The subtropics of the Northern Hemisphere also show a secondary maximum of $C(K_3,K_2)$ which may be attributed to the intense Hadley circulation in the Northern Hemisphere. The contribution to $C(K_3,K_2)$ from different parts of the atmosphere is shown in Figure 11. The positive value of $C(K_3,K_2)$ in the lower and upper layers of the subtropics due to the Hadley circulation causes the secondary maximum in the Northern Hemisphere. Contributions to $C(K_3,K_2)$ exist mainly in the lower layers of middle and high latitudes where the baroclinic eddies, e.g., cyclones and anticyclones, are active. One should notice that a broad part of the upper layers in the Northern Hemispheres display negative values of $C(K_3,K_2)$ which reduce higher values of $C(K_3,K_2)$ in the lower layers and makes the mean value of $C(K_3,K_2)$ smaller in the Northern Hemisphere than in the Southern Hemisphere.

The distribution of $C(K_3,K_2)$ is roughly similar to that of $C(P,K_3)$ in Figure 7, especially the distribution of the negative values of both quantities. Owing to the short residence time of K_3, one may expect that the conversion between potential energy and K_2 is not postponed significantly by the existence of K_3. In other words, the rapid conversion from total potential energy to K_2 may imply that the distribution of $C(P,K_3)$ and $C(K_3,K_2)$ have to be very similar except for the distortion due to the contributions of $D(K_3)$. The artificial model atmosphere may not be able to simulate this part* well, but the coexistence of negative $C(K_3,K_2)$ and $C(P,K_3)$ in the upper layers of the Northern Hemisphere shows partly the similarity between the distribution of $C(P,K_3)$ and $C(K_3,K_2)$.

To elucidate the contributions of various terms in (3.20)(except $C(K_3,K_2)C$ which is only a few percent of $C(K_3,K_2)$) from different parts of the atmosphere, the latitudinal and latitude-height distributions of these terms are shown in Figures 8b and 8d and Figures 12 to 14, respectively. Figures 8a and 8b show that the latitudinal contribution to $C(K_3,K_2)$ and $C(K_3,K_2)A1$ are similar. One must recall that $C(K_3,K_2)$ consists of several terms. Figures 8c and 8d show that the contributions to $C(K_3,K_2)$ from $C(K_3,K_2)B$ and $C(K_3,K_2)A2$ are more or less opposite such that their contributions may cancel each other and

* It has been shown in this study that the mean value of $C(P,K_3)$ is larger than $C(K_3,K_2)$ in the NCAR GCM January simulation.

may not modify significantly the contribution from $C(K_3,K_2)A1$ to $C(K_3,K_2)$. The significant parts of $C(K_3,K_2)A2$ and $C(K_3,K_2)B$ are from the tropical regions of both hemispheres where Hadley circulations exist. Figures 11 and 12 show that $C(K_3,K_2)$ and $C(K_3,K_2)A1$ are similar except for the presence of negative $C(K_3,K_2)$ in the upper layer of the tropics. Figures 13 and 14 show that $C(K_3,K_2)A2$ presents positive values only over the upper layers of the middle latitudes where $C(K_3,K_2)B$ has negative values.

Figure 9 shows the latitudinal distribution of $D(K_2)$ and $D(K_3)$. Both quantities show significant dissipation in the region between 60^o and 70^o of both hemispheres. $D(K_2)$ and $D(K_3)$ come mainly from the lower layers of the model atmosphere as shown in Figures 15 and 16.

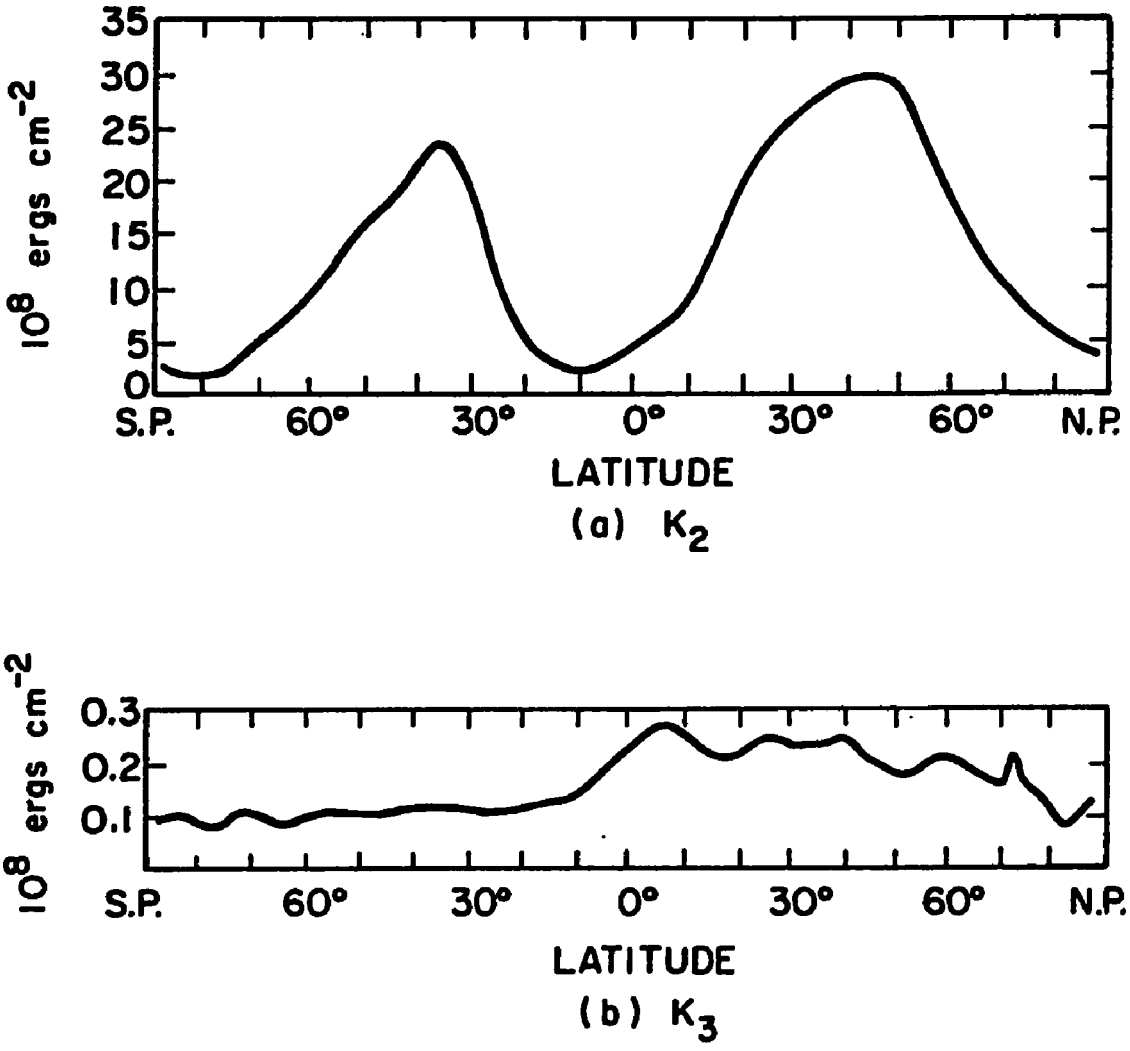


Fig. 4. Contributions to K_2 and K_3 from different latitude bands. Unit: 10^8 ergs cm^{-2} (10^5 joules m^{-2}).

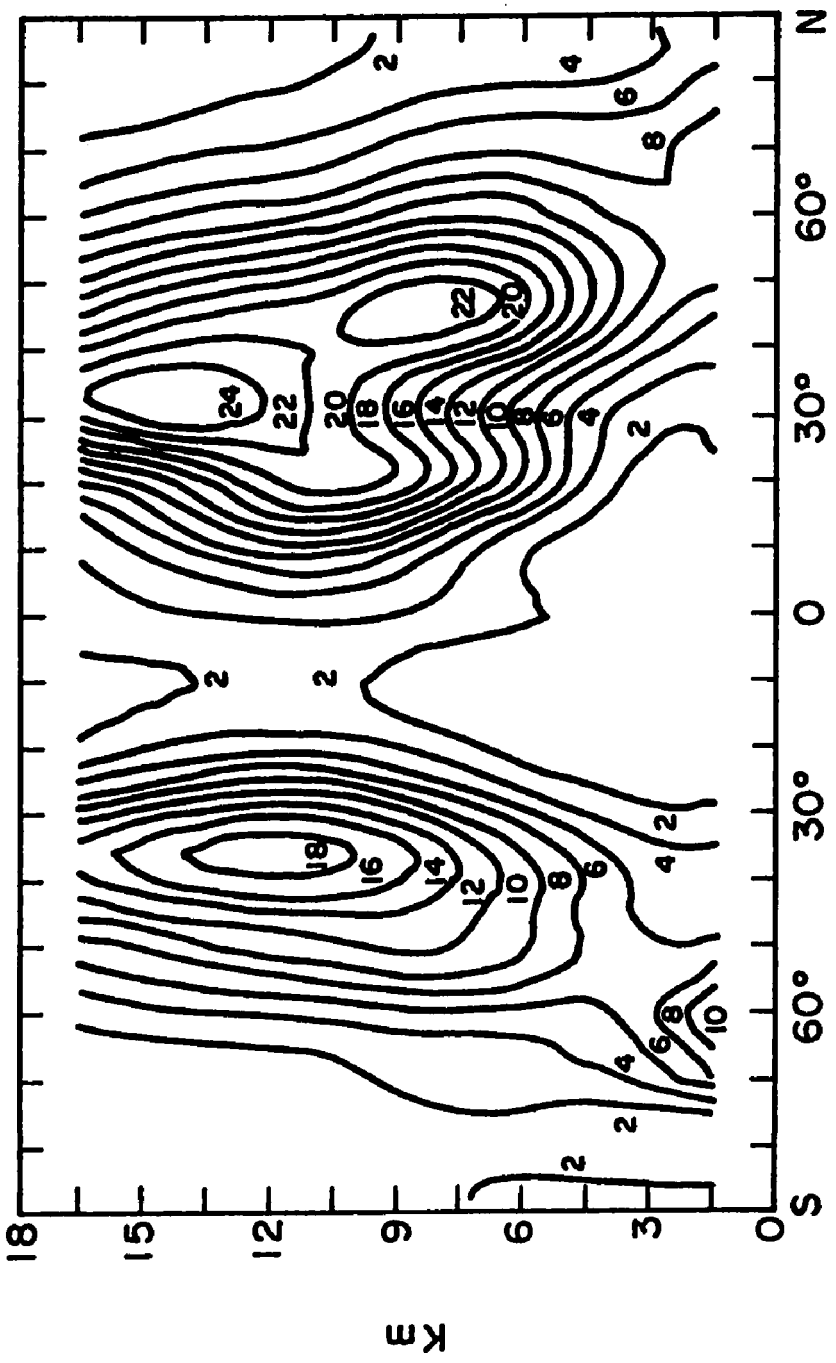


Fig. 5. Latitude-height distribution of 30-day (day 71-100) mean of zonally averaged K_2. Unit: 10^2 ergs cm^{-3} (10 Joule m^{-3}).

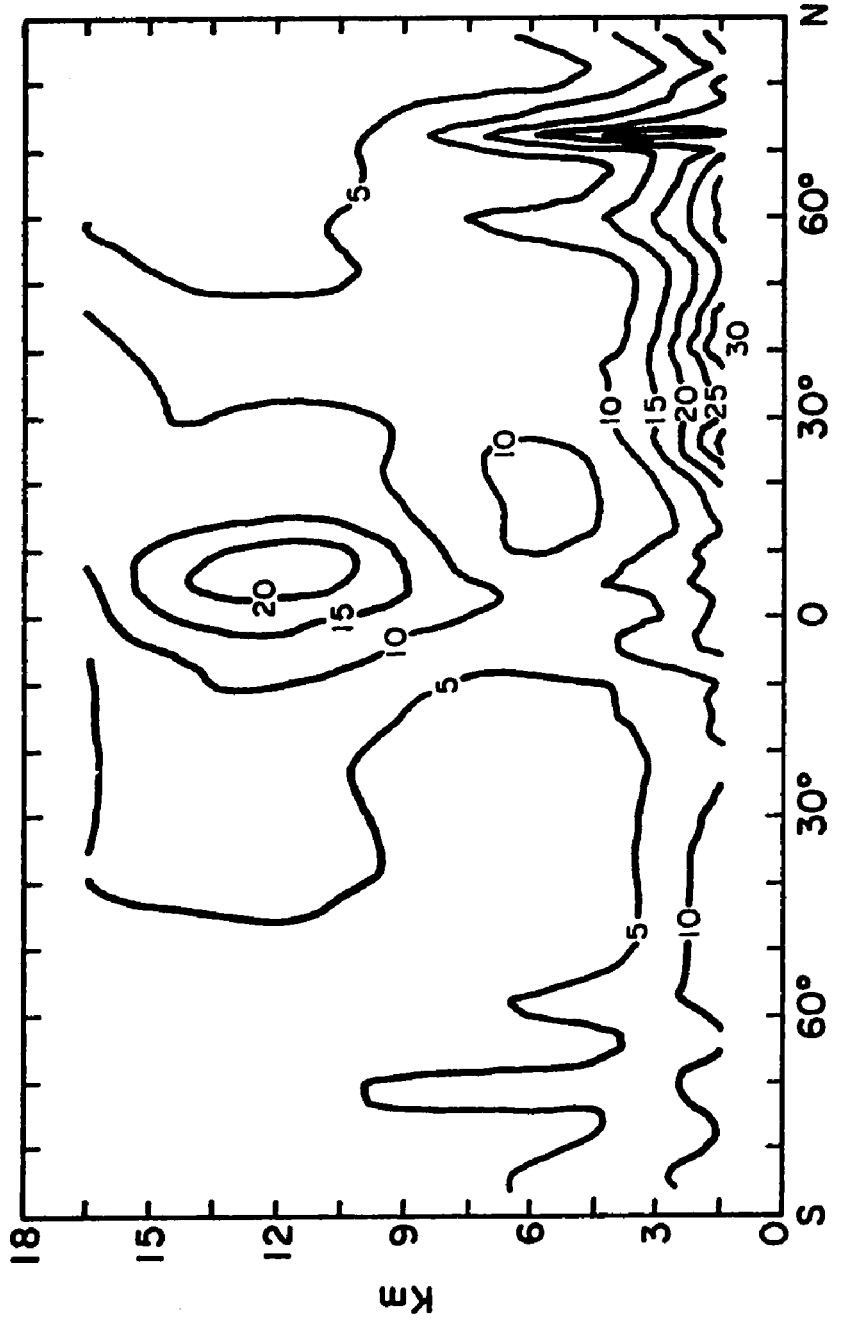


Fig. 6. Latitude-height distribution of 30-day (day 71-100) mean of zonally averged K_3.
Unit: ergs cm^{-3} (10^{-1} Joule m^{-3}).

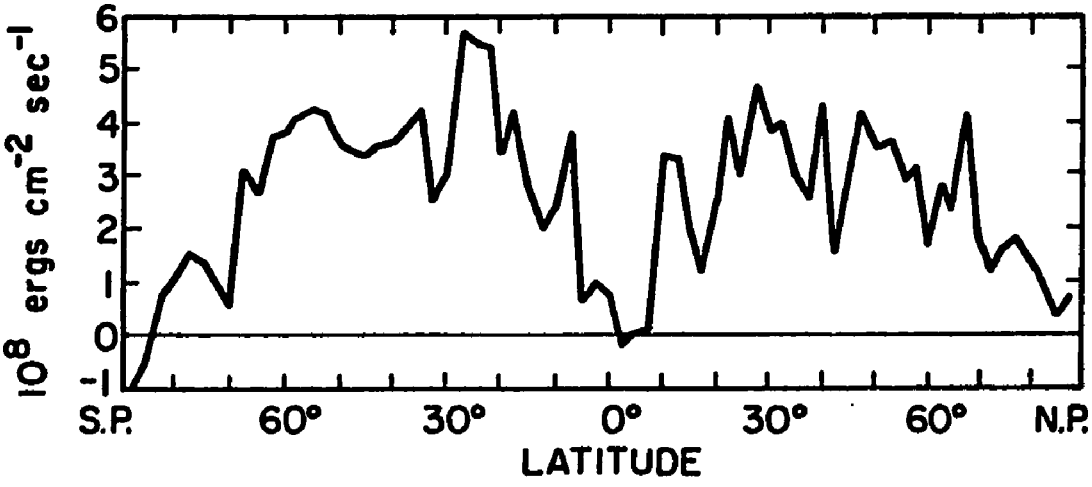


Fig. 7. Contributions to $C(P, K_3)$ from different latitude bands. Unit: 10^3 ergs cm^{-2} sec^{-1} (Watts m^{-2}).

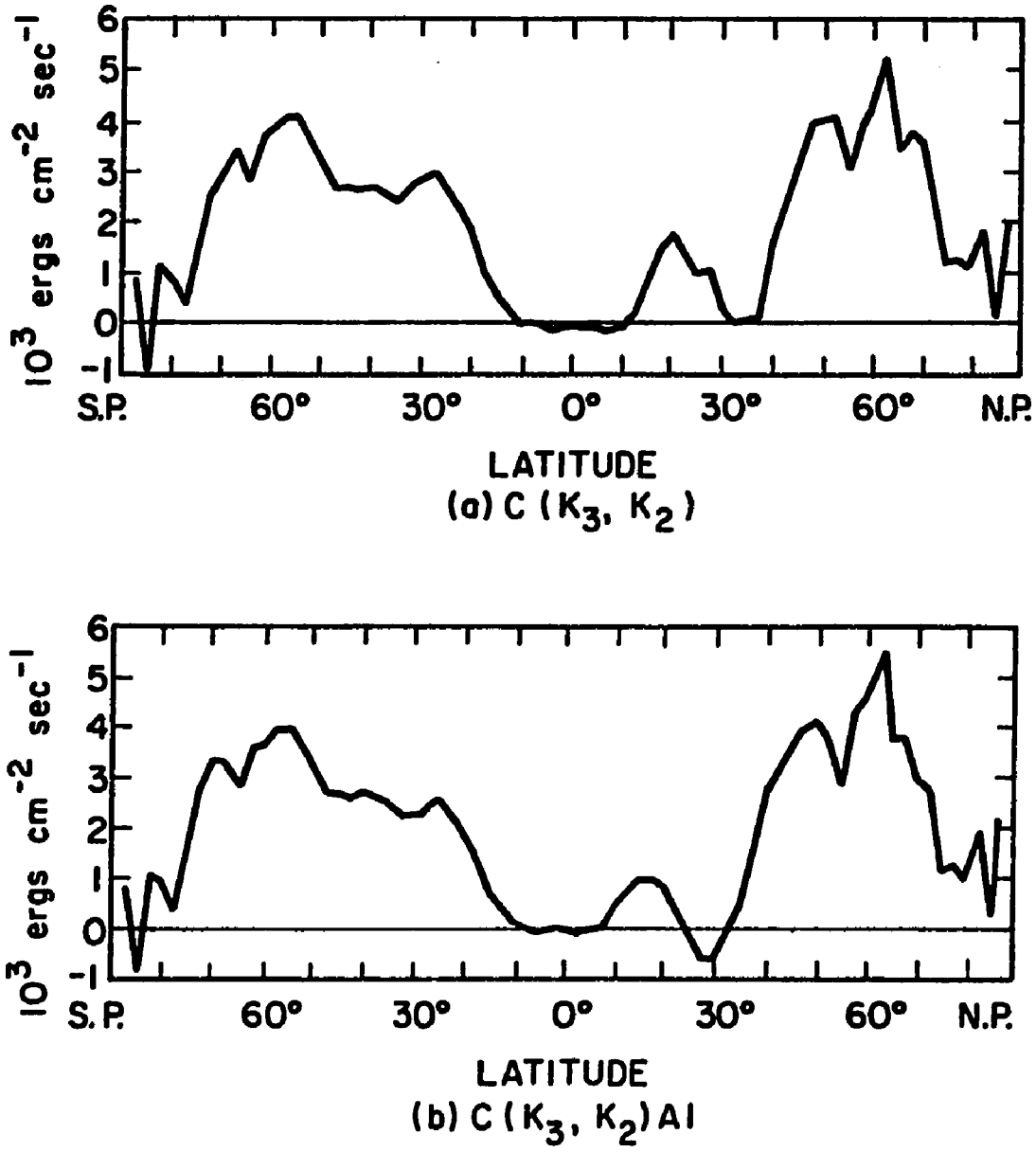


Fig. 8 (a & b). Contributions to (a) $C(K_3,K_2)$ and (b) $C(K_3,K_2)Al$ from different latitude bands. Unit: 10^3 ergs cm^{-2} sec^{-1} (Watts m^{-2}).

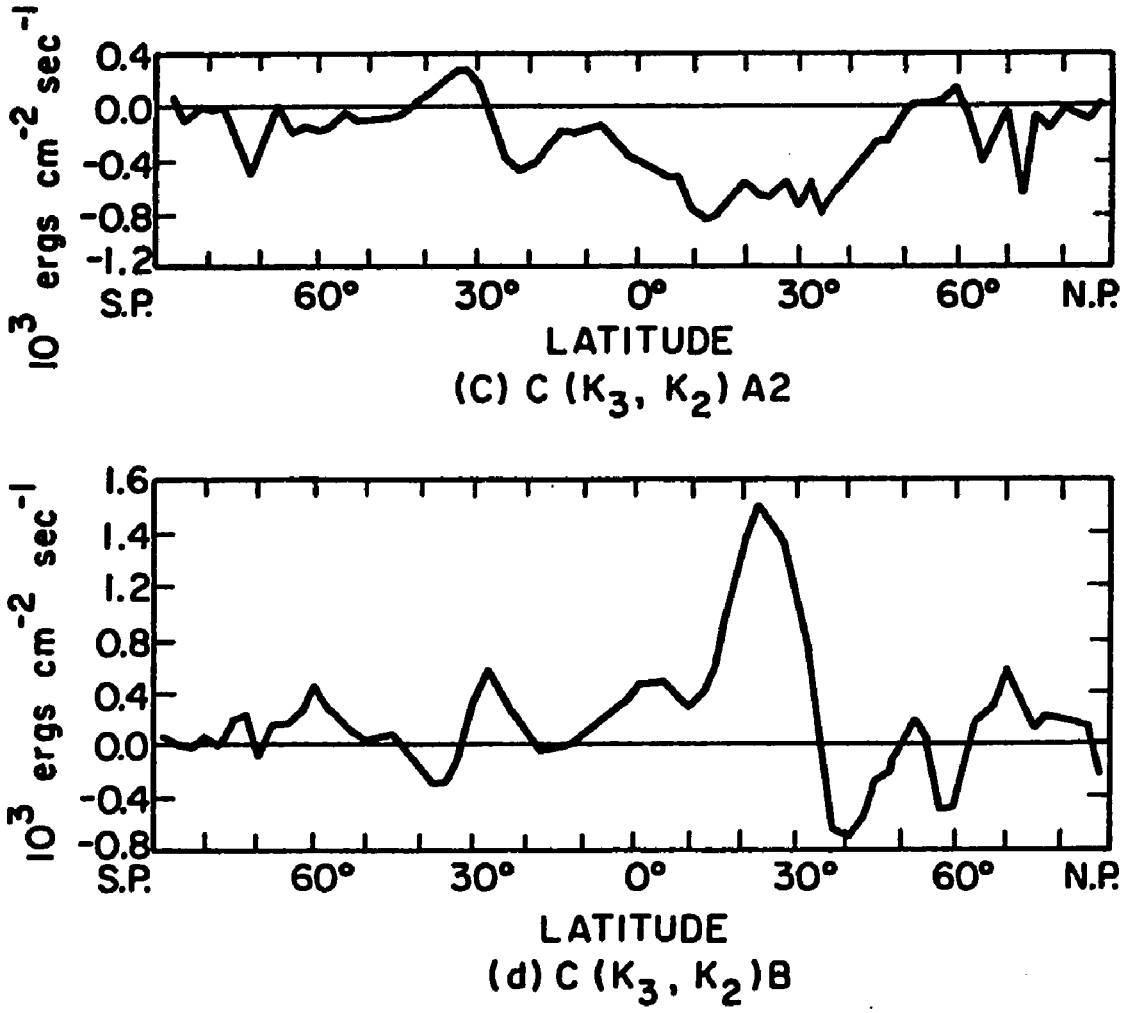


Fig. 8 (c & d). Contributions to (c) $C(K_3,K_2)A2$ and (d) $C(K_3,K_2)B$ from different latitude bands. Unit: 10^3 ergs cm^{-2} sec^{-1} (Watts m^{-2}).

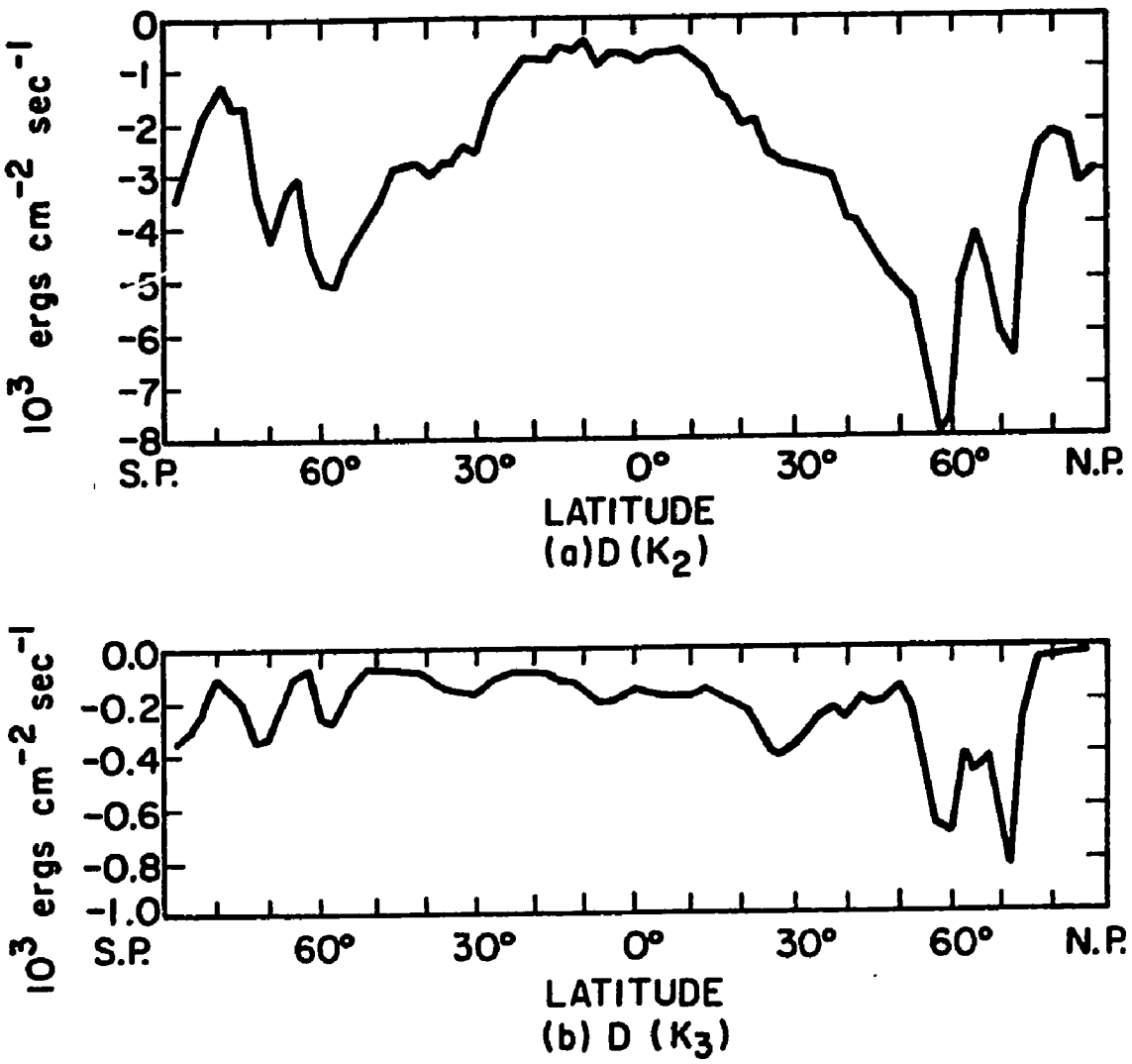


Fig. 9. Contributions to (a) $D(K_2)$ and (b) $D(K_3)$ from different latitude bands. Unit: 10^3 ergs cm^{-2} sec^{-1} (Watts m^{-2}).

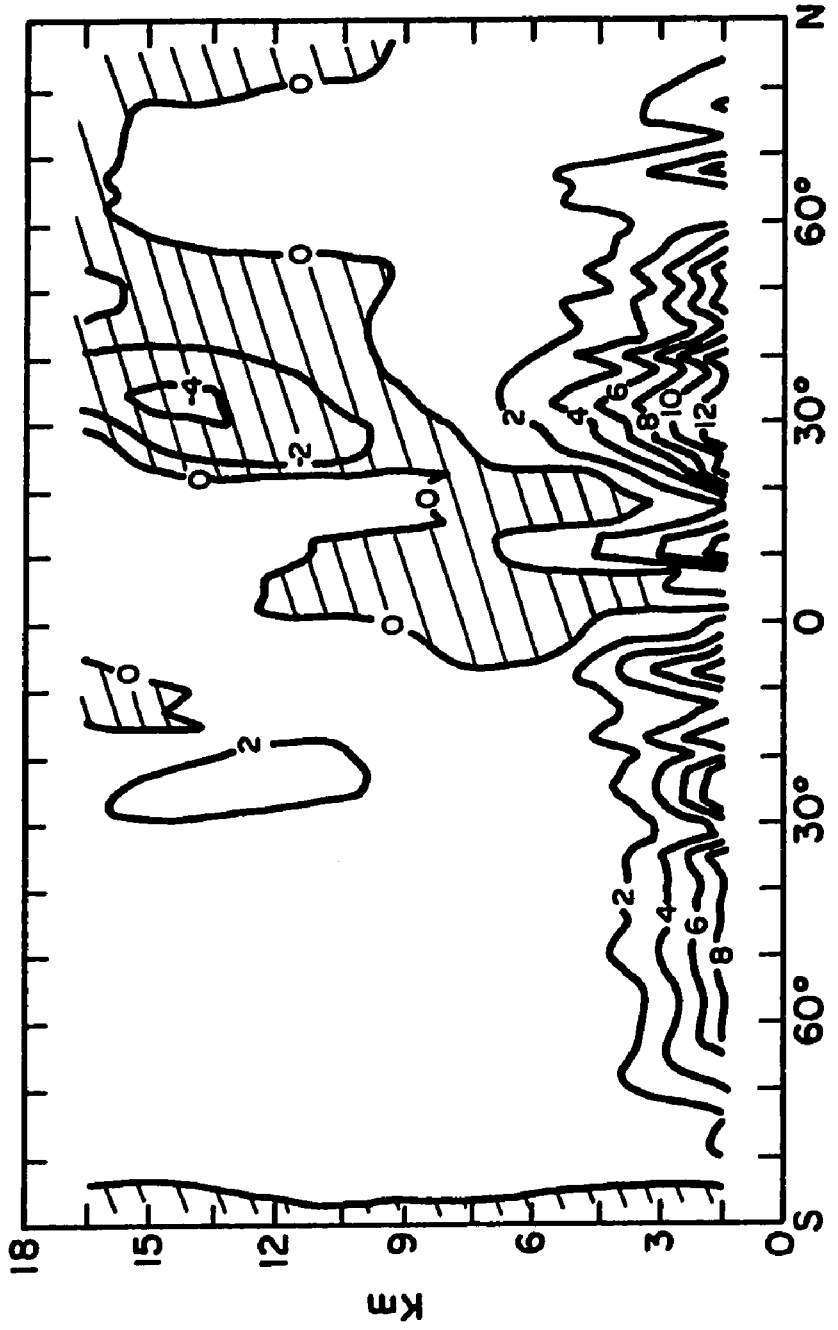


Fig. 10. Latitude-height distribution of 30-day (day 71-100) mean of zonally averaged $C(P,K_3)$. Unit: 10^{-3} erg cm^{-3} sec^{-1}.

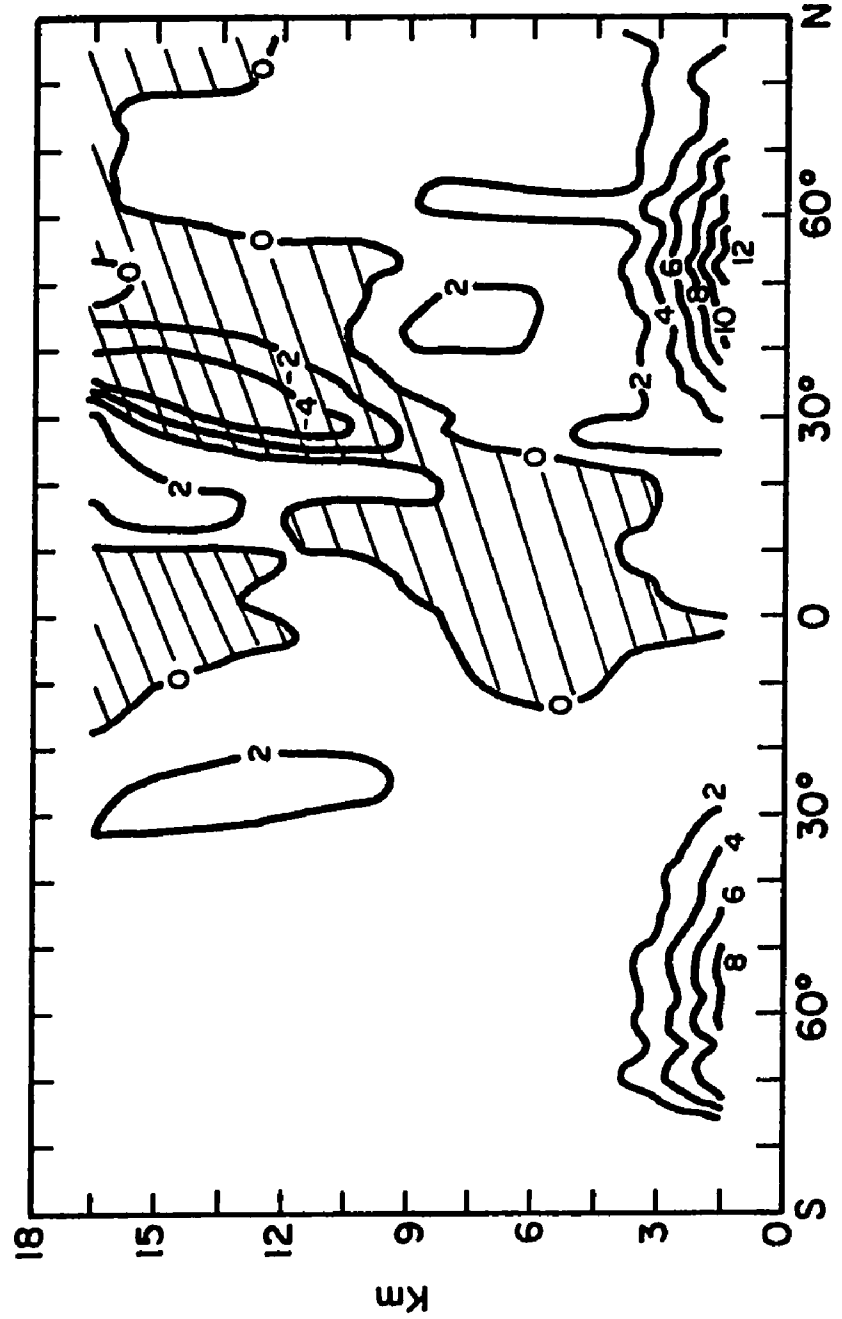


Fig. 11. Latitude-height distribution of 30-day (day 71-100) mean of zonally averaged $C(K_3,K_2)$. Unit: 10^{-3} erg cm^{-3} sec^{-1}.

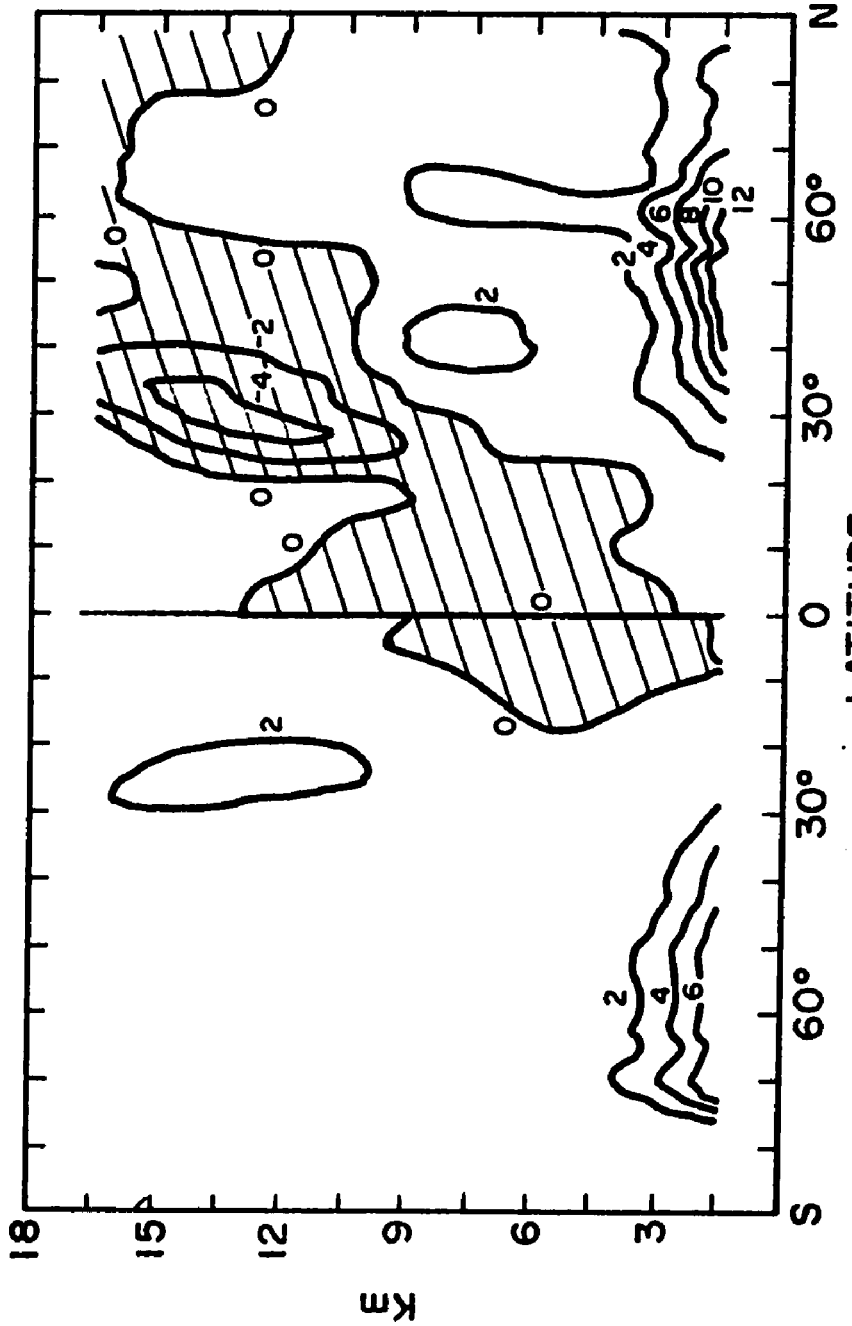


Fig. 12. Latitude-height distribution of 30-day (day 71-100) mean of zonally averaged $C(K_3, K_2)Al$. Unit: 10^{-3} erg cm^{-3} sec^{-1}.

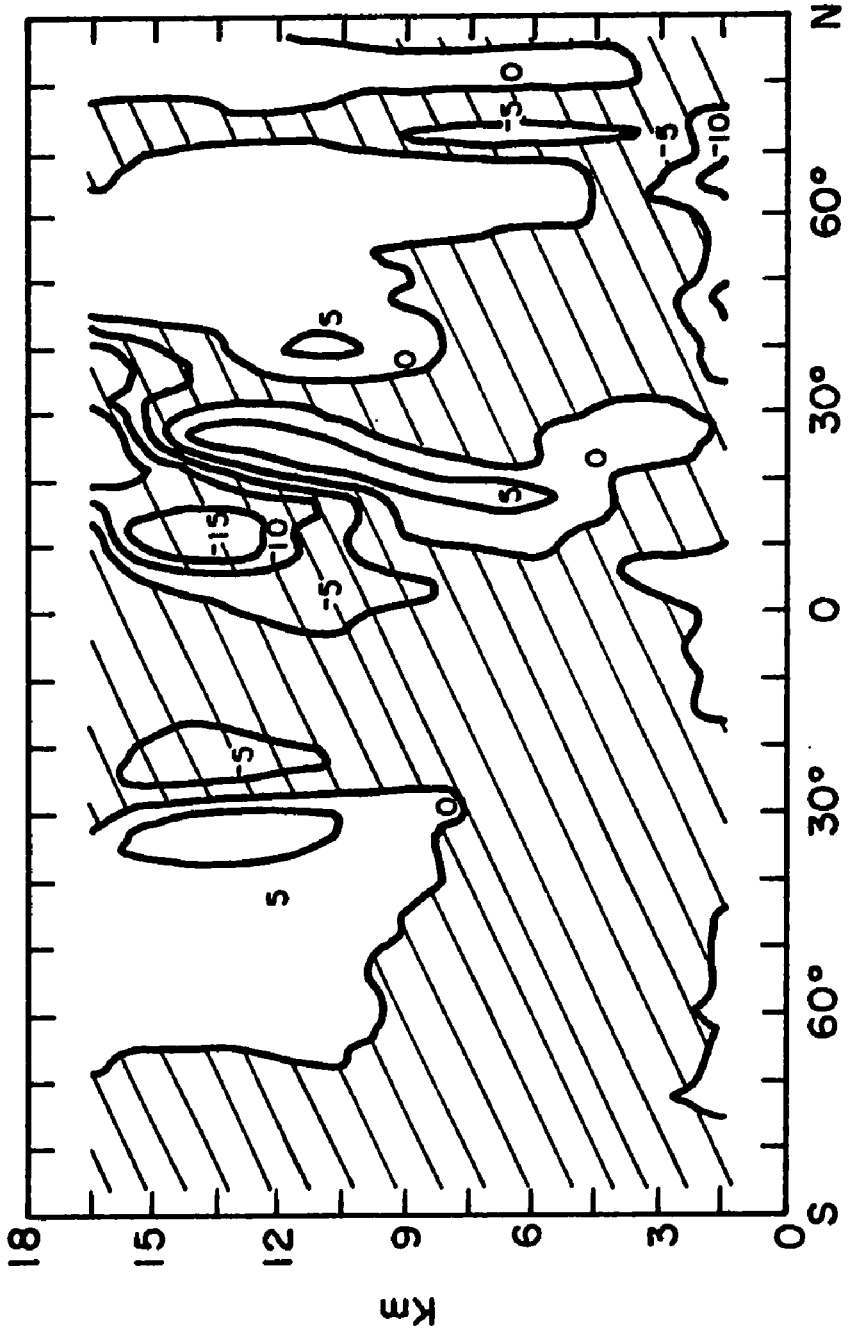


Fig. 13. Latitude-height distribution of 30-day (day 71-100) mean of zonally averaged $C(K_3,K_2)A2$.
Unit: 10^{-4} erg cm^{-3} sec^{-1}.

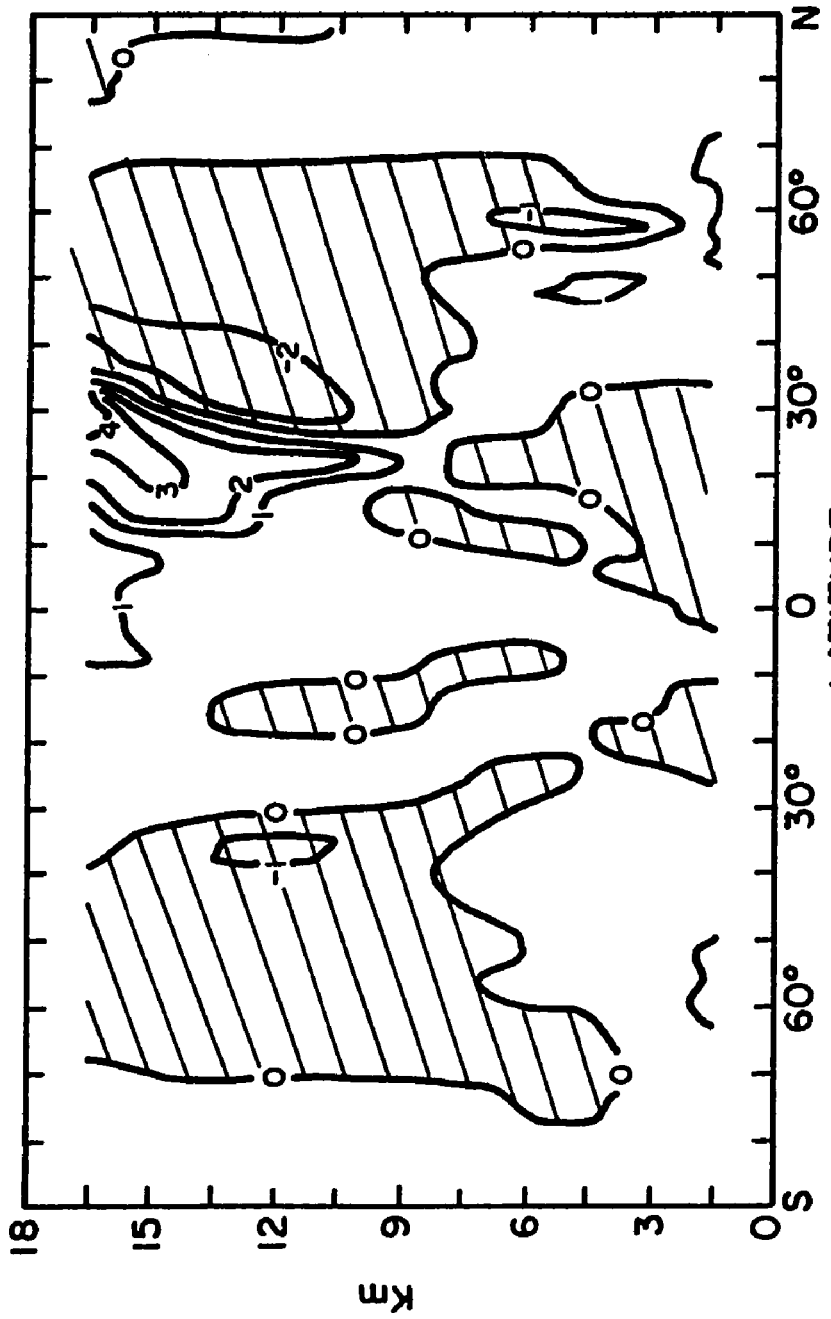


Fig. 14. Latitude-height distribution of 30-day (day 71-100) mean of zonally averaged $C(K_3,K_2)B$. Unit: 10^{-3} erg cm^{-3} sec^{-1}.

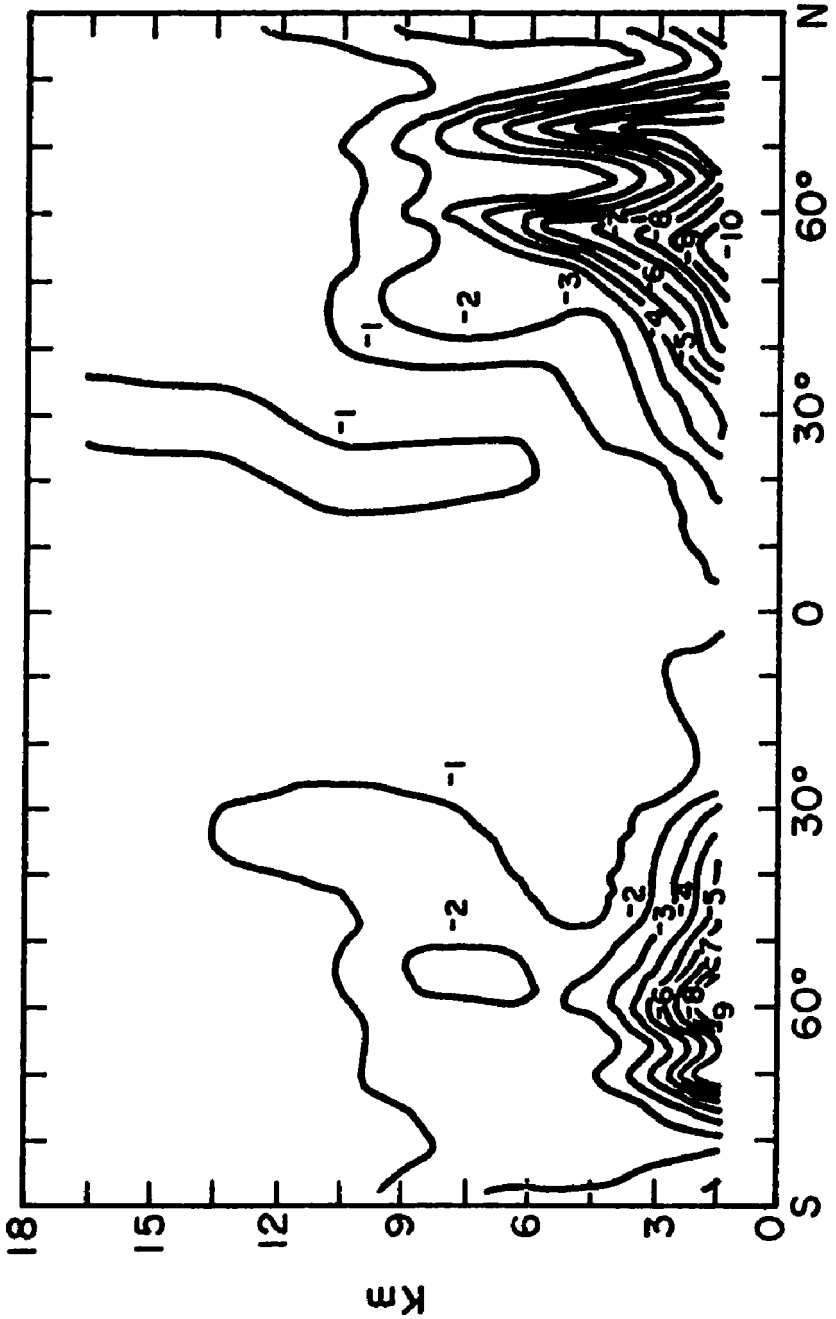


Fig. 15. Latitude-height distribution of 30-day (day 71-100) mean of zonally averaged $D(K_2)$. Unit: 10^{-3} erg cm^{-3} sec^{-1}.

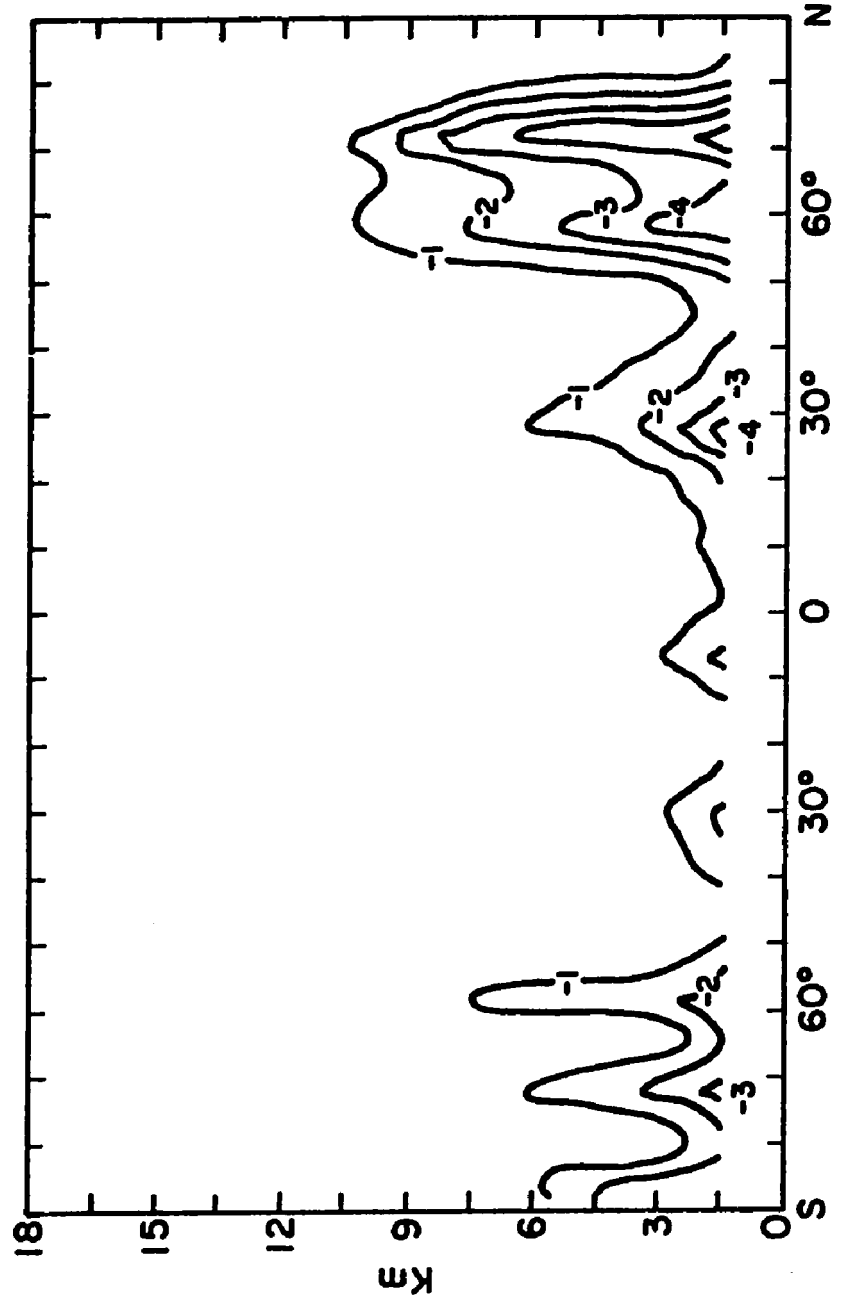


Fig. 16. Latitude-height distribution of 30-day (day 71-100) mean of zonally averaged $D(K_3)$. Unit: 10^{-4} erg cm^{-3} sec^{-1}.

Chapter IV

The Observational Study

The computations of energy quantities based upon the data produced by the GCM yield energy properties that behave as the model dictates. Therefore, a model may not reproduce all aspects of energy processes in the real atmosphere. For this reason it is desirable to calculate the energy parameters by using real data which correspond to the actual events in the atmosphere.

Using wind data at our disposal, the first and second terms of $C(K_3,K_2)$ in (2.27) can be evaluated. As is well known, it is difficult to give a proper estimate of the horizontal divergence in the atmosphere by the direct method from the observational wind. This difficulty might make the precise evaluation of the second term of (2.27) inaccurate. However a computation of this term is done by employing the direct calculation of divergence from the available wind field to give an estimate of its magnitude.

4.1 Data

The observational data used in this chapter are provided by William R. Burrows from his study of the kinetic energy of the Northern Hemisphere in the spectral domain for the summertime. The data consists of the

0000 GMT and 1200 GMT height and wind fields for the period of August 1 to 15, 1970. The height field which is continuous from the North Pole to the Equator is available through the U.S. Navy Fleet Numerical Weather Center (FNWC). The wind data come from the National Meteorological Center (NMC) analysis for an operational six-layer primitive equation forecast model (Shuman and Havermale, 1968) on an octagonal grid which covers the region from the North Pole to about 20°N; and from an operational tropical forecast model on a Mercator grid extending from about 48°S to 48°N (Bedient et al, 1967). To obtain a horizontally continuous wind for the Northern Hemisphere, Burrows (1974) employs a 16-point Bessel interpolation scheme to arrange the wind data in a 3° latitude-longitude grid system and to merge the wind data from these two sources in the ring between 27° to 33°N by a linear interpolation.

The data are for the levels: surface, 850 mb, 700 mb, 500 mb, 300 mb, 250 mb, 200 mb, and 100 mb. It should be noticed that the wind data at the surface of the whole Northern Hemisphere, and at 850 mb and 100 mb over the tropical region are supplemented by climatological statistics.

4.2 The Calculation of Energy and Energy Conversion

The first step of evaluating the energy quantities is to divide the horizontal wind vector into its divergent and nondivergent parts. The procedure is to calculate the vorticity from the horizontal wind at each grid point, and solve the Poisson equation,

$$\nabla^2\psi = \zeta \tag{4.1}$$

to obtain the stream function by the spectral method. The stream function and vorticity can be expressed in terms of spherical harmonics,

$$\psi(\theta,\lambda,t) = \sum_{m,n} \psi_n^m Y_n^m(\theta,\lambda) \tag{4.2}$$

$$\zeta(\theta,\lambda,t) = \sum_{m,n} \zeta_n^m Y_n^m(\theta,\lambda) \tag{4.3}$$

where n is the set of all non-negative integers, while the $Y_n^m(\theta,\lambda)$ are non-zero for $-n\leq m\leq n$, wherein m takes on integral values. By definition,

$$Y_n^m = P_n^m(\mu)e^{im} \qquad i\equiv\sqrt{-1}$$

where the normalized associated Legendre function,

$P_n^m(\mu)$, are given by Rodrigues' formula,

$$P_n^m(\mu) = \frac{1}{2^n n!}\left((2n+1)\frac{(n-m)!}{(n+m)!}\right)^{1/2}(1-\mu)^{m/2}\frac{d^{n+m}}{d\mu^{n+m}}(\mu^2-1)^n$$

In the above formulas $\mu = \cos\theta$, θ is co-latitude. As defined, the Y_n^m satisfy the following orthogonality condition;

$$\int_0^{2\pi}\int_0^{\pi} Y_n^m(y_n,^{m'})^* \sin\theta d\theta d\lambda = 4\pi\delta m,m'\delta n,n' \qquad (4.4)$$

where the star denotes complex conjugation.

Substituting (4.2), (4.3) in (4.1), and applying (4.4) (the orthogonality condition of Y_n^m), we find,

$$\psi_n^m = -\frac{a^2}{n(n+1)}\zeta_n^m \qquad (4.5)$$

where a is the earth's radius. Notice that ζ_n^m can be obtained from the vorticity field through the relation,

$$\zeta_n^m = \frac{1}{4\pi}\int_0^{2\pi}\int_0^{\pi}\zeta(Y_n^m)^* a^2 d\mu d\lambda$$

The nondivergent velocity can be calculated from the streamfunction

$$u_2 = \frac{1}{a}\frac{\partial \psi}{\partial \theta}$$

$$v_2 = \frac{1}{a \sin\theta}\frac{\partial \psi}{\partial \lambda} \qquad (4.6)$$

Substitute (4.2) in (4.6), then substitute (4.5) in the resulting equations,

$$u_2 = a\sqrt{1-\mu^2} \sum_{n,m} \frac{\zeta_n^m}{n(n+1)} \frac{dP_n^m}{d\mu} e^{im\lambda} \qquad (4.7)$$

$$v_2 = \frac{a}{\sqrt{1-\mu^2}} \sum_{n,m} \frac{im\zeta_n^m}{n(n+1)} P_n^m e^{im\lambda} \qquad (4.8)$$

The triangular (expansion basis forms a triangle in m, n space) truncation

$$0 \leq n \leq 25$$

$$-n \leq m \leq n$$

is applied for the practical computation. The selection of the order of truncation is based upon the resolution of the grid.

As indicated earlier, the available data fields cover only the Northern Hemisphere. It is therefore necessary to assume symmetry or antisymmetry for the data fields about the equator. Antisymmetry is assumed for

the vorticity from the observation of its distribution such that only odd (parity of n-m) Legendre functions are used in the expansion of (4.2). This implies that the stream function is antisymmetric, and alternately, u_2 symmetric and v_2 antisymmetric about the equator.

The divergent wind is obtained by substraction of the nondivergent wind from the total wind, rather than from the evaluation of the gradient of velocity potential. The reasons for this are; the NMC wind analysis has smoothed the wind field in such a way that the horizontal divergence may be reduced, and the divergent wind whose magnitude is an order less than the nondivergent wind is sensitive to finite difference error. In other words, the method of obtaining the divergent wind by solving the Poisson equation for the velocity potential may not be proper as far as the NMC wind data are concerned. In fact, the divergent wind generated here may be slightly overestimated. However, this overestimate might compensate the reduction in magnitude of the divergent wind due to NMC wind analysis.

We next concern ourselves with the numerical integration of various physical properties. The energy parameter per unit area is defined as follows:

$$\Lambda = \frac{1}{gs} \int_o^{p_o} \int_o^{\pi/2} \int_o^{2\pi} A.a^2 \cos\phi d\lambda d\phi dp \qquad (4.9)$$

where A is an arbitrary physical quantity per unit mass and s the area of the Northern Hemisphere. The data are available at the isobaric surfaces shown in Figure 17.

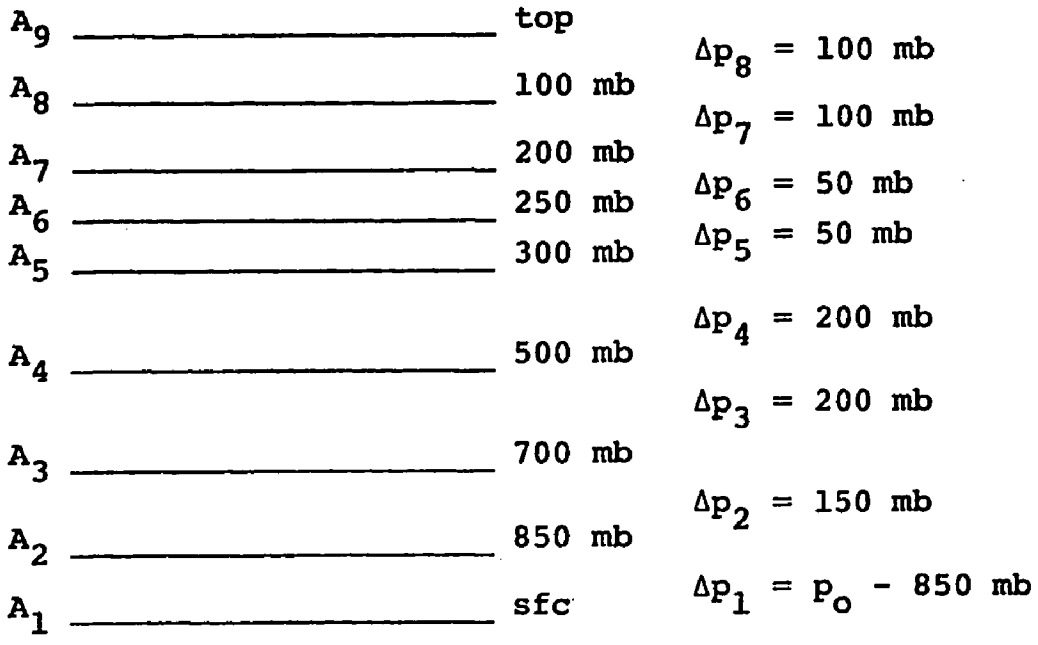


Fig. 17: The vertical grid used in calculations. A is a physical quantity per unit mass at a given level. p_o is the surface pressure.

However, due to the limited vertical resolution it is necessary to make a numerical integration with respect to pressure. We apply the trapezoidal rule for the vertical integration of (4.9). The contribution from any arbitrary level is

$$\Lambda_i = \frac{1}{\pi g} \int_o^{\pi/2} \int_o^{2\pi} A_i \frac{(\Delta p_{i-1} + \Delta p_i)}{2} \cos\phi \, d\lambda \, d\phi \qquad (4.10)$$

It should be noticed that the surface pressure, p_o, is a function of location such that Δp_1 may be changed from place to place. For this reason, we let $(\Delta p_{i-1} + \Delta p_i)/2$ remain inside the integral. Here $\Delta p_{i-1} = 0$ when $i-1 = 0$ and $\Delta p_i = 0$ when $i = 9$. In addition, if A is not available from the surface or at the top of the atmosphere, we simply assume that $A_1 = A_2$ or $A_9 = A_8$. From these considerations, we find

$$\Lambda = \sum_{i=1}^{9} \Lambda_i \tag{4.11}$$

4.3 Kinetic Energies of Divergent Flow and Nondivergent Flow

Values of K, K_2 and K_3 averaged over the period of August 1 to 15, 1970 are shown in Table 9.

Table 10: Mean value of the kinetic energy quantities, K, K_2, and K_3 over the period of August 1 to 15, 1970. Unit: 10^5 joule m^{-2} (10^8ergs cm^{-2})

K	K_2	K_3	$K_2/(K_2+K_3)$	$K_3/(K_2+K_3)$
7.39	6.39	0.71	90%	10%

It is of interest to compare the kinetic energy, K, of our calculation and those of previous studies. The

value of K for August 1963 obtained by Wiin-Nielsen (1967) is 9.11×10^5 joule m^{-2} which is somewhat higher than ours. The reason that Wiin-Nielsen obtained a higher value of K may be that the data which he used cover only the area north of 20°N in such a way that he does not have a weighting factor to account for the contribution from the tropics to reduce his value of K. Recently, Peixoto and Oort (1974) used a collection of 5 years of daily upper air data covering the area of the globe north of 10°S from the so-called MIT general circulation library and obtained a slightly lower value for K. The mean value of August obtained by them is $K = 7.37 \times 10^5$ joule m^{-2} to which our value of K is very close. This comparison shows that the particular period we studied is meteorologically typical for the month of August. Table 9 shows that a discrepancy exists between K and the sum of K_2 and K_3. According to (2.3) and (2.8) this discrepancy may be caused by the nonvanishing of the integral of $\vec{V}_2 \cdot \vec{V}_3$ over the Northern Hemisphere. Since (2.8) shows that $\vec{V}_2 \cdot \vec{V}_3$ integrates to zero over a closed domain, it is obvious that the requirement of a closed domain in (2.8) cannot be achieved by the integration over a hemisphere. In fact, the discrepancy between K and $K_2 + K_3$ which is small, as we expect, is not the major concern in this study, and we will focus our attention on K_2 and K_3.

K_2 and K_3 are 90% and 10% of $K_2 + K_3$ respectively. K_3 is an order smaller than K_2. However, as far as the separation of the horizontal wind vector into its divergent and nondivergent parts is concerned, it should be noticed that we may underestimate K_2 and overestimate K_3. This is because we truncate the nondivergent wind when we apply the spectral method to solve (4.1). The unresolved part of the nondivergent wind, of course, goes into the divergent winds obtained by substraction of the nondivergent wind from the total wind.

The contributions to K_2 and K_3 from different pressure levels and latitudes are displayed in Figures 18 and 19. As for the height distribution, K_2 and K_3 have maxima between 300 mb and 200 mb in the vicinity of the jet stream. The tropical easterlies give a relatively small peak of K_2 in the latitudinal distribution in addition to the peak of this quantity due to the strong westerlies in the middle latitudes. K_3 shows relatively high values in the middle latitudes and equator.

To obtain further insight into the contributions to K_2 and K_3 from the different parts of the atmosphere, the latitude-height distribution of these two quantities are presented in Figures 20 and 21. It should be noticed that since we intend to express K_2 and K_3 as a function of latitude and pressure, it is convenient to express the

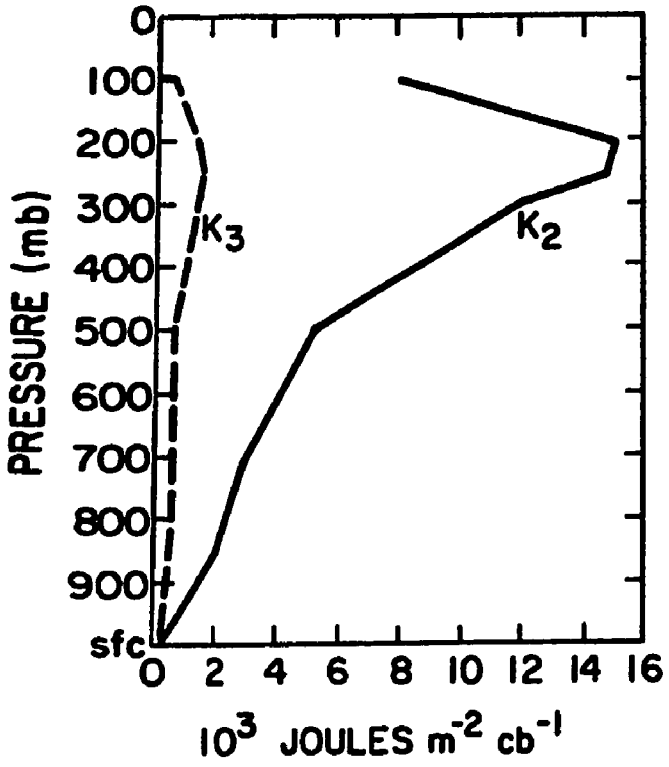


Fig. 18: Vertical profile of zonally averaged K_2 and K_3 as a function of pressure. Unit: 10^3 joule m^{-2} cb^{-1}.

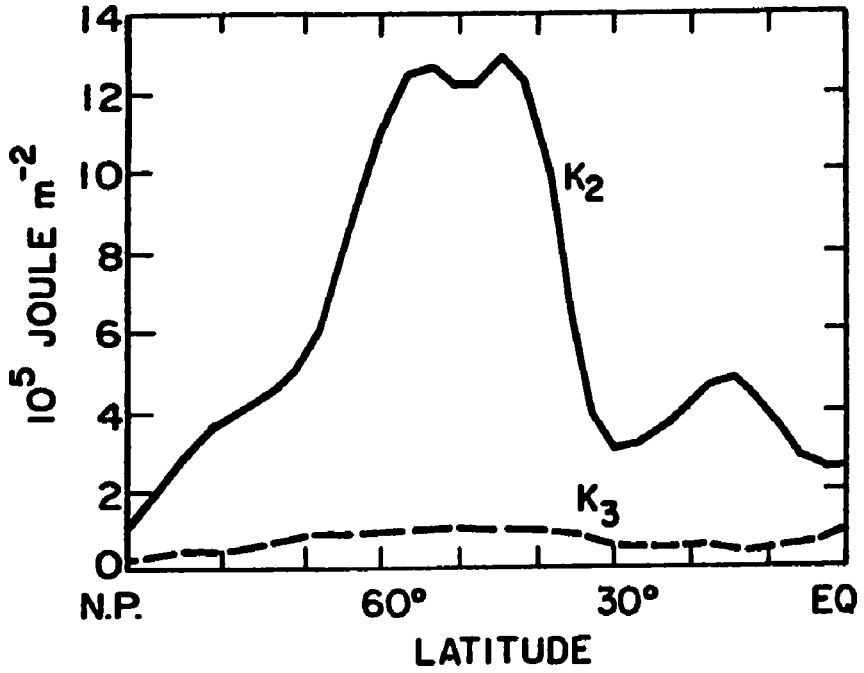


Fig. 19: Contributions to K_2 and K_3 from different latitude bande. Unit: 10^5 joule m^{-2} (10^8ergs cm^{-2}).

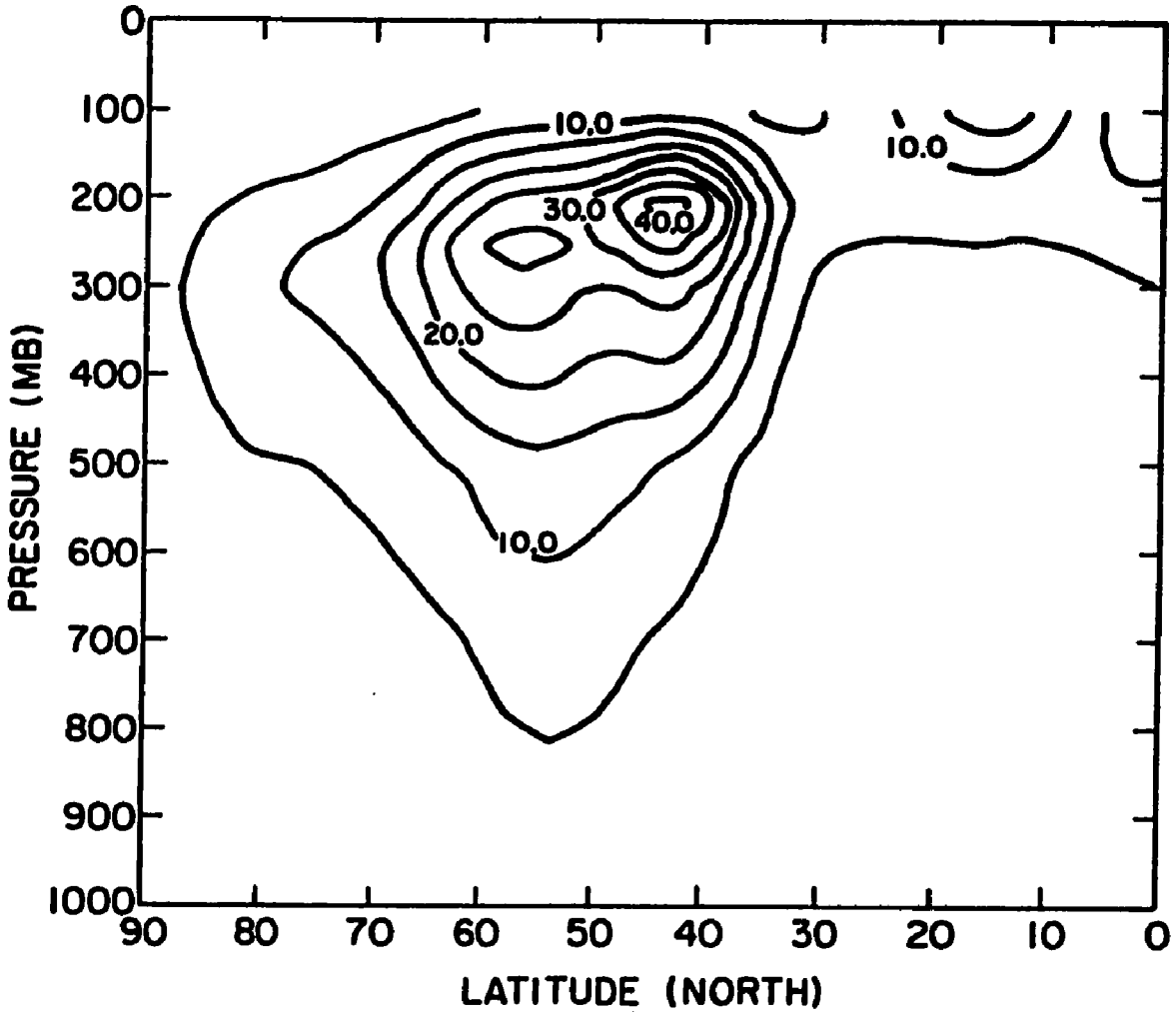


Fig. 20: Latitude-height distribution of zonally averaged K_2. Unit: 10^3 joules m^{-2} cb^{-1}.

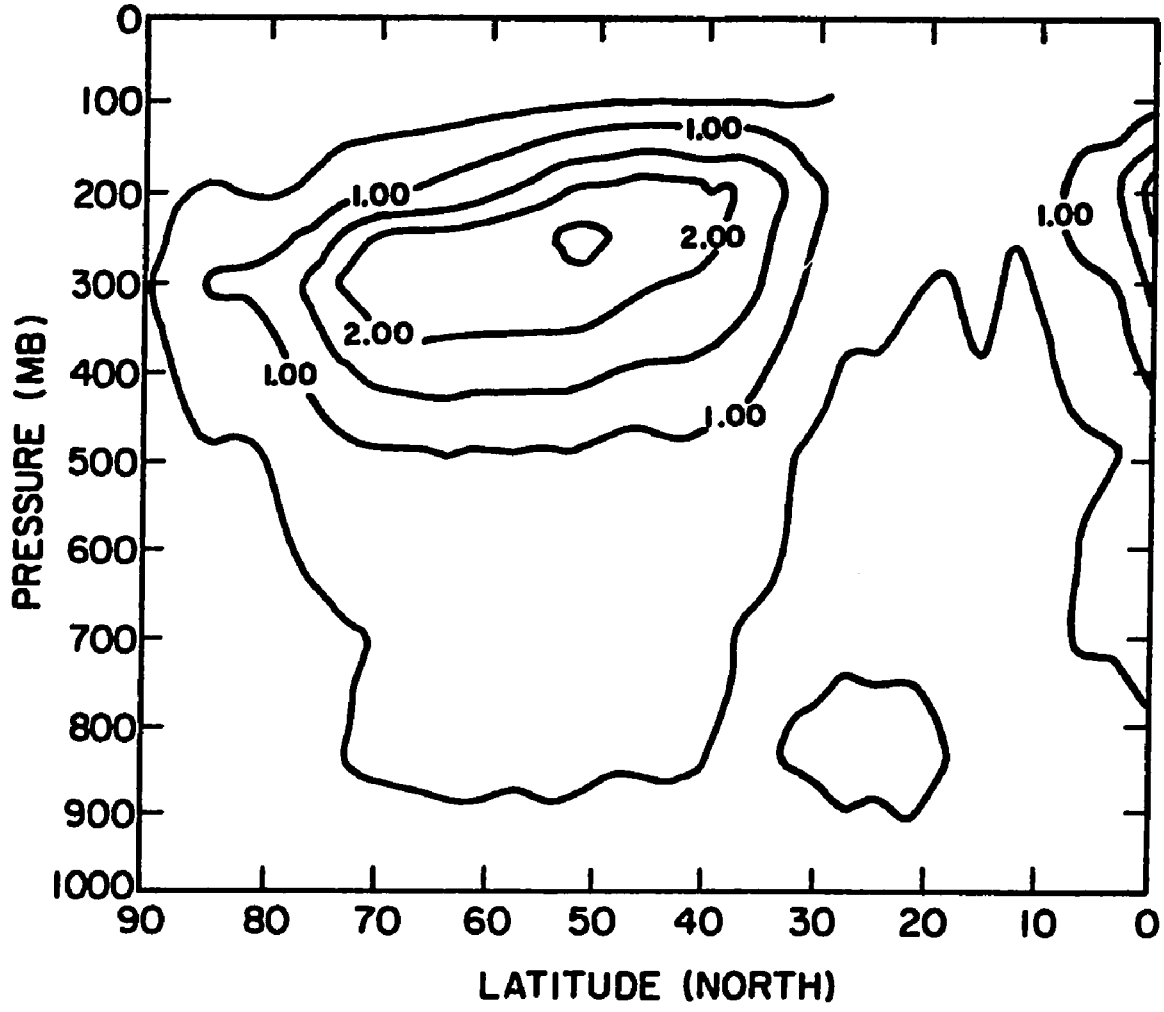


Fig. 21: Latitude-height distribution of zonally averaged K_3. Unit: 10^3 joules m^{-2} cb^{-1}.

amounts in the unit: joule m^{-2} cb^{-1}. To relate this unit to the conventional one for energy (energy per unit mass which has the dimension of the square of velocity) simply multiply the numbers showing in Figures 20 and 21, and also Figure 18 by the acceleration of gravity or about 10m sec^{-2} such that the energy unit becomes m^2 sec^{-2}.

The distribution of K_2 which is very similar to K (not shown) shows a maximum in the vicinity of the jet stream. The distribution of K_3 is surprising because it has its maximum in the vicinity of that of K_2. The weak cyclonic and anticyclonic activities in the summertime do not seem to give significant contributions to the divergent wind field. Therefore, no appreciable K_3 occurs in the lower layer of the atmosphere. However, it has been shown that the inertial-gravity wave motion may give contributions to the kinetic energy divergent wind field (Blumen, 1972; Veronis, 1956). From this consideration, the high value of K_3 appearing in the vicinity of the maximum westerlies indicates that the major contribution to the generation of K_3 may come from the geostrophic adjustment of the jet stream meandering over the particular period which we investigated. The appearance of high values of K_3 in the upper tropics does not seem to be caused by the upper branch of the Hadley cell.

4.4 Energy Conversions

$C(K_3,K_2)$, the energy conversion between K_3 and K_2, consists of three terms in (2.27). A theoretical discussion has been made in section 2.2 to distinguish each term in (2.27) for different numerical models and mechanisms. For the convenience of discussing the computational results, it is illustrative to represent each term in (2.27) by different symbols,

$$C(K_3,K_2)A1 = -\frac{1}{g}\int_o^{p_o}\int_s f\vec{V}_2\cdot(\vec{k}X\vec{V}_3)dsdp$$

$$C(K_3,K_2)A2 = -\frac{1}{g}\int_o^{p_o}\int_s \zeta_2\vec{V}_2\cdot(\vec{k}X\vec{V}_3)dsdp$$

$$C(K_3,K_2)B = -\frac{1}{g}\int_o^{p_o}\int_s k_2\nabla\cdot\vec{V}_3 dsdp$$

$$C(K_3,K_2)C = -\frac{1}{g}\int_o^{p_o}\int \omega_3\vec{V}_2\cdot\frac{\partial\vec{V}_3}{\partial p}\,dsdp$$

Here we reserve $C(K_3,K_2)A$ for the first term of (2.27) and $C'(K_3,K_2)$ for the sum of $C(K_3,K_2)A + C(K_3,K_2)B$. The purpose of splitting $C(K_3,K_2)A$ into $C(K_3,K_2)A1$ and $C(K_3,K_2)A2$ is to compare the importance of the role played by the Coriolis effect and the relative vorticity.

Table 11: Mean values and standard deviation of $C(K_3,K_2)A1$, $C(K_3,K_2)A2$, $C(K_3,K_2)B$ and $C(P,K_3)$ for the period of August 1 to 15, 1970. Unit: watts m^{-2} (10^3ergs cm^{-2} sec^{-1}).

	$C(K_3,K_2)A1$	$C(K_3,K_2)A2$	$C(K_3,K_2)B$	$C(P,K_3)$
Mean Values	0.588	-0.030	-0.032	0.620
Standard Deviation	0.945	0.1091	0.116	1.018

$C(K_3,K_2)A$ is 0.558 watts $m^{-2}sec^{-1}$ by summing up $C(K_3,K_2)A1$ and $C(K_3,K_2)A2$ shown in Table 10. The comparison of $C(K_3,K_2)A2$ and $C(K_3,K_2)A$ gives a ratio between them of 5%. In other words, the major contribution to $C(K_3,K_2)A$ comes from $C(K_3,K_2)A1$.

$C(K_3,K_2)B$ and $C(K_3,K_2)C$, which have been discussed in section 2.2, originate from the vertical advection of momentum, or the vertical advection and twisting of vorticity. As far as the scale analysis is concerned, $C(K_3,K_2)B$ and $C(K_3,K_2)C$ are an order less than $C(K_3,K_2)A$. Even though no numerical evaluation of $C(K_3,K_2)C$ can be done here, the smallness of $C(K_3,K_2)B$ is confirmed by the numerical result of a computation shown in Table 10 where $C(K_3,K_2)B/C(K_3,K_2)A = 6\%$.

If the magnitude of $C(K_3,K_2)C$ is assumed to be as small as $C(K_3,K_2)B$, $C(K_3,K_2)$ should possess a magnitude in the range of 0.5 to 0.6 watt m^{-2} for the period we investigated in this study.

We have shown in section 2.2 that $C(K_3,K_2)A1$ is the only channel in the quasi-geostrophic model through which conversion between K_3 and K_2 can be carried out when f is assumed constant. The comparison between $C(K_3,K_2)$ in the foregoing and $C(K_3,K_2)A1$ shown in Table 10 verifies that the quasi-geostrophic theory explains most of the conversion between K_3 and K_2. The more sophisticated model, e.g. balance-model or primitive equation model, introduces only a small correction by the appearance of $C(K_3,K_2)A2$, $C(K_3,K_2)B$ and $C(K_3,K_2)C$ in regard to energy conversion.

As far as numerical weather prediction is concerned, the study of the energetics of the atmosphere is a good way to evaluate the physics of the model. A small loss in the energy conversion may result in a large error in a long range forecast because of the growth of error. In this regard, the quasi-geostrophic model may not be able to give good forecasts. Therefore, a more elaborate balanced model, or a primitive equation model, is called for.

$C'(K_3,K_2)$, the sum of $C(K_3,K_2)A$ and $C(K_3,K_2)B$ is 0.528 watt m^{-2} which is slightly smaller than

$C(P,K_3) = 0.62$ watt m^{-2}. Recall that an assumption has been made in the vertical integration of (4.1); if information for a given quantity is not available at the surface, we assume that the value of this quantity at the surface is equal to that at 850 mb. This assumption which was applied to the integration of $C(P,K_3)$ might give an overestimate on $C(P,K_3)$. In addition, no numerical evaluations of $D(K_3)$ and $C(K_3,K_2)C$ are available. Under these circumstances, we cannot make a definite conclusion for the energy cycle as shown in Figure 1. But from our numerical results, it is quite obvious that the direction of energy conversion is as we expected from the theoretical consideration in Chapter 2, i.e., energy goes from the potential energy to the kinetic energy of the divergent wind, and, then from the latter to the kinetic energy of the nondivergent wind.

A check of the reasonableness of our computation of energy conversions may be obtained by a comparison with the values obtained by observational studies of the energy conversion from available potential energy to kinetic energy. The latter energy conversion is usually denoted by C(A,K). Several estimates have been made of

this energy conversion by different investigators. Oort (1964) gave 2.3 watts m^{-2} for the annual mean of C(A,K), and Wiin-Nielsen (1968) 2.5 watts m^{-2}. Apparently, these estimates are higher than our numerical result of $C(P,K_3)$ or $C'(K_3,K_2)$. It should be noted that C(A,K) is smaller during the summertime (Wiin-Nielsen, 1967; Krueger, et al, 1965). Recently, Oort and Peixoto (1974) used 5 years of daily data from the MIT general circulation library to make an extensive, calculation which shows C(A,K) = 1.0 watt m^{-2} in July. In fact, our calculations of $C(P,K_3)$ and $C'(K_3,K_2)$ are very close to Oort and Peixoto's.

In order to examine the extent to which K_3 is catalytic we may compare the residence times of K_3 and K_2. Since $D(K_3)$ and $C(K_3,K_2)C$ are supposedly small, it may be reasonable to assume that $C(K_3,K_2)$ is about 0.6 watts m^{-2} over the period concerned in this study. This gives us a residence time of K_3 and K_2 of 1.4 days and 12.3 days respectively. Recall that K_3 is somewhat overestimated in our calculation. This would imply that the residence time of K_3 is less than what appears here. Nevertheless, the residence time of K_3 is an order less than that of K_2. In conclusion, the short residence time of K_3 indicates that K_3 transforms to K_2, almost immediately.

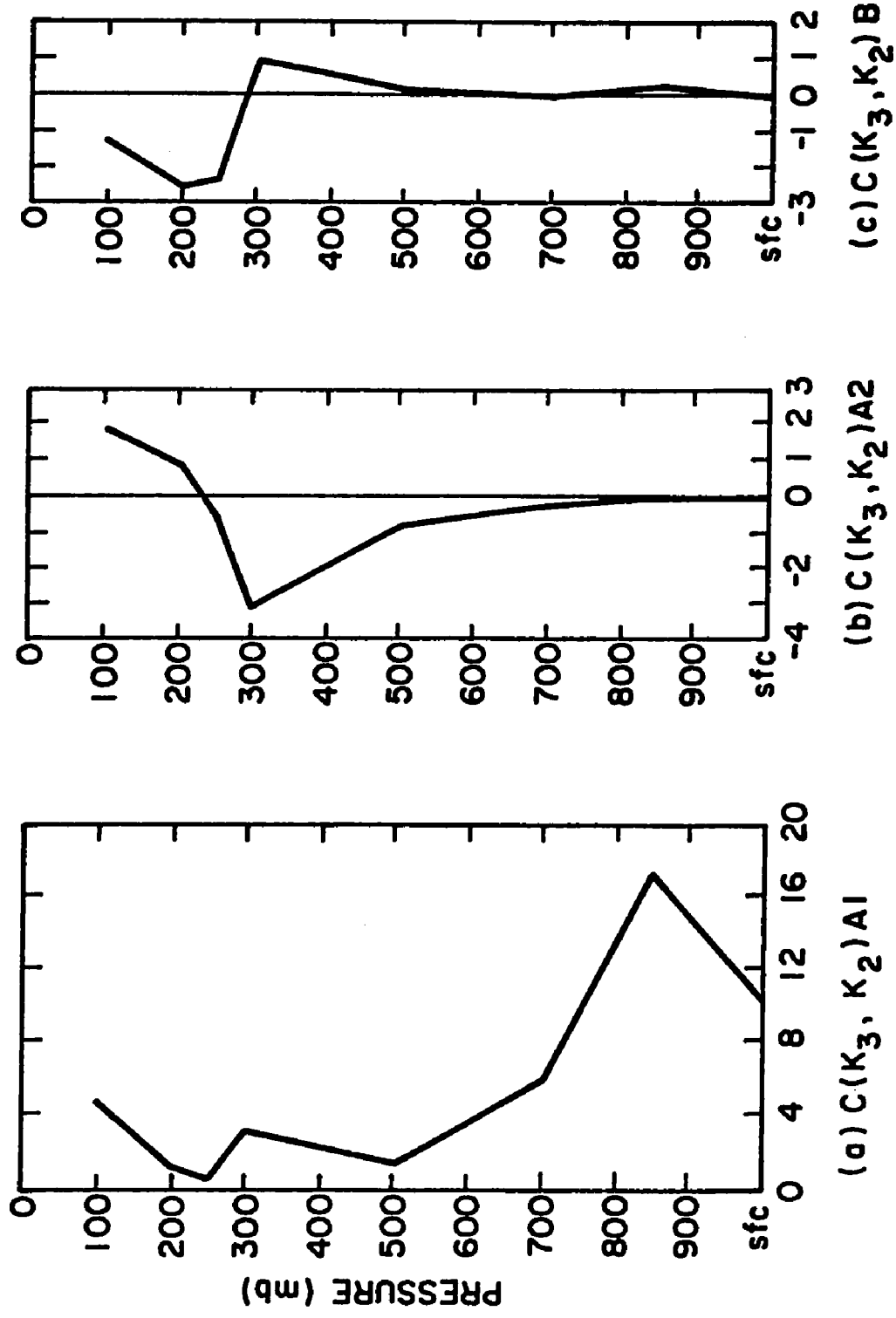


Fig. 22: Vertical profile of (a) $C(K_3,K_2)A1_4$ (b) $C(K_3,K_2)A2$, (c) $C(K_3,K_2)B$ as a function of pressure. Unit: 10^{-3} joule m^{-2} cb^{-1} sec^{-1}.

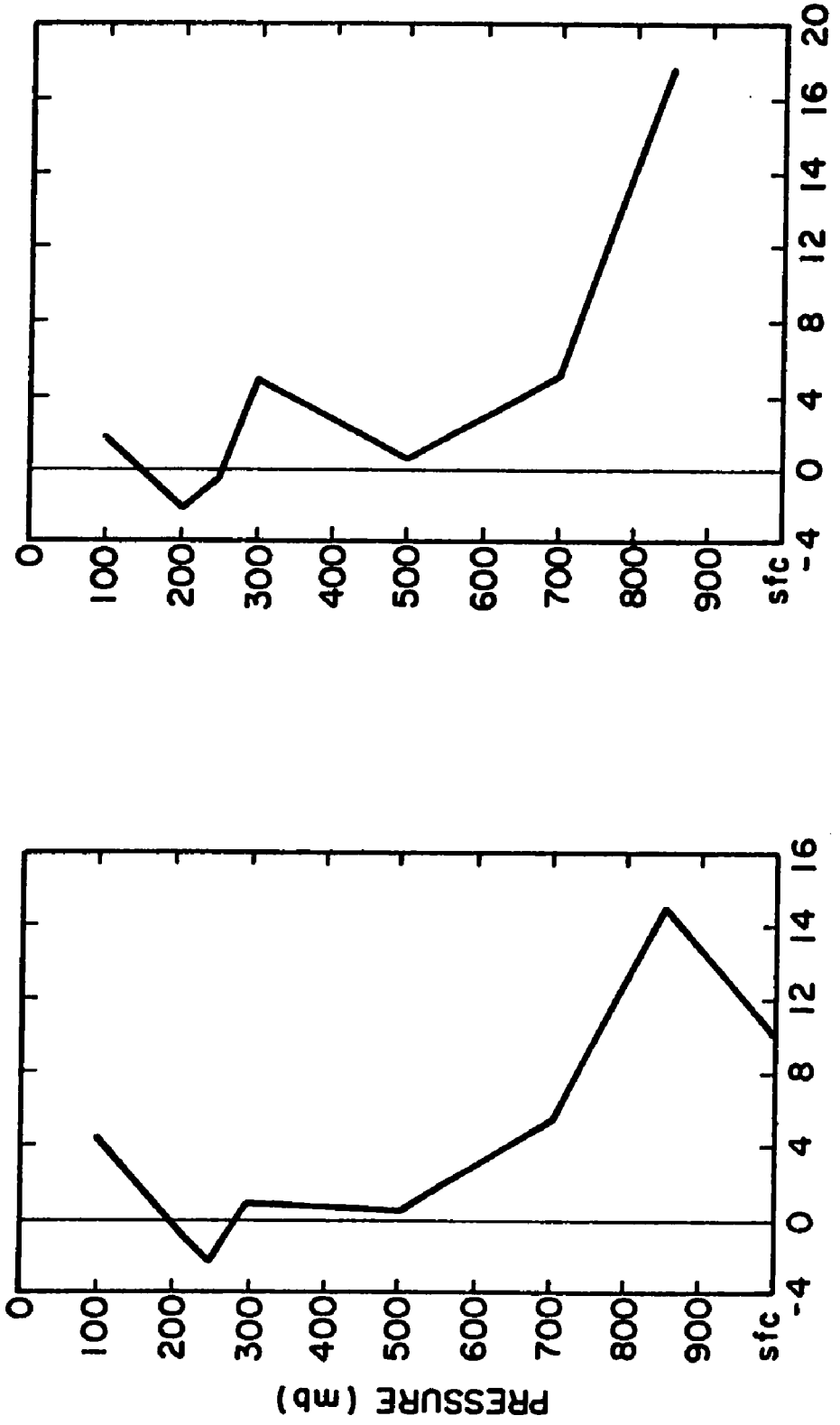


Fig. 22: Vertical profile of (d) $C'(K_3,K_2)$ and (e) $C(P,K_3)$ as a function of pressure. Unit: 10^{-3} joule m^{-2} cb^{-1} sec^{-1}.

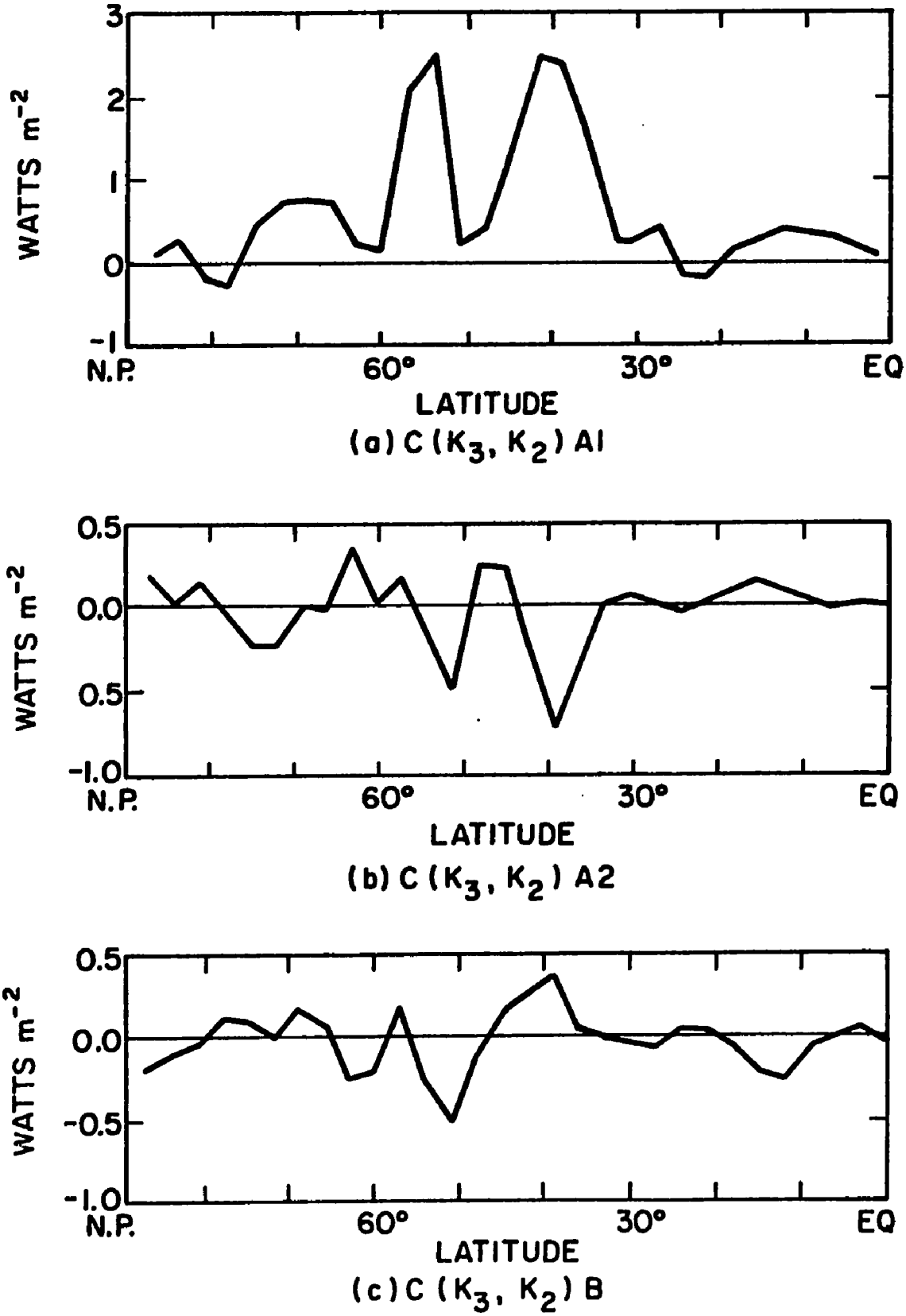
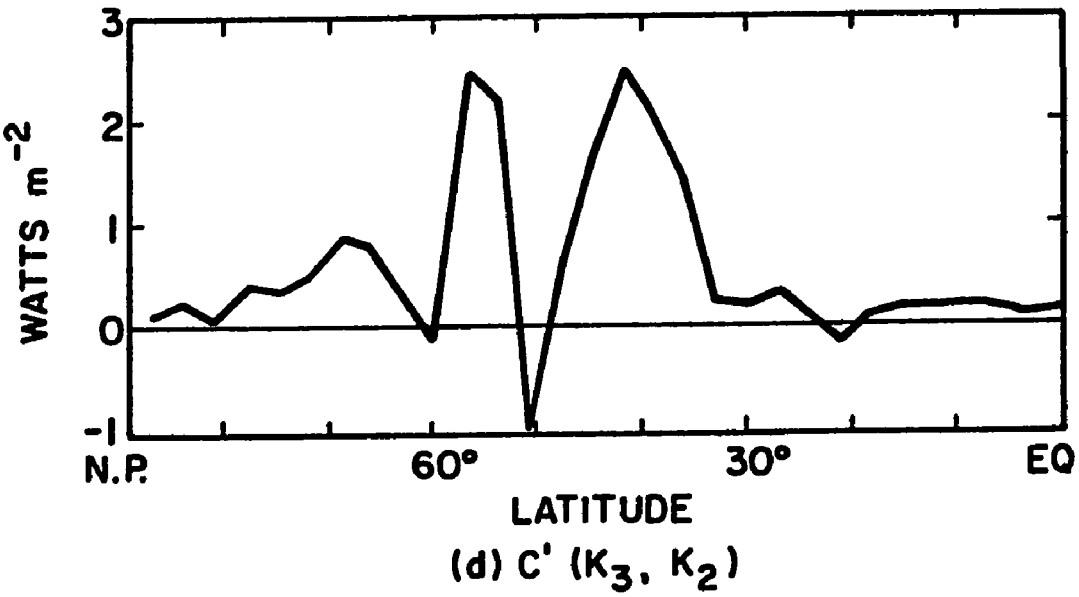


Fig. 23: Contributions to (a) $C(K_3,K_2)A1$, (b) $C(K_3,K_2)A2$ and (c) $C(K_3,K_2)B$ from different latitude bands. Unit: watts m^{-2} (10^3ergs cm^{-2} sec^{-1}).



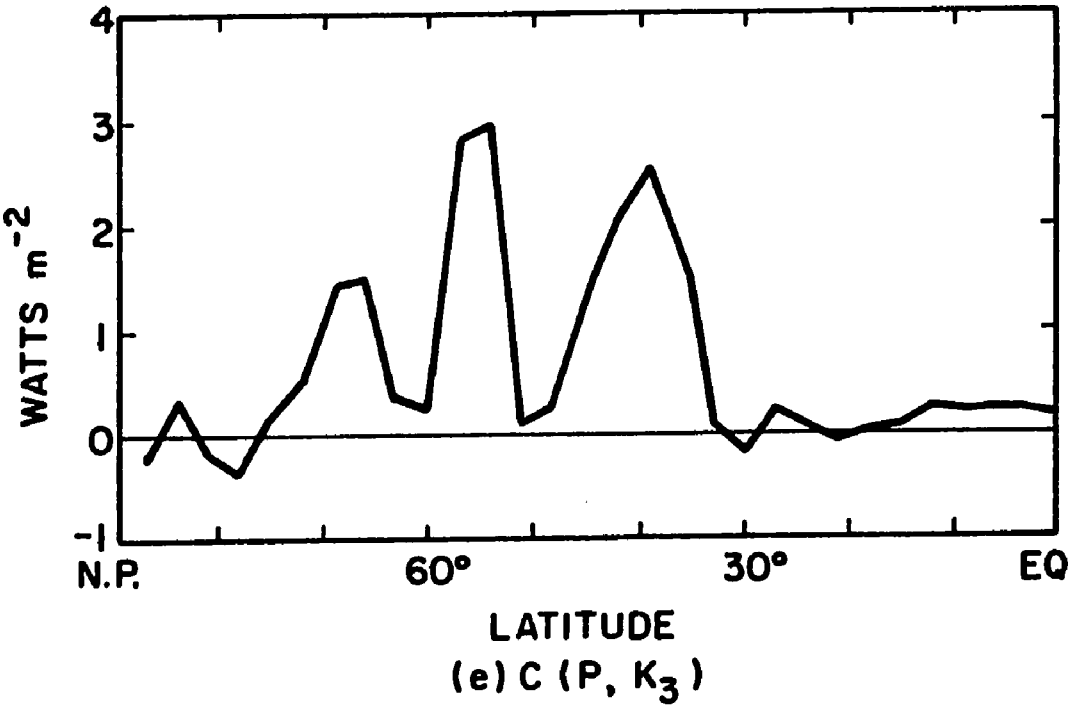


Fig. 23: Contributions to (d) $C'(K_3,K_2)$ and (e) $C(P,K_3)$ from different latitude bands. Unit: watts m^{-2} (10^3ergs cm^{-2} sec^{-1}).

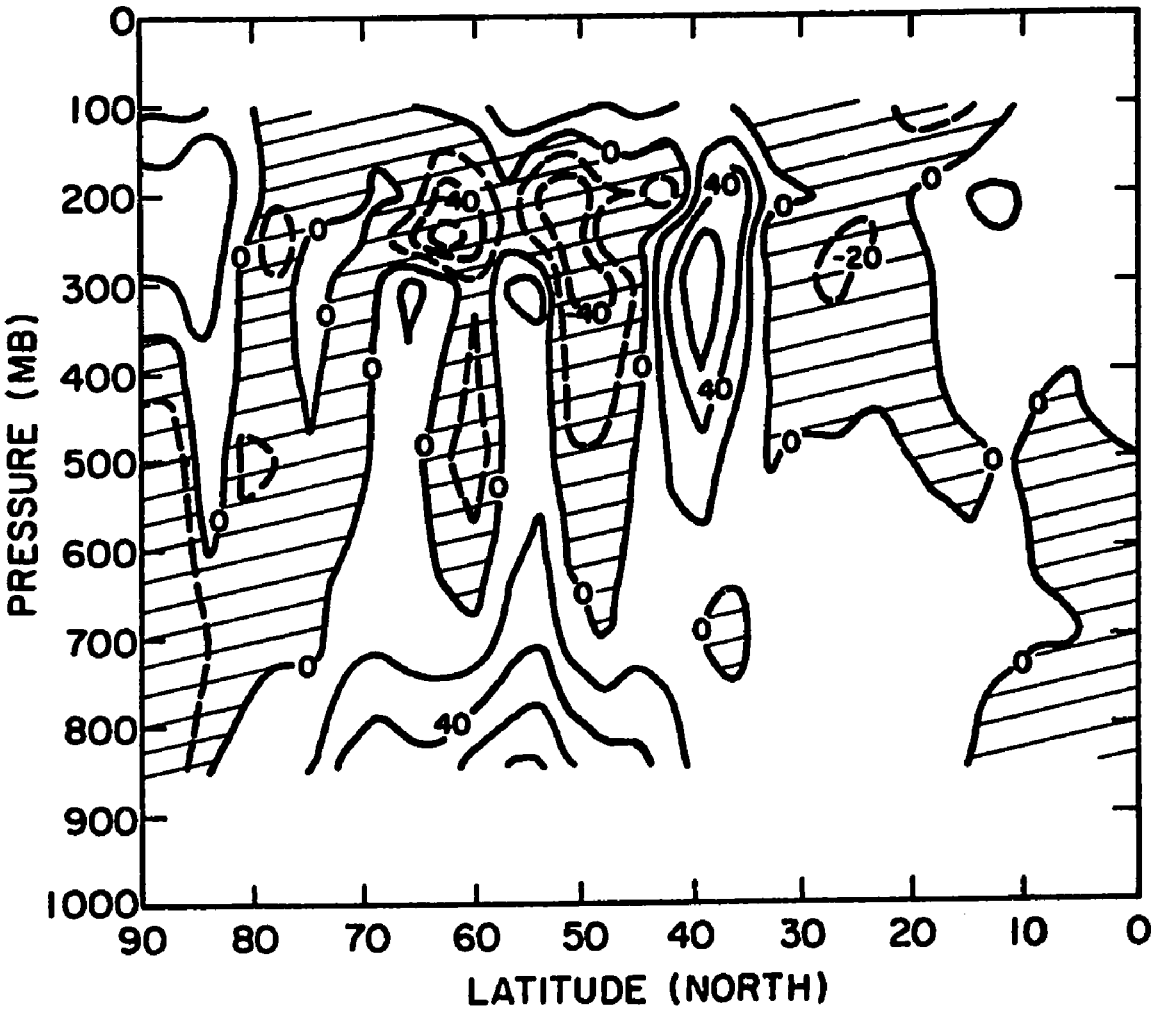


Fig. 24: Latitude-height distribution of zonally averaged $C(P,K_3)$. Unit: 10^{-3} watt m^{-2} cb^{-1}.

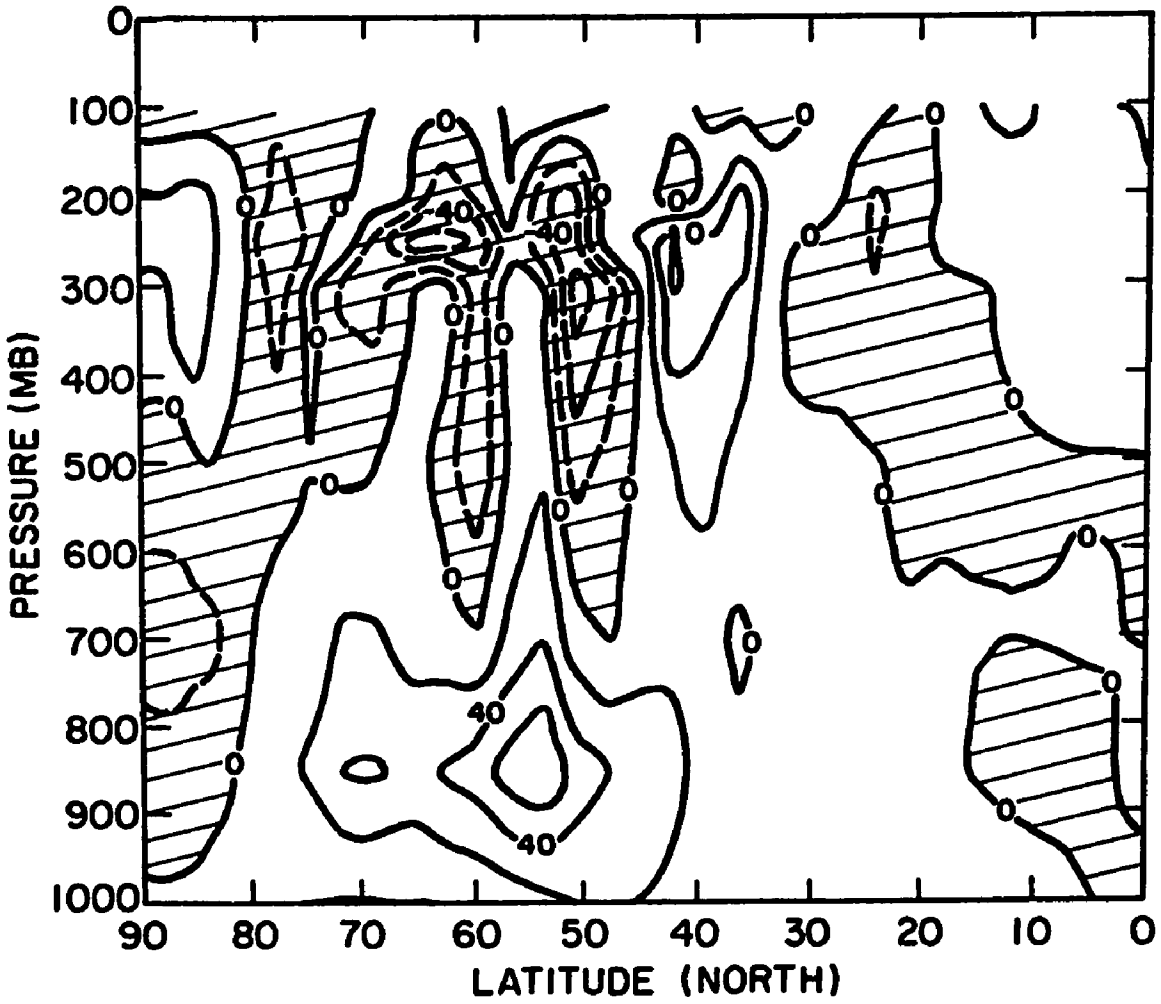


Fig. 25: Latitude-height distribution of zonally averaged $C'(K_3,K_2)$. Unit: 10^{-3} watt m^{-2} cb^{-1}.

The various energy conversions as functions of pressure are shown in Figure 22. The major contribution to $C(K_3,K_2)A1$, Figure 22a, exists in the lower layer of the atmosphere where the ageostrophic motion is significant such that the Coriolis effect makes the conversion from K_3 to K_2 more possible. The vertical profile of $C(K_3,K_2)A2$, Figure 22b, is opposite to that of $C(K_3,K_2)A1$. The significant part of $C(K_3,K_2)A2$ is in the upper atmosphere, but it has negative values below 250 mb. Comparing the integrands of these two quantities and their vertical profiles, we may easily find that the vorticity field is prominent in the upper atmosphere. $C(K_3,K_2)B$, Figure 22c, is also significant in the upper layer of the atmosphere where K_2 is large.

Figure 22d is the vertical profile of the sum of Figures 22a to 22c. On the whole, the conversion from K_3 to K_2 occurs mainly in the lower atmosphere. A negative part of $C'(K_3,K_2)$ appears in the upper atmosphere where K_3 has high values. This negative part of $C'(K_3,K_2)$ might be viewed as an energy conversion from K_2 to K_3, if the contribution from $C(K_3,K_2)C$ cannot erase this negative value. $C'(K_3,K_2)$ is small between 300 mb and 500 mb, but we are not able to say that the barotropic assumption is a good approximation there because $C(K_3,K_2)C$ is unknown,

and the fluctuation of $C'(K_3,K_2)$ is large in this layer as will be made clear later.

The vertical profile of $C(P,K_3)$, Figure 22e, is similar to $C'(K_3,K_2)$ except $C(P,K_3)$ has a second maximum at 300 mb. It is interesting to notice that the vertical distribution of $C(P,K_3)$ is very similar to Kung's (1967) distribution for his so-called generation term, $\overline{-V\cdot\nabla\phi}$, where the bar means an average over North America. The major contribution to $C(P,K_3)$ also comes from the lower layer of the atmosphere.

The latitudinal distributions of various energy, conversions are shown in Figure 23. As discussed in section 2.1 $C(P,K_3)$ is performed by the baroclinic process which mainly exists in the middle latitudes. This may explain why $C(P,K_3)$ is dominate over the middle latitudes shown in Figure 23e. Furthermore, the short residence time of K_3, and possibly small $D(K_3)$ make $C'(K_3,K_2)$ follow $C(P,K_3)$ rapidly so that $C'(K_3,K_2)$ possesses a prominant part in the middle latitudes as shown in Figure 23d. This may also explain the high similarity of the distribution of $C(P,K_3)$ and $C'(K_3,K_2)$ as shown in Figures 24 and 25. Notice that $C(K_3,K_2)C$ is assumed small here for the argument above. Two large maxima of $C'(K_3,K_2)$ and $C(P,K_3)$ appear in the vicinity of

50°N and 60°N. These are more distinctive on the height-latitude distribution of both quantities (see Figures 24 and 25) where two negative maxima exist in the vicinity of the maximum westerlies. The peaks between 50°N and 60°N, and 60°N and 80°N are mainly established by the contribution from the lower layer, while another maximum that appears in contrast in the upper layer forms the peak between 30°N and 50°N.

Chapter 5

Conclusion

5.1 Concluding Remarks

According to Helmholtz' theorem, the horizontal wind vector can be divided into its divergent and non-divergent parts. Correspondingly, the horizontal kinetic energy of the whole hydrostatic atmosphere can also be divided into the kinetic energy of divergent and non-divergent flow, i.e., K_3 and K_2. It is shown that energy converts from the total potential energy to the kinetic energy of divergent flow and then to kinetic energy of nondivergent flow. The energy reservoir of K_3 is obviously important and is the only passage through which total potential energy can be transformed into the kinetic energy of nondivergent flow.

The energy conversions between total potential energy and K_3, $C(P,K_3)$, and between K_3 and K_2, $C(K_3,K_2)$ have been derived from the primitive equations. Further analysis of the energy conversions has been made to compare the difference between balanced and unbalanced models. It is found that $C(P,K_3)$ and $C(K_3,K_2)$ are equal in energetically consistent, balanced models of the atmosphere, but may be different in models based upon the primitive equations. This suggests that a study of the

energy budget of K_3, using a primitive equations model, will show the extent to which K_3 is catalytic.

The history data generated by the NCAR GCM of a January simulation have been used to evaluate all energy parameters. The NCAR GCM is formulated in the z-coordinate system, but the small slopes of isobaric surfaces make the energy parameters in the z-coordinate system approximately equal to the corresponding quantities in the p-coordinate system.

The global mean value of K_3 is 1.2% of K_2+K_3 which is 14.7×10^8 erg cm^{-2}. The global mean of $C(P,K_3)$, $C(K_3,K_2)$, $D(K_2)$ and $D(K_3)$ are 2.85×10^3 erg cm^{-2} sec^{-1}, 1.74×10^3 erg cm^{-2} sec^{-1}, 2.52×10^3 erg cm^{-2} sec^{-1} and 0.22×10^3 erg cm^{-2} sec^{-1} respectively. Some discrepancies were shown in the energy diagram of the NCAR GCM (K & W, 1971). In view of the energy inconsistency in the GCM, we may not be able to expect the quasi-balance between $C(P,K_3)$ and $C(K_3,K_2) + D(K_3)$, and between $C(K_3,K_2)$ and $D(K_2)$. The positive values of $C(P,K_3)$ and $C(K_3,K_2)$ clearly show that energy converts from total potential energy to K_3 and then from K_3 to K_2.

$K_3/C(K_3,K_2)$ and $K_2/C(K_3,K_2)$ show that the residence times of K_3 and K_2 are 3 hours and 9.6 days respectively. Furthermore, $C(K_3,K_2)$ is mainly determined by $C(K_3,K_2)Al$ which is due to the Coriolis effect and is the only term

of the energy conversion between K_2 and K_3 in a quasi-geostrophic model. Also, the difference between $C(K_3,K_2)$ corresponding to the primitive equation models and balanced models is very small. These results assure the quasi-catalytic role of K_3.

The NMC wind data and FNWC height field of August 1 to 15 of 1970 were also used to evaluate the energies and energy conversions. $K_3/(K_2 + K_3)$ and $K_2/(K_2 + K_3)$ are 10% and 90% respectively. The spectral method is applied to find the nondivergent wind. The truncation is at (n, ℓ=25). The divergent wind is obtained by subtracting the nondivergent wind from the total wind. This procedure requires an accurate determination of the nondivergent wind.

$C(K_3,K_2)$ consists of three parts in (2.27), but the term involving vertical velocity cannot be evaluated due to the missing vertical velocity. Usually, this term is small as shown by scale analysis. However, we are able to obtain an acceptable approximation to $C(K_3,K_2)$ from the computation of the first two terms in (2.27). $C(P,K_3)$ and $C(K_3,K_2)$ are 0.62 watts m^{-2} (0.62×10^3 erg cm^{-2} sec^{-1}) and 0.526 watts m^{-2} (0.526×10^3 erg cm^{-2} sec^{-1}) respectively. $C(K_3,K_2)$ is mainly determined by $C(K_3,K_2)A1$ which is the Coriolis effect.

The computations made in this study are based upon two different data sets and two different schemes of wind separation. Regardless of the difference of approach and data sources, we obtain essentially the same features of the energetics.

Finally, it should be pointed out that the scheme of separating the horizontal wind vector into its divergent and nondivergent parts is very crucial in this study, for the determination of K_3, and small terms in $C(K_3,K_2)$ are sensitive to numerical procedures.

5.2 Suggestions for Future Study

The historical data of the NCAR GCM used in this study are output of a simulation for January. Since many studies have found that the energetics, e.g., Wiin-Nielsen (1967), Oort and Peixoto (1974), and the dynamic structure, e.g. Palmen and Newton (1971), of the atmosphere in winter are different from those in summer, it would be desirable to carry out this study for a summer month.

The data set used for the observational study covers only 15 days of the first half month of August, 1970. Even though the results are promising and consistent with what is expected from the theoretical presentation, the observational study should be extended in time to obtain more reliable and representative estimates of various

energetic parameters. We may thus increase our understanding of their seasonal and annual variation.

This study has shown that $C(P,K_3)$ and $C(K_3,K_2)$ are dominant in middle and high latitudes where the activity of baroclinic eddies exists. Saltzman (1970) reviewed observational studies of the atmospheric energetics in the wave-number domain by one-dimensional Fourier analysis. He pointed out that the energy conversion between the total potential energy and kinetic energy mainly occurs through the baroclinic eddies of the medium scale which corresponds to the most unstable waves predicted by the theory of baroclinic instability, e.g. Kuo (1952). To extend the diagnostic study of $C(P,K_3)$ and $C(K_3,K_2)$ in this report to the spectral domain will definitely promote our knowledge of the atmospheric energetics in the different spatial scales.

It is well known that the primitive equations have two types of solutions: inertial-gravity waves and slow-moving meteorologically significant waves. The introduction of improper initial conditions from observational data will cause the excitation* of inertial-gravity waves

*The excitation of these gravity waves is known as the "initialization shock".

of considerable amplitude and may spoil the forecast. Many attempts, e.g. Morel and Talagrand (1974), have been made to design a damping scheme avoiding the growth of inertial-gravity waves during the initial stage of a numerical integration of the primitive equations. The occurrence of large inertial-gravity waves may make the variation K_3 and the possible connected imbalance between $C(P,K_3)$ and $C(K_3,K_2)$ important. The investigation of the behavior of K_3, $C(P,K_3)$, and $C(K_3,K_2)$ during the initial stage of the numerical integration of the primitive equations may present a way to evaluate different initialization schemes and therefore allow one to design a more proper damping scheme to suppress the initialization shock to a tolerable level without influencing the slow-moving meteorologically significant motions.

Numerous studies investigating the cyclone development, e.g. Pettersen and Smebye (1971), Smith (1973), and others, have been attempted, but the energetics of a cyclone system is still unclear. Recently, Pearce (1974) called attention to the diagnostic study of synoptic-scale system. The variation of K_3 and the connected imbalance $C(P,K_3)$ and $C(K_3,K_2)$ may be important in the development of a cyclone system. An extension of the study to consider the energetics of a cyclone in a

limited area may yeild insight into the nature of energy conversions occurring in the synoptic-scale system.

Appendix A

The Derivation of the Potential Energy Equation

A.1 The Potential Energy Equation in the p-Coordinate System

The potential energy of the atmosphere is

$$E_P = \int_o^\infty \int_s gz\rho dzds \qquad (A.1)$$

From the hydrostatic equation $\rho dz = - dp/g$, therefore

$$E_P = \frac{1}{g} \int_o^{p_o} \int_s \Phi dpds = \frac{1}{g} \int_s (\Phi p)\Big|_o^{p_o} ds$$

$$- \frac{1}{g} \int_\infty^o \int_s pd\Phi ds = \frac{1}{g} \int_o^\infty \int_s pd\Phi ds \qquad (A.2)$$

$$= \frac{1}{g} \int_o^{p_o} \int_s RTdpds$$

when the earth's surface is not at sea level, $\frac{1}{g} \int_s \Phi p\big|_{p_o} ds$ must be retained.

The internal energy of the atmosphere is:

$$E_I = \int_o^\infty \int_s C_v T\rho dzds = \frac{1}{g} \int_o^{p_o} \int_s C_v Tdsdp \qquad (A.3)$$

(A.2) and (A.3) tell us that the potential and internal energy are proportional under the hydrostatic assumption (Haurwitz, 1941).

The combination of the potential and internal energy is known as the <u>total potential energy</u>, or simply the <u>potential energy</u> (Lorenz, 1955)

$$P = \frac{1}{g}\int_o^{p_o}\int_s (R + C_v)T\,dpds = \frac{1}{g}\int_o^{p_o}\int_s C_p T\,dpds \qquad (A.4)$$

The equation of potential energy can be obtained from (A.4)

$$\frac{dP}{dt} = \frac{1}{g}\int_o^{p_o}\int_s C_p \frac{\partial T}{\partial t}\,dpds \qquad (A.5)$$

Consider next the thermodynamic equation

$$\frac{\partial T}{\partial t} + \vec{V}\cdot\nabla T + \omega\frac{\partial T}{\partial p} - \frac{\alpha\omega}{C_p} = \frac{Q}{C_p} \qquad (A.6)$$

Combining (A.6) and (2.47), the continuity equation, and substituting the resulting equation in (A.5), we obtain,

$$\frac{dP}{dt} = -\frac{C_p}{g}\int_o^{p_o}\int_s \nabla\cdot(\vec{V}T)\,dsdp - \frac{C_p}{g}\int_o^{p_o}\int_s \frac{\partial}{\partial p}(\omega T)\,dsdp$$

$$+ \frac{1}{g}\int_o^{p_o}\int_s \alpha\omega\,dsdp + \frac{1}{g}\int_o^{p_o}\int_s Q\,dsdp$$

By Gauss' theorem and boundary conditions at the top and bottom of the atmosphere,

$$\frac{dP}{dt} = \frac{1}{g}\int_o^{p_o}\int_s \alpha\omega ds dp + \frac{1}{g}\int_o^{p_o}\int_s Q ds dp \qquad (A.7)$$

This equation was obtained by White and Saltzman (1956). As far as the thermodynamic forcing is concerned, the first term on the right-hand side of (A.7) is considered as the energy conversion between the potential and kinetic energy due to the process of rising of warm air masses and sinking of cold air masses.

The vertical motion of the rising and sinking air masses will induce the horizontal motion of the fluid to satisfy the conservation of mass. We can, therefore, consider the generation of kinetic energy of the fluid motion from the point of view of dynamics. Applying the equation of state, the hydrostatic equation, and the continuity equation, we are able to transform (A.7) to a new expression

$$\frac{dP}{dt} = -\frac{1}{g}\int_o^{p_o}\int_s \Phi\nabla\cdot\vec{V} ds dp + \int_o^{p_o}\int_s Q ds dp \qquad (A.8)$$

(A.8) tells us if Φ and $\nabla\cdot\vec{V}$ have net positive correlation over the entire domain of the atmosphere, the potential energy can then be converted into kinetic energy. From the meteorological observation, divergence (or convergence) is usually associated with the high pressure (or low pressure) which posses higher height (or lower height)

such that the conversion from the potential energy to kinetic energy can be achieved.

In order to make the physical argument of energy conversion, $C(K_3,K_2)$, clear in our study, we express (A.8) in another form by applying Gauss' theorem,

$$\frac{dP}{dt} = \frac{1}{g}\int_o^{p_o}\int_s \vec{V}\cdot\nabla\Phi ds dp + \frac{1}{g}\int_o^{p_o}\int_s Q ds dp \qquad (A.9)$$

The energy conversion representing the first term on the right-hand side of (A.9) can be interpreted as the work done by the pressure gradient force on the cross-contour flow (Kung, 1966). For the consistency of notation and physical argument laid down in Section 2.1, we may write (A.9) in the form

$$\frac{dP}{dt} = \frac{1}{g}\int_o^{p_o}\int_s \vec{V}_3\cdot\nabla\Phi_1 ds dp + \frac{1}{g}\int_o^{p_o}\int_s Q ds dp \qquad (A.10)$$

The first term in the right-hand side of (A.10) can be viewed as the work done by the pressure gradient force on the cross-contour flow of the divergent field. (A.9) and (A.10) can be expressed symbolically,

$$\frac{dP}{dt} = - C(P,K) + G(P) \qquad (A.11)$$

and

$$\frac{dP}{dt} = - C(P,K_3) + G(P) \qquad (A.12)$$

A.2 The Potential Energy Equation in the z-Coordinate System of NCAR GMC

The model atmosphere of the NCAR GMC is extended vertically from Z_H to Z_T; therefore the potential energy and internal energy of this model atmosphere should be of the form

$$E_{PZ} = \int_{Z_H}^{Z_T} \int_S g\rho z dz ds \tag{A.13}$$

$$E_{IZ} = \int_{Z_H}^{Z_T} \int_S C_v T\rho dz ds \tag{A.14}$$

The rate change of E_{PZ} and E_{IZ} for a general type of atmosphere have been fully discussed and derived by Wiin-Nielsen (1968). We modify slightly his formulation to fit the atmosphere on the GMC for the purpose of our study here. An identity which was shown by Wiin-Nielsen (loc. cit.)

$$\int_V \frac{\partial (b\rho)}{\partial t} dV = \int_V \frac{db}{dt} \rho dV \tag{A.15}$$

will be used in the following derivation of the potential energy equation, where b is an arbitrary scalar variable defined everywhere in the atmosphere.

The rate of change of E_{PZ} is

$$\frac{dE_{PZ}}{dt} = \int_{Z_H}^{Z_T} \int_s g\frac{\partial}{\partial t}(\rho z)\,dsdz = \int_{Z_H}^{Z_T} \int_s g\rho\frac{dz}{dt}dsdz$$
$$= \int_{Z_H}^{Z_T} \int_s g\rho w\,dsdz \qquad (A.16)$$

The rate of change of E_{IZ} is

$$\frac{dE_{IZ}}{dt} = \int_{H}^{Z_T} \int_s Cv\frac{\partial}{\partial t}(\rho T)\,dsdz = \int_{Z_H}^{Z_T} \int_s Cv\frac{dT}{dt}\rho\,dsdz \qquad (A.17)$$

Combining thermodynamic equation and continuity equation to a single equation, we get

$$Cv\frac{dT}{dt} = -\frac{p}{\rho}\nabla\cdot\vec{V} + Q \qquad (A.18)$$

Substituting (A.18) in (A.17),

$$\frac{dE_{IZ}}{dt} = -\int_{H}^{Z_T} \int_s p\nabla\cdot\vec{V}\,dsdz + \int_{Z_H}^{Z_T} \int_s Q\,dsdz \qquad (A.19)$$

(A.19) is similar to (A.8). (A.19) can be changed to a new form following the discussion of Chapter 2 by using Gauss' theorem is the hydrostatic equation,

$$\frac{dE_{IZ}}{dt} = -\int_{H}^{Z_T} \int_s \vec{V}\cdot\nabla\, p\,dsdz + \int^{Z_T} \int_s g\rho w\,dsdz$$
$$-\int_s (pw)_{Z_b}\,ds + \int_{H}^{Z_T} \int_s Q\,dsdz \qquad (A.20)$$

The third term on the right-hand side of (A.20) represents the vertical flux term coming from the bottom boundary condition of the GCM. We may expect that this term is small because w at Z=H is usually very small. Combining (A.16) and (A.20), we obtain the potential energy equation

$$\frac{dP}{dt} = \frac{d(E_{PZ} + E_{IZ})}{dt} = - \int_H^{Z_T} \int_s \vec{V} \cdot \nabla p \, ds \, dz + \int_H^{Z_T} \int_s (pw) \, ds + \int_H^{Z_T} \int_s Q \, ds \, dz \tag{A.21}$$

or

$$\frac{dP}{dt} = - \int_H^{Z_T} \int_s \vec{V}_3 \cdot \nabla p_1 \, ds \, dz + \int_H^{Z_T} \int_s (pw)_{Z_b} \, ds + \int_H^{Z_T} \int_s Q \, ds \, dz \tag{A.23}$$

Here we may also express (A.22) and (A.23) in symbolic form which are similar to (A.11) and (A.12).

Appendix B

The Physical Interpretation of $C(K_3,K_2)$, An Example -- Cyclone

The energy conversion $C(K_3,K_2)$ expressed in (2.27) contains three parts which come from different physical processes as one checks the derivation of (2.27). To illustrate qualitatively the physical processes causing this energy conversion from the point of view of momentum, let us consider a simple case, say, a cyclone, in which a divergent field, namely, the motion toward the center of cyclone, is superimposed upon a rotational field, the tangential motion of cyclone.

The analogy between the rotational motions of a rigid body and a fluid tells us that the local vorticity of flow is equal to a half of its local angular velocity. To simplify our physical argument here, we may assume that $f + \zeta$, absolute vorticity, is uniform over the area covered by a cyclone. The inward motion of the divergent field will move the fluid elements of relatively high angular momentum from the outer portion of the cyclone inward. In order to satisfy the conservation of angular momentum, the exchange of fluid elements with differential angular momentum will produce a tangential force. This qualitative discussion can be, indeed, cleared up by a simple mathematical argument.

ΔL, the change of angular momentum per unit mass of a fluid element moving from the radial distance r to $r - \Delta r$, is:

$$\Delta L = \frac{1}{2}(f + \zeta)r^2 - \frac{1}{2}(f + \zeta)(r - \Delta r)^2$$

Assume

$$\Delta r << r$$

$$\Delta L \simeq (f + \zeta)r\Delta r$$

where $\Delta L/\Delta t$ is equal to the torque, $\tau = rF_1$, where F_1 is the tangential force. Therefore,

$$rF_1 = (f + \zeta)r\frac{\Delta r}{\Delta t}$$

or

$$F_1 = (f + \zeta)\frac{\Delta r}{\Delta t} = (f + \zeta)V_r$$

where V_r is the radial motion, i.e., $\vec{V}_3$ in this study. We may write it in a vector form

$$\vec{F}_1 = \vec{V}_3 x \vec{k}(f + \zeta_2)$$

The work done by this force on the tangential motion, i.e. rotational motion is

$$\vec{V}_2 \cdot \vec{F}_1 = \vec{V}_2 \cdot [\vec{V}_3 x \vec{k}(f + \zeta_2)] \tag{B.1}$$

or

$$\vec{V}_2 \cdot \vec{F}_1 = -(f + \zeta_2)\vec{V}_2 \cdot (\vec{k} x \vec{V}_3)$$

The right-hand side of (B.1) is the integrand of the first term in (2.27). Note that the contribution made by the intrinsic rotation of the earth to this energy conversion can be simply explained in the following; The Coriolis force induced by the inward motion of the divergent field is $\vec{V}_3 x \vec{k} f$, this force does a work on the rotational motion $\vec{V}_2 \cdot (\vec{V}_3 x \vec{k} f)$ or $-f\vec{V}_2 \cdot (\vec{k} x \vec{V}_3)$.

The discussion above concerns only the motion in the horizontal plane. If we assume that the divergent field of a cyclone is superimposed on the lower part of the cyclone, as is the case in the atmosphere, a vertical upward motion will be triggered by the inward motion of the divergent field such that the mass conservation can be satisfied. However, the induced vertical motion will present a channel for the exchange of the momentum of the fluid elements at different levels.

A simple mathematical treatment similar to that of angular momentum for (B.1) can clarify this point; let us assume that the rotational motion of a fluid element is $\vec{V}_2(p - \Delta p)$ and $\vec{V}_2(p)$ at level $p - \Delta p$ and p respectively,

and Δp is an infinitesimal change at p. We may, therefore, be able to expand the rotational motion at level $p - \Delta p$ with respect to that at level p as follows:

$$\vec{V}_2(p - \Delta p) = \vec{V}_2(p) - \frac{\partial \vec{V}_2}{\partial p}\Delta p + 0(\Delta p^2)$$

or

$$\vec{V}_2(p - \Delta p) - \vec{V}_2(p) = - \frac{\partial V_2}{\partial p}\Delta p + 0(\Delta p^2)$$

Assuming $\Delta p << p$, and neglecting $0(\Delta p^2)$ terms, ΔM, the change of momentum per unit mass as the fluid element moves upward Δp, can be expressed,

$$\Delta \vec{M} = \Delta \vec{V}_2 \simeq -\frac{\partial \vec{V}_2}{\partial p}\Delta p$$

The force induced by this change of momentum is

$$\vec{F}_2 = \frac{\Delta \vec{M}}{\Delta t} = \frac{\Delta \vec{V}_2}{\Delta t} = - \frac{\partial \vec{V}_2}{\partial p} \frac{\Delta p}{\Delta t} \simeq -\omega_3 \frac{\partial V_2}{\partial p} \qquad \text{(B.2)}$$

(B.2) tells us that the vertical motion, ω_3 convects the momentum of the rotational motion and results in a local force acting on this motion. The work done by this force on the rotational motion is,

$$\vec{V}_2 \cdot \vec{F}_2 = - \vec{V}_2 \cdot \omega_3 \frac{\partial \vec{V}_2}{\partial p} = - \omega_3 \frac{\partial k_2}{\partial p} \qquad \text{(B.3)}$$

The last form on the right-hand of (B.3) is the integrand of the second integral in (2.21). Although no force is directly generated by ω_3, it presents the way to redistribute the momentum of the rotational motion. This redistribution process of momentum of the rotational motion, in turn, offers a possiblity to speed up (or slow down) the energy conversion between the divergent and nondivergent field due to the process of the first term of (2.27).

Note that the second term of (2.27) is expressed as

$$-\frac{1}{g}\int_o^{p_o}\int_s k_2 \nabla\cdot\vec{V}_3 ds dp$$

which can be established by applying Gauss' theorem to

$$-\frac{1}{g}\int_o^{p_o}\int_s \omega_3 \frac{\partial k_2}{\partial p} ds dp.$$

For the convenience of interpretation, the former expression can be given in another form,

$$\frac{1}{g}\int_o^{p_o}\int_s k_2 \frac{\partial \omega_3}{\partial p} ds dp$$

by using the continuity equation. $\frac{\partial \omega_3}{\partial p}$, the differential vertical motion offers the possibility to stretch or

contract the vortex line of the rotational motion. The stretching or contracting of vortex line will change the tangential motion of the rotational field under the conservation of angular momentum. As a matter of fact, $\frac{\partial \omega_3}{\partial p}$ is induced by $\nabla \cdot \vec{V}_3$ or vice verse. In effect, $\nabla \cdot \vec{V}_3$ can offer the same effect as $\frac{\partial \omega_3}{\partial p}$ for the argument in this paragraph.

ω_3 convects vertically not only the momentum of the rotational motion but also that of the divergent motion. The final term of $C(K_3,K_2)$ in (2.27) can, therefore be explained in the same manner as has been done for the second term of $C(K_3,K_2)$ above. One should notice that $\vec{V}_2$ is normal to $\vec{V}_3$ in the example given here such that $\vec{V}_2 \cdot \omega_3 \frac{\partial \vec{V}_3}{\partial p}$ may be zero (this may not be true in the real atmosphere).

One should also notice that the vertical exchange of momentum of the flow at different levels inducing energy conversion from K_3 to K_2 is not only by means of the second and third processes described in this appendix, but also by means of the first process that involves $\vec{V}_2$ and $\vec{V}_3$ which will vary through the vertical column.

Appendix C

The Scheme of Filling Wind Data at Poles

The wind at the north pole (N.P.) and south pole (S.P.) are determined by the wind at 87.5°N and 87.5°S, respectively, using the following scheme

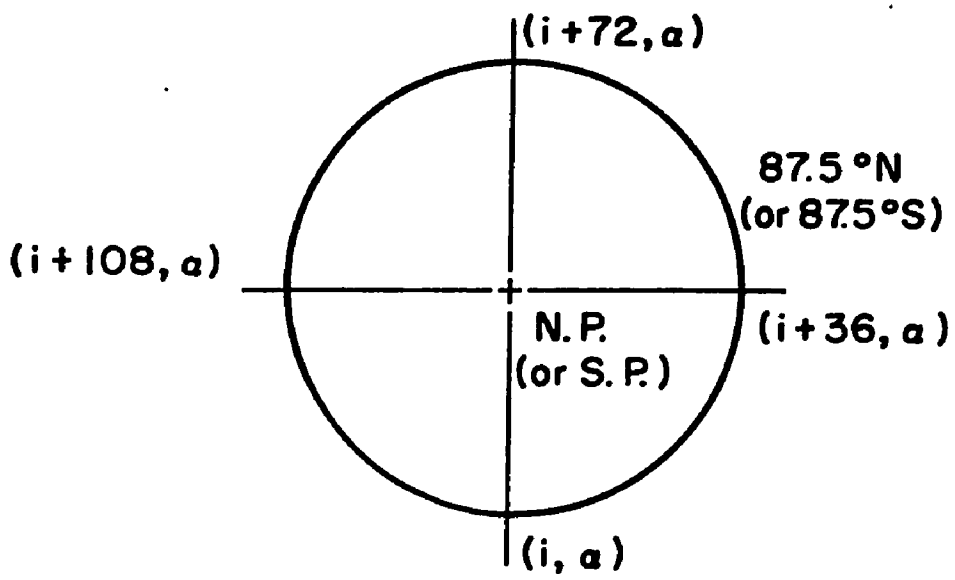


Fig. C1: A coordinate system in which the origin is located at the pole

Figure C1 shows a coordinate system in which the origin is located at the pole. Here, $1 \leq i \leq 144$, and $\alpha = 2$ (or 72) for the south (or north) pole. This coordinate system rotates $2\frac{1}{2}°$ as one switches from one grid point, e.g., (i,α), to the next one, e.g. $(i+1,\alpha)$.

The values of wind at the N.P. (or S.P.) corresponding to a given grid point (i,α) are calculated by

$$u(i,\alpha\pm1) = \frac{1}{4}[u(i,\alpha) - u(i+72,\alpha) + v(i+108,\alpha) - v(i+36,\alpha)] \quad \text{(C.1)}$$

$$v(i,\alpha+1) = \frac{1}{4}[u(i+36,\alpha) - u(i+108,\alpha) + v(i,\alpha) - v(i+72,\alpha)] \quad \text{(C.2)}$$

where $\alpha = 2$ (or 72), we use $\alpha-1$ (or $\alpha+1$) for the index on the left-hand side. Some rules are also applied to indices on the right-hand side;

$i+32 > 144$; replace $i+32$ by $(i+32) - 144$

$i+72 > 144$; replace $i+72$ by $(i+72) - 144$

$i+108 > 144$; replace $i+108$ by $(i+108) - 144$

The foregoing calculation gives 144 values of wind components, u and v, at the poles. This is not physically realistic. We, therefore, have to introduce a scheme of finding one wind vector at the pole.

We fix the coordinate system in Figure C1 by letting i=1 in such a way that the wind vectors at the pole corresponding to different grid points, (i,α), rotate around the pole. However, the average wind vector at the pole is determined by

$$u_{\text{at the pole}} = \frac{1}{144} \sum_{i=1}^{144} u(i,\alpha\pm1)\cos(ix2\tfrac{1}{2}°) \qquad \text{(C.3)}$$

$$v_{\text{at the pole}} = \frac{1}{144} \sum_{i=1}^{144} v(i,\alpha\pm1)\cos(ix2\tfrac{1}{2}°) \qquad \text{(C.5)}$$

where $\alpha+1$ for N.P. and $\alpha-1$ for S.P.

Appendix D

Verification for the Direct Method of Dividing the Horizontal Wind Vector into its Divergent and Nondivergent Parts

(2.1) and (2.2) imply that wind components may be expressed as

$$u = u_2 + u_3$$

$$v = v_2 + v_3$$

where

$$u_2 = -\frac{1}{a}\frac{\partial \psi}{\partial \phi},\ v_2 = \frac{1}{a\cos\phi}\frac{\partial \psi}{\partial \lambda}$$

$$u_3 = \frac{1}{a\cos\phi}\frac{\partial \psi}{\partial \lambda},\ v_3 = \frac{1}{a}\frac{\partial \psi}{\partial \phi}$$

The zonal average of u and v,

$$\bar{u} = \bar{u}_2 + \bar{u}_3 = \bar{u}_2 \qquad \text{(D.1)}$$

$$\bar{v} = \bar{v}_2 + \bar{v}_3 = \bar{v}_3 \qquad \text{(D.2)}$$

where $(\overline{\ \ }) \equiv \frac{1}{2\pi}\int_0^{2\pi} (\ \ )d\lambda$. (D.1) and (D.2) provide one method for verifying the scheme of wind separation. Another verification comes from the definitions of divergent and nondivergent flow. The former processes

$$\nabla\cdot\vec{V}_3 = \text{Divergence} = \nabla\cdot\vec{V} \qquad \text{(D.3)}$$

$$\nabla X\vec{V}_3 = 0$$

and the latter

$$\nabla\cdot\vec{V}_2 = 0 \qquad \text{(D.4)}$$

$$\nabla X\vec{V}_2 = \text{Vorticity} = \nabla X\vec{V}$$

Figures D1, D2, D3, and D4 shows respectively the height-latitude distribution of $\bar{u}$, $\bar{v}$, $\bar{u}_2$, and $\bar{v}_3$ for time step 41040 of the NCAR GCM. Tables D1, D2, D3, D4, D5, and D6 show respectively the divergence and vorticity of $\vec{V}$, $\vec{V}_2$, and $\vec{V}_3$ field at level 3, i.e. 9 kms, for time step 41040 of the NCAR GCM.

The comparisons of Figures D1 to D4 and Tables D1 to D6 following criteria (D.1), (D.2), (D.3), and (D.4) show us that the scheme of separating the horizontal wind vector into its divergent and nondivergent parts is clearly an acceptable method.

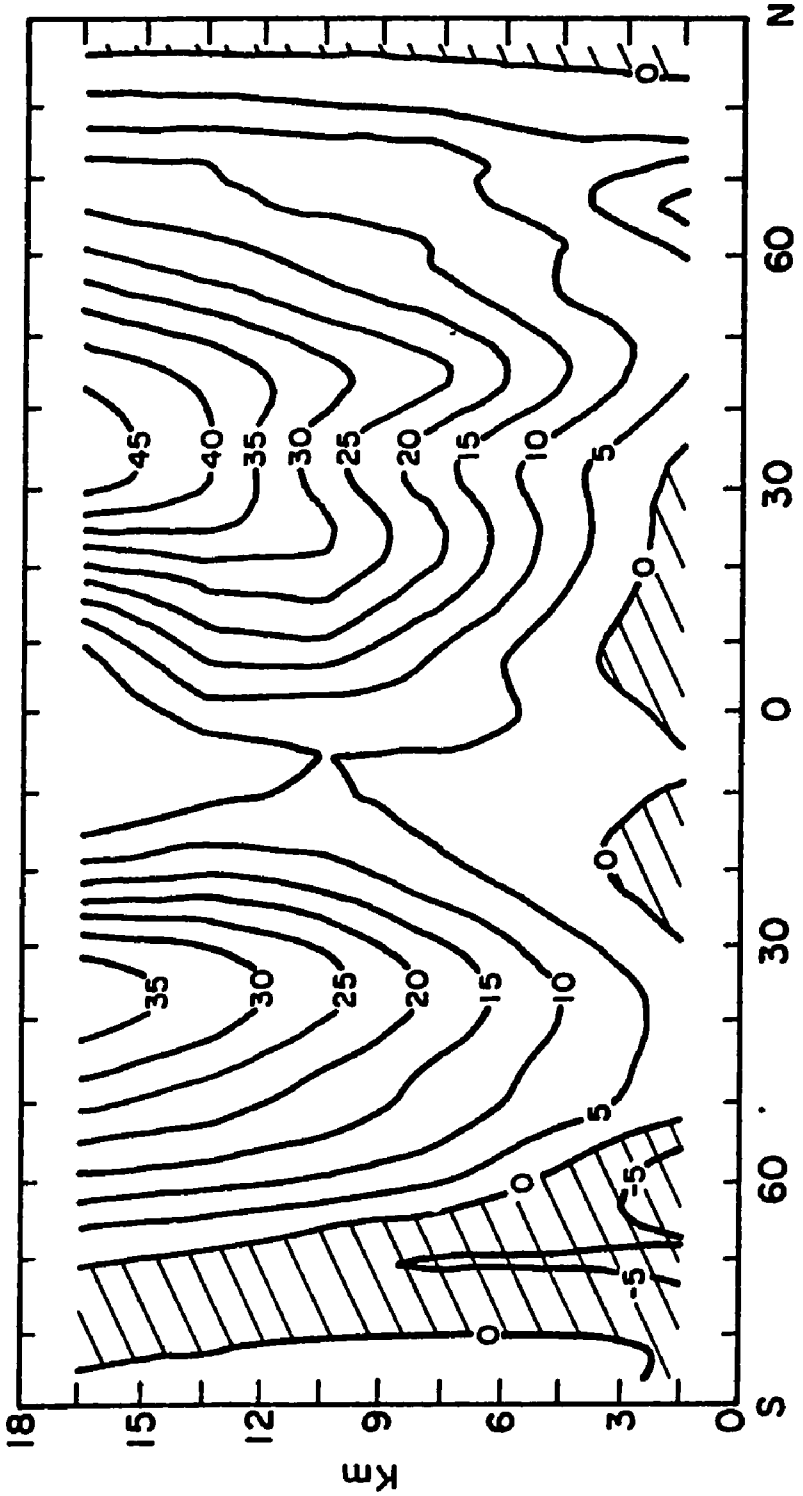


Fig. D1. Latitude-height distribution of $\bar{u}$ for time step 41040 of the NCAR GCM. Unit: m/sec.

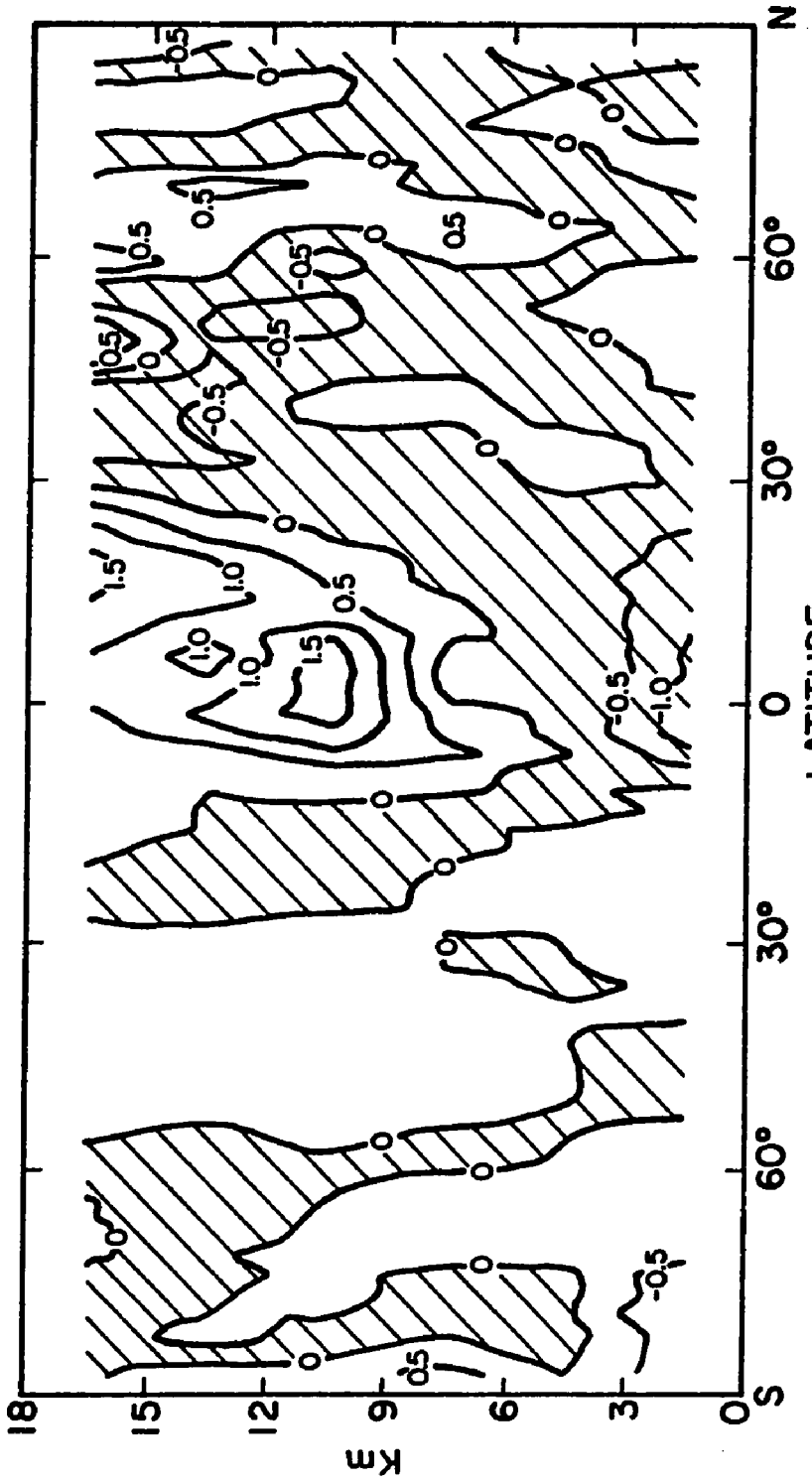


Fig. D2. Latitude-height distribution of $\bar{v}$ for time step 41040 of the NCAR GCM. Unit: m/sec.

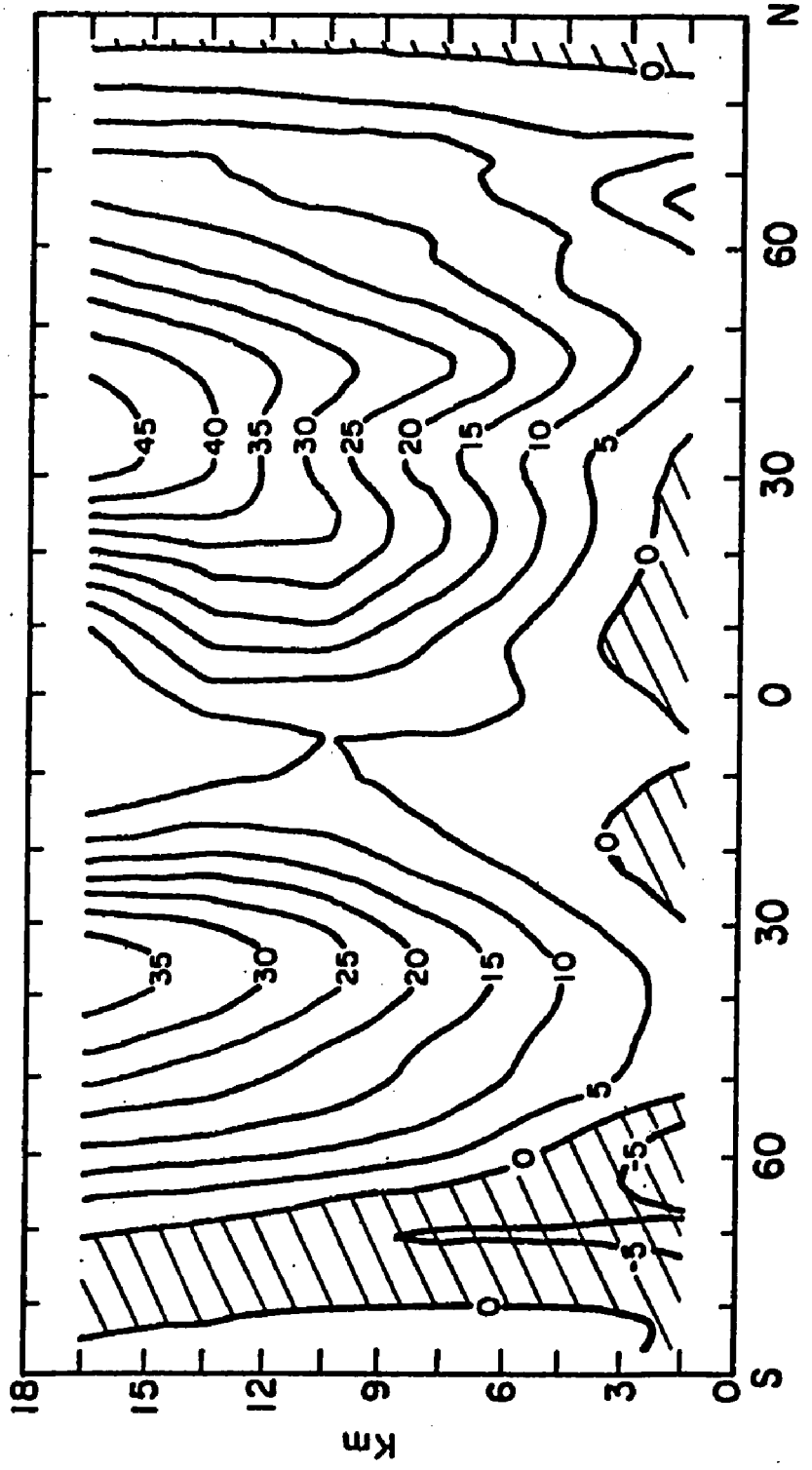


Fig. D3. Latitude-height distribution of $\bar{u}_2$ for time step 41040 of the NCAR GCM. Unit: m/sec.

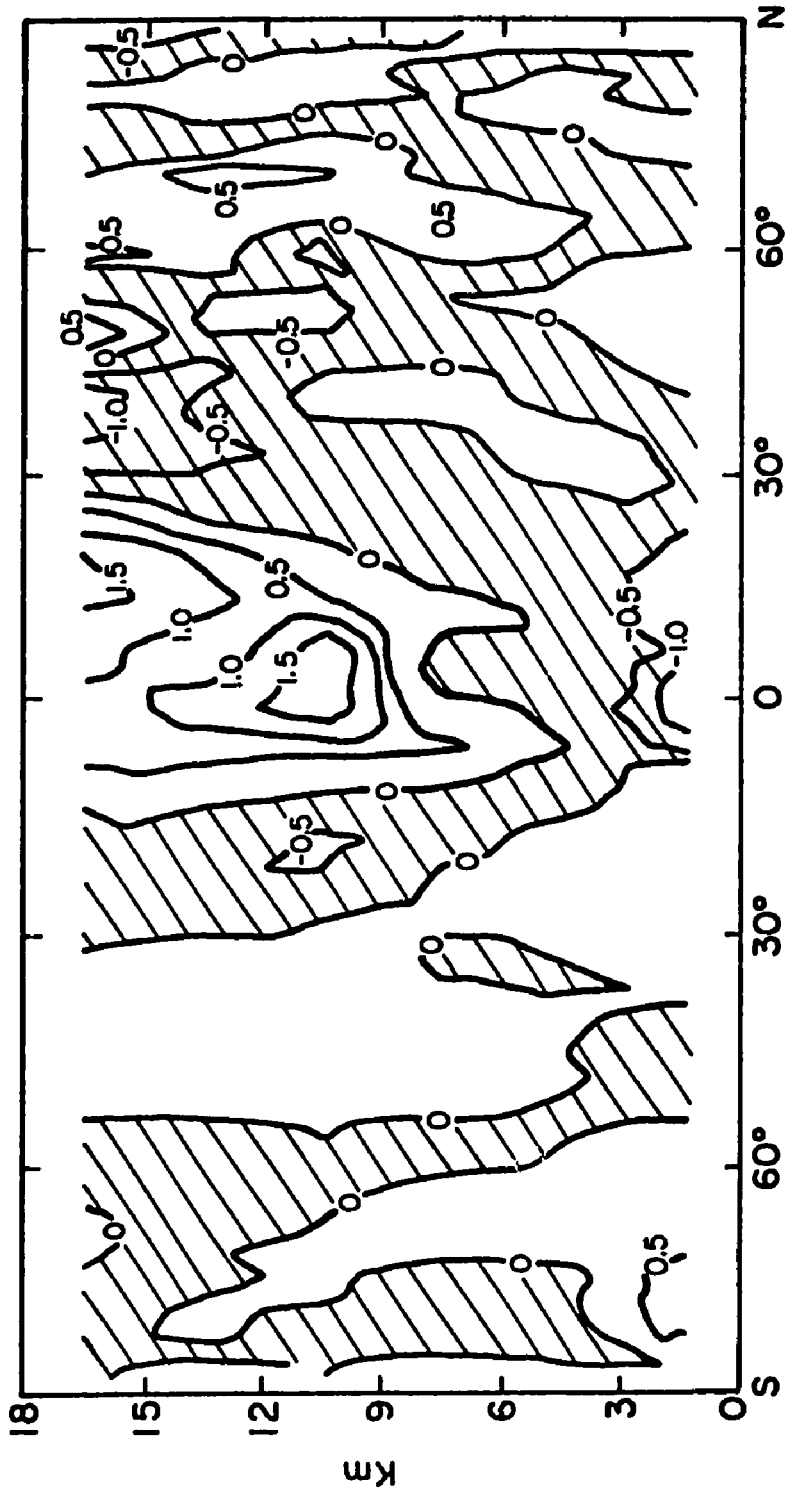


Fig. D4. Latitude-height distribution of $\bar{v}_3$ for time step 41040 of the NCAR GCM. Unit: m/sec.

Table D1: Divergence calculated from $\hat{V}$ field at 7.5 km level of the NCAR GCM for time step 41040. Unit: $10^{-6}sec^{-1}$.

Latitude/ Longitude	80°N	70°N	60°N	50°N	40°N	30°N	20°N	10°N	0°	10°S	20°S	30°S	40°S	50°S	60°S	70°S	80°S
0°	-2.6294	4.8995	4.5751	-1.0143	-3.6101	1.3577	-0.9091	0.3772	0.6638	3.0764	-0.4451	-2.1502	1.8720	8.3279	-2.9418	5.9912	-0.6512
20°	-3.7179	1.6739	-0.7639	-5.1649	-1.0039	-0.6876	4.1780	-0.6456	0.7544	-0.9115	4.6057	3.5360	0.7886	4.1202	0.5861	-0.4062	11.436
40°	1.6446	-2.3782	-3.6058	-2.2256	-0.4560	0.6194	-3.0943	1.7113	2.6523	-2.3667	3.3536	-2.2018	-5.3024	-2.3372	8.4051	-2.3712	-12.443
60°	3.0655	4.3230	2.7579	2.4582	0.4499	6.0287	0.3959	-1.7979	3.4570	-0.0699	-1.4187	-4.4344	1.0152	3.4635	6.3494	-0.4287	0.4266
80°	-10.121	-0.7442	0.9514	2.0854	-3.6924	-2.3403	0.6507	-1.6397	-2.6288	7.5624	4.8040	-0.9680	-0.2657	-1.1205	-0.3904	4.1496	-1.6073
100°	9.2932	12.071	1.7398	-4.2600	-3.4402	-2.5234	-0.5453	-0.2687	-6.1306	4.1698	-5.1428	0.9325	0.5417	0.4621	3.7295	-4.3067	-2.0143
120°	-5.3989	-1.9276	-0.6031	2.6153	-1.9383	5.3612	1.1529	-0.2595	3.2631	2.5976	2.9067	-2.4369	-1.5305	3.1047	4.0064	-3.6549	1.9341
140°	-4.1906	11.773	3.5464	6.6666	-2.9691	-4.6195	-0.1169	2.3722	-2.0745	2.0056	0.7122	-2.1646	-2.6273	-1.0819	13.771	8.1195	-7.0019
160°	-0.0271	11.718	-1.2139	-2.1595	4.1537	-0.3515	1.0367	0.8416	1.9893	-3.9628	-2.3314	0.4051	4.7537	-1.4227	2.5392	-9.1802	5.1633
180°	-2.0421	-1.8929	9.8150	-3.7115	-1.5072	-1.1556	-1.4270	-2.7096	-0.2464	3.9595	0.0246	-1.6468	-1.0038	5.1645	14.147	-1.0222	-5.4283
200°	-3.2183	-28.595	13.131	-0.6962	2.0116	2.3126	2.0824	-2.9782	3.4597	-2.4902	4.3606	1.6332	-4.3384	4.2767	1.2823	-8.3573	6.5237
220°	-5.3007	8.3479	-8.1885	-2.9048	-5.2421	1.3352	-2.1390	0.0976	10.946	-5.2191	10.727	-3.1005	1.2426	-9.3338	-19.194	11.900	-6.5273
240°	2.4024	13.923	-0.3286	1.4289	5.6387	3.4969	-0.9906	-0.5033	7.8765	-1.3317	-3.3306	-1.5728	3.6314	11.300	8.4933	7.0849	-2.3433
260°	-14.762	-52.080	-2.1566	5.2051	-0.1735	-0.7747	-2.0319	-1.4598	-7.4056	5.3672	2.1542	-0.4042	6.4110	3.4988	5.2827	2.6348	4.2638
280°	-1.3834	15.694	-4.4033	-6.1440	1.1370	1.9292	0.2184	-0.1604	1.8126	-0.3411	0.9330	0.5140	12.131	4.8128	-1.9962	-1.8885	1.4022
300°	7.1065	5.4017	0.9247	-0.5779	-0.1535	-0.7761	-0.1546	0.6993	1.9815	-4.6345	-3.9268	-0.0781	3.8023	1.5258	-0.2747	0.37659	0.5682
320°	-3.8032	6.5968	-1.2063	-6.8502	1.6601	-1.3077	1.6486	-2.1724	1.1408	-0.0585	-2.6190	-0.5068	-5.6997	5.2300	-0.0539	1.8967	9.8862
340°	3.6040	2.5320	-1.3034	4.0035	-4.0087	-0.6033	0.6824	-0.0593	-3.7275	1.6075	-2.3990	-4.7558	1.6438	-2.3566	-28.123	-0.6527	-3.3175

Table D2: Vorticity calculated from $\vec{V}$ field at 7.5 km level of the NCAR GCM for time step 41040. Unit: $10^{-5}sec^{-1}$.

Latitude/ Longitude	80°N	70°N	60°N	50°N	40°N	30°N	20°N	10°N	0°	10°S	20°S	30°S	40°S	50°S	60°S	70°S	80°S
0°	-1.1302	1.2564	1.8163	-1.1890	-0.8275	0.5220	1.7833	0.4641	-0.4574	-0.7692	-2.8466	1.4736	1.6098	5.4197	5.8597	2.7254	2.6946
20°	-1.4687	2.6724	-4.4514	-2.4242	-3.6020	-2.7541	-0.4017	1.2177	-1.1917	0.0790	-1.3588	0.3372	0.0720	0.2034	-3.2303	-4.4673	0.7033
40°	-2.6339	1.4059	-0.5544	1.5297	-2.0638	0.9993	2.2009	0.5964	-1.4049	-0.9442	1.3495	0.4709	3.3241	-3.4108	-2.0998	0.2055	2.1375
60°	-3.6949	1.1578	-4.1667	-0.7184	1.0218	1.3927	1.0151	0.9293	-2.2448	0.4445	1.9970	2.0052	2.6771	0.1807	-4.9390	1.9934	-1.0959
80°	-1.2176	0.1132	-0.1531	-4.0453	-0.9250	-2.6530	-0.6155	-1.7881	0.2116	1.0469	-0.5469	-1.5173	-1.8142	0.7690	-2.9584	3.9797	-1.3769
100°	0.7278	-3.1751	2.2669	-1.9469	-0.0425	0.5300	-0.4537	-1.0329	-1.2498	1.3925	-1.0228	-1.0831	-1.2113	3.2942	1.3950	0.6624	-1.5309
120°	1.8017	-6.1655	-2.9204	2.9533	2.3257	1.2539	1.4195	0.0155	-2.6281	0.0490	0.0719	0.5100	-3.2475	4.0354	4.0949	0.2345	1.8618
140°	1.1049	0.8655	-2.6511	-4.1702	-2.4665	-1.0040	1.0043	-0.2046	0.9413	-0.8936	-1.3049	1.8971	-1.2084	2.9945	-2.7205	3.1136	-3.7930
160°	1.1459	-0.1903	-4.0024	-1.6019	2.6608	1.1965	1.0846	-0.4797	-0.3292	0.9660	0.5982	-1.2939	-3.0224	1.4556	5.3829	-1.5797	-1.0980
180°	3.8806	0.2860	0.4042	5.2377	3.1634	-0.9745	-1.7018	0.1521	-0.9336	1.6939	-0.3936	2.7269	-1.3249	-0.9431	0.8951	-1.3266	2.3837
200°	-2.0793	-2.4686	0.9068	-2.6428	-3.3370	-2.6512	2.1952	-0.5999	-2.6255	-0.5584	-2.7944	2.4895	0.0657	-3.8033	5.3912	-2.2693	2.6576
220°	-0.9147	2.3347	1.3611	-0.8940	-5.5718	-2.1843	2.8484	-0.2677	0.9225	-1.4045	-0.3534	2.5253	0.7826	5.0735	5.8068	3.9536	1.1436
240°	-0.9256	3.2019	-0.6440	-5.2128	-3.4402	0.8675	2.9100	0.4147	0.3859	-2.1554	-1.8753	1.3401	-0.3130	-3.6311	-2.4782	-1.4693	-0.9233
260°	0.3668	-3.8724	0.1281	1.2609	-2.1338	4.0181	2.2548	-0.1160	0.1889	-1.4759	-2.5003	-0.2849	3.6053	4.6838	-0.1237	-4.5194	-1.3216
280°	3.7096	4.4782	0.1071	-0.8875	0.1182	1.4511	0.0235	-0.4037	0.4455	-0.3410	-1.2980	3.7453	-0.6056	-0.1770	2.0973	2.0321	1.2268
300°	0.7764	0.6019	-0.8030	-0.0777	-4.3137	-0.3000	-0.3567	1.6803	-0.3625	-2.9666	-0.0138	0.1645	-2.2469	-0.6905	0.7460	0.1503	0.8027
320°	-0.6811	0.4961	-1.9369	0.0119	1.0243	1.5315	0.7241	0.3755	0.5705	-0.4987	-0.7156	-0.1168	-1.8405	6.7435	0.2087	0.5764	2.9610
340°	-1.7820	0.5141	-1.5439	-3.2732	0.5771	0.7714	-0.7925	0.4561	-0.8554	0.3215	-1.4758	0.0820	-3.2042	0.0443	2.4742	5.1771	4.4424

Table D3: Divergence calculated from $\tilde{V}_2$ field at 7.5 km level of the NCAR GCM for time step 41040. Unit: $10^{-6}sec^{-1}$.

Latitude/ Longitude	80°N	70°N	60°N	50°N	40°N	30°N	20°N	10°N	0°	10°S	20°S	30°S	40°S	50°S	60°S	70°S	80°S
0°	6.0612	0.2451	0.1348	-0.1186	-0.4324	-0.3834	0.1095	0.7361	1.2672	1.6227	1.5814	1.0855	0.4602	0.0049	-0.1979	-0.7943	-2.6744
20°	3.0277	-0.6458	-0.5083	-0.4833	-0.569	-0.7010	-0.6244	-0.2580	0.4085	1.3699	2.3078	2.6303	2.1830	1.4562	0.9113	0.1543	-2.8802
40°	6.4228	0.0650	-0.3230	-0.0732	0.1828	0.1564	-0.1753	-0.6380	-0.8580	-0.5597	0.0873	0.5261	0.3950	0.0975	0.3649	1.8025	1.3857
60°	7.4301	2.2731	1.3098	0.9660	1.0045	1.0203	0.7068	0.0997	-0.4344	-0.6286	-0.6449	-0.7803	-1.1100	-1.4301	-1.3305	-0.8237	-4.3427
80°	9.3504	2.5937	1.2714	-0.0254	-0.7531	-0.9422	-0.9313	-1.0292	-0.8667	-0.4783	-0.3307	-0.7355	-1.5472	-2.1406	-2.3193	-2.9300	-14.158
100°	13.861	5.9383	3.0829	-1.2093	-2.4311	-3.0683	-3.3902	-3.4490	-3.0083	-2.0499	-1.1269	-0.8546	-1.2915	-1.8445	-1.8665	-1.5381	-5.1515
120°	14.497	-0.1435	-0.2890	-1.0259	-1.8023	-2.1742	-2.3613	-2.5634	-2.5494	-2.1135	-1.5267	-1.2029	-1.1868	-1.4119	-1.9296	-2.5435	-13.060
140°	3.6676	1.8436	1.1357	0.3386	0.0746	0.4218	0.8865	1.0295	0.8334	0.7030	0.5062	0.2673	0.1417	0.1046	-0.8254	-3.7910	-32.010
160°	6.7357	0.7309	1.7253	1.5097	1.8525	2.5650	3.2871	3.6401	3.4134	2.8234	2.4342	2.7141	3.5755	4.1521	2.7909	-2.1292	-20.053
180°	-11.684	-2.2254	0.5153	0.6476	0.6010	0.7422	0.9633	1.1298	1.1803	1.1765	1.4555	2.4692	4.1685	5.2815	3.5245	-2.2232	-9.7390
200°	-21.139	-2.9466	-0.6447	0.2493	0.4332	0.1623	-0.4185	-1.2541	-1.9262	-1.8395	-0.7241	1.2431	3.6793	5.4491	3.8259	-2.3781	-6.2041
220°	-42.931	-3.5303	-1.6435	0.0367	0.9252	1.4636	1.6327	1.2831	0.2220	-0.6633	-0.3701	1.2663	3.6882	5.8993	5.5188	-0.0441	-5.7247
240°	-22.331	-2.7017	-0.6400	0.1073	0.6519	1.0208	1.9159	2.4057	1.8716	0.5068	-0.2968	0.1996	1.7176	3.3232	3.9766	2.3555	0.8690
260°	-21.039	0.2782	0.1616	0.3534	0.0033	-0.3178	-0.3137	-0.2993	-0.7228	-1.6276	-2.2532	-1.8941	-0.8411	0.1464	1.1095	3.0976	8.2458
280°	-6.3212	0.6841	0.2272	-0.0526	-0.1902	-0.6653	-1.2820	-1.9543	-2.7360	-3.5561	-3.9333	-3.4285	-2.3528	-1.2579	0.3142	3.8816	19.283
300°	2.4282	1.5834	1.1453	0.6545	0.3787	-0.0056	-0.4777	-1.0641	-1.8991	-2.8680	-3.4914	-3.4293	-2.8900	-2.0733	-0.1319	4.6638	17.990
320°	5.1416	3.5302	1.5649	1.0541	0.9106	0.8091	0.7830	0.7047	0.3649	-0.3374	-1.1596	-1.6229	-1.6099	-1.3622	-0.3407	3.4404	18.713
340°	5.1436	2.7838	0.8305	0.1375	-0.1754	0.0011	0.5979	1.2569	1.4718	1.2949	0.6983	-0.0294	-0.4459	-0.5858	-0.6005	0.3295	2.225

Table D4: Vorticity calculated from $\bar{v}_j$ field at 7.5 km level of the NCAR CCM for time step 41040. Unit: 10^{-5}sec^{-1}.

Latitude / Longitude	80°W	70°W	60°W	50°W	40°W	30°W	20°W	10°W	0°	10°S	20°S	30°S	40°S	50°S	60°S	70°S	80°S
0°	-1.1115	1.2574	1.8173	-1.1887	-0.8295	0.5220	1.7838	0.4564	-0.4575	-0.7692	-2.8446	1.4736	1.6099	5.4199	5.8606	2.7314	2.6775
10°	-1.4537	2.6753	-4.4497	-2.4236	-3.6019	-2.7541	-0.4518	1.2176	-1.1917	0.0792	-1.3586	0.3372	0.0714	0.2014	-3.2350	-4.4751	0.6134
20°	-2.6113	1.4120	-0.5545	1.5296	-2.0646	0.9990	2.2029	0.5965	-1.4250	-0.9444	1.3493	0.4705	3.3232	-3.4126	-2.1048	0.1856	2.0123
30°	-3.7370	1.1677	-4.1679	-0.7225	1.0206	1.3922	1.0149	0.9293	-2.2448	0.4444	1.9967	2.0048	2.6766	0.1806	-4.9375	2.0006	-1.0663
40°	-1.2319	0.1552	-2.1545	-4.0457	-0.9253	-2.6534	-0.6163	-1.7885	0.2114	1.0469	-0.5469	-1.5176	-1.8146	0.7682	-2.9547	4.0015	-1.3156
50°	0.7055	-3.1781	2.2176	-1.9456	-0.0418	0.5303	-0.4535	-1.0330	-1.7520	1.3924	-1.0229	-1.0832	-1.2114	3.2941	1.3949	0.6606	-1.6000
60°	1.7884	-4.1764	-2.6199	2.9540	2.3916	1.2548	1.4254	0.0162	-2.6278	0.0192	0.0775	0.5111	-3.2459	4.0373	4.0949	0.2673	1.8987
70°	1.1182	0.8767	-2.6516	-4.1737	-2.6665	-1.0239	1.0045	-0.2543	0.9416	-0.8933	-1.3046	1.8968	-1.7016	2.9329	-2.7213	3.1182	-3.7782
80°	1.1366	-3.1780	-4.3008	-1.6018	2.6623	1.1963	1.0843	-0.4799	-0.3737	0.9659	0.5379	-1.2947	-3.0239	1.4534	5.3802	-1.5817	-1.1360
90°	3.8443	0.7826	3.4080	5.7903	3.1644	-0.9742	-1.7018	0.1570	-0.9336	1.6939	-0.3935	2.7280	-1.3219	-0.9378	0.9003	-1.3799	2.3817
100°	-2.1799	-2.4722	0.9091	-2.6804	-3.3357	-2.6506	2.1925	-0.5998	-2.6256	-0.5584	-2.7942	2.4905	0.0682	-3.7987	-5.3856	-2.2719	2.6225
110°	-0.8139	2.3427	1.3102	-0.8950	-5.5721	-2.1843	2.8434	-0.2677	0.9725	-1.4046	-0.3535	2.5256	0.7830	5.0750	5.8105	3.9586	1.1159
120°	-0.9736	3.2170	-0.6454	-5.2166	-3.6637	0.8674	2.9099	0.4144	0.3858	-2.1557	-1.8759	1.3393	-0.3142	-3.6323	-2.4774	-1.4650	-0.9426
130°	0.1993	-3.0312	0.1710	1.2599	-2.1339	4.0182	2.2549	-0.1159	0.1889	-1.4763	-2.5012	-0.2963	3.6034	4.6821	-0.1230	-4.5123	-1.3934
140°	3.4946	4.4564	0.1265	-0.8878	0.1178	1.4528	0.0235	-0.4337	0.4458	-0.3410	-1.2981	3.7453	-0.6058	-0.1771	2.0989	2.0412	1.2098
150°	0.7215	0.5462	-0.8258	-0.0784	-4.3143	-0.3004	-0.3169	1.0852	-0.3625	-2.9445	-0.0136	0.1649	-2.2445	-0.6906	0.7445	0.1486	0.7871
160°	-3.6969	0.4841	-1.5390	0.0120	1.0245	1.5317	0.7741	0.3755	0.5726	-0.4986	-0.7154	-0.1165	-1.8422	7.7427	0.2038	0.5590	2.8994
170°	-1.7877	0.1744	-1.5483	-3.2727	0.5777	0.7719	-0.7824	0.4141	-0.8154	0.3215	-1.4759	0.0821	-3.2037	0.0451	2.4741	5.1707	4.4344

Table D1: Divergence calculated from $\bar{V}_3$ field at 7.5 km level of the NCAR CCM for time step 41040.Unit: $10^{-6}sec^{-1}$.

Latitude/ Longitude	80°N	70°N	60°N	50°N	40°N	30°N	20°N	10°N	0°S	10°S	20°S	30°S	40°S	50°S	60°S	70°S	80°S
0°	-3.2351	4.8750	4.5416	-1.0025	-3.5469	1.3961	-0.9700	0.3636	0.6171	2.9141	-0.5033	-2.2588	1.8260	0.3274	-2.9221	6.0706	-0.3838
22°	-4.0797	1.7388	-0.7133	-5.1166	-0.9469	-0.6175	4.2434	-0.6198	0.7135	-1.0485	4.1749	3.2730	0.7703	3.9745	0.5951	-0.4217	11.724
45°	1.0323	-2.3547	-1.5725	-2.2186	-0.4743	0.6238	-3.6758	1.7751	2.7381	-2.3137	3.3449	-2.2545	-5.3419	-2.3469	8.3686	-2.5514	-12.582
67°	2.3254	4.0957	2.6719	2.6216	0.4483	5.9747	0.3752	-1.1079	3.5004	-0.0071	-1.3542	-4.3543	1.1762	3.6965	0.4824	-0.3463	0.8609
90°	-10.956	-1.0036	0.8243	2.0879	-3.6175	-2.2461	0.6498	-1.1368	-2.5432	7.6175	4.8341	-0.9744	-0.2118	-0.9064	-0.1585	4.4426	-0.1915
112°	7.9571	11.981	1.7313	-6.1351	-3.1875	-2.7165	-0.8062	-0.1761	-5.8798	4.3347	-1.3301	0.6183	0.5708	0.5466	3.9161	-4.1529	-1.4992
135°	-6.8836	-1.9137	-0.5347	7.7178	-1.8130	1.4786	1.7783	3.0934	3.5151	2.8029	3.0593	-2.3166	-1.4118	3.2459	4.1993	-3.4005	3.2602
157°	-4.6737	11.489	3.6274	6.6347	-2.9756	-4.6616	-0.9016	2.2632	-2.1639	1.9313	0.6616	-2.1916	-2.6415	-1.0924	13.853	8.4986	-3.8009
180°	0.6464	11.681	-1.3643	-2.3138	3.9684	-0.4083	0.9080	0.7774	1.9479	-4.2412	-2.1348	0.6337	4.1961	-1.6379	2.2611	-0.9673	7.1687
202°	-0.8736	-1.4706	5.7636	-3.7762	-1.5673	-1.2708	-1.1230	-2.3226	-0.2648	3.6418	0.1229	-1.8537	-1.4207	6.9364	13.994	-0.7998	-4.4546
225°	-6.7063	-28.388	13.274	-0.7212	1.9683	2.7964	2.1242	-2.4628	3.6173	-2.3062	0.6331	1.4289	-4.2064	3.9318	1.1997	-0.1195	7.1641
247°	-8.7019	6.7210	-6.0241	-2.4206	-4.3581	1.1882	-2.2062	0.2836	0.424	-6.1129	10.764	-3.2271	1.0737	-9.9238	-19.746	11.904	-1.9149
270°	6.6861	16.283	-0.2487	1.6187	6.5886	3.2963	-1.6814	-0.6838	2.4298	-1.3846	-3.3293	-1.1927	3.4136	19.967	0.0917	6.8494	-2.6302
292°	-12.136	-42.418	-2.1727	6.6187	-0.1729	-0.7879	-2.0806	-1.6336	-2.3333	6.1303	2.2795	-0.3167	6.4911	3.4381	5.1919	2.5350	3.4392
315°	-0.7139	16.424	-6.8362	-6.1388	1.9160	1.9917	0.2474	-0.0250	2.0882	-0.0144	1.0260	0.6149	12.364	6.9186	-2.0277	-2.0767	-0.5261
337°	0.0136	5.7138	0.8982	-0.6434	-0.3613	-0.7711	-0.1161	0.7219	2.1716	-6.6177	-1.7774	-0.1647	6.6913	1.6332	-0.2615	0.1897	-1.2307
360°	-6.3178	6.6832	-1.3630	-6.9256	1.5783	-1.3886	1.1723	-2.2479	1.1543	-0.0247	-2.1239	-0.6445	-5.1382	5.3443	-0.0199	1.6525	0.0149
382°	2.6851	2.6131	-1.3861	3.9877	-1.9511	-0.6234	0.6726	-2.1833	-1.8744	1.1783	-2.4429	-4.7129	1.6884	-2.2913	-28.842	-0.6816	-3.5400

Table D6: Vorticity calculated from $\tilde{V}_3$ field at 7.5 km level of the NCAR GCM for time step 41040. Unit: $10^{-8}sec^{-1}$.

Latitude/ Longitude	80°N	70°N	60°N	50°N	40°N	30°N	20°N	10°N	0°	10°S	20°S	30°S	40°S	50°S	60°S	70°S	80°S
0°	-18.650	-0.9808	-0.6531	-0.2489	-0.0024	0.0531	0.0612	0.0521	0.0272	0.0102	-0.0071	-0.0616	-0.1016	-0.1788	-0.8869	-5.9948	17.095
20°	-14.968	-2.9254	-1.7589	-0.6143	-0.1536	0.0396	0.1060	0.1004	0.0145	-0.1399	-0.2192	0.0119	0.6724	2.0198	4.6942	7.7381	8.9923
40°	-22.539	-6.0775	0.1190	1.0785	0.7547	0.3173	0.0028	-0.0812	0.0426	0.1877	0.2571	0.4309	0.8755	1.7833	5.0053	19.915	12.515
60°	42.129	-9.9407	1.2045	2.0183	1.2111	0.5794	0.1821	-0.0176	-0.0074	0.0984	0.2290	0.4156	0.5300	0.1736	-1.4652	-7.2221	-29.604
80°	13.450	7.5082	1.3926	0.3805	0.2727	0.4412	0.5257	0.4322	0.2227	0.0039	-0.0209	0.2531	0.4474	-0.1715	03.6886	-21.774	-61.352
100°	22.299	3.0289	-0.7359	-1.3162	-0.7762	-0.2939	-0.0672	0.0986	0.2048	0.1425	0.0213	0.0362	0.1313	0.0947	0.1294	1.7693	69.014
120°	13.319	-9.1635	-0.5541	-0.6893	-0.8584	-0.8907	-0.8959	-0.6650	-0.3247	-0.2732	-0.5975	-1.0623	-1.6304	-1.9284	-0.0004	17.263	-36.845
140°	-14.052	-11.162	0.4271	-0.0156	-0.0805	-0.1029	-0.2345	-0.2808	-0.2694	-0.3248	-0.2470	0.2995	1.1732	1.6796	0.7731	-4.6494	-14.769
160°	7.3265	-11.265	-1.5338	0.0021	0.5049	0.4871	0.3323	0.1643	0.0432	0.0574	0.3052	0.8212	1.5451	2.2528	2.6807	2.0273	37.999
180°	36.324	-6.5263	-4.7617	-2.6247	-1.0040	-0.3463	-0.0698	0.0535	0.0643	0.0380	-0.1593	-1.0478	-2.9968	-5.3100	-5.2094	3.3229	1.9731
200°	10.062	3.5315	-2.2600	-2.3604	-1.2631	-0.5576	-0.2633	-0.0974	0.0217	0.0162	-0.2432	-0.9752	-2.5165	-4.6398	-5.5469	2.0115	34.189
220°	-0.7962	-8.0387	0.8605	1.0417	0.2762	0.0287	-0.0129	-0.0478	-0.0019	0.0917	0.0645	-0.1006	-0.4544	-1.4689	-3.6842	-5.0054	27.649
240°	47.977	-15.087	1.4445	1.7997	0.5775	0.0861	0.0495	0.0620	0.0751	0.2696	0.5918	0.8628	1.1960	1.1931	0.8834	-4.2649	20.301
260°	16.777	8.7999	3.0447	1.0291	0.0615	-0.1689	-0.1436	-0.0638	0.0600	0.3821	0.9099	1.4210	1.8661	1.7231	-0.6956	-7.0916	71.817
280°	21.505	21.801	0.5685	0.3404	0.4437	0.2527	0.0849	-0.0037	-0.0265	0.0102	0.0534	0.0753	0.2238	0.1022	-1.5541	-9.1111	17.033
300°	54.917	35.896	2.7638	0.7020	0.5599	0.3512	0.1774	0.0464	-0.0334	-0.0793	-0.2093	-0.4268	-0.3960	0.1555	1.4993	1.7483	15.553
320°	04.2039	7.9902	2.1741	-0.1585	-0.4346	-0.2340	-0.0600	-0.0249	-0.0532	-0.0801	-0.1475	-0.3457	-0.3457	0.7743	4.9263	17.432	61.549
340°	-39.272	-10.353	-0.6463	-0.5672	-0.5982	-0.3305	-0.0746	0.0117	0.0100	-0.0168	0.0482	-0.0182	-0.4338	-0.8442	0.1117	6.3971	7.9983

References

Arakawa, A., 1962: Nongeostrophic Effects in Baroclinic Prognostic Equations, Proc. Intern, Symp. Numerical Weather Prediction, Tokyo, 161-175.

Arakawa, A., 1966: Computational Design for Long-Term Numerical Integrations of the Equations of Atmospheric Motion, J. Computational Phys., Vol. 1, 119-143.

Bedient, H.A., W.G. Collins, and G. Dent, 1967: An Operational Tropical Analysis System, Mon. Wea. Rev., Vol. 95, 942-949.

Berkofsky, L., and E.A. Bertoni, 1955: Mean Topographic Charts for the Entire Earth, Bull. Amer. Meteo. Soc., Vol. 36, 350-354.

Blumen, W., 1972: Geostrophic Adjustment, Rev. Geophy. and Space Phys., Vol. 10, 485-528.

Burrows, W.R., 1974: Merging of Data on NMC Octagonal and Mercator Grids for Hemispheric Analysis, J. Atmos. Sci., Vol. 102, 76-81.

Charney, J.G., 1948: On the Scale of Atmospheric Motions, Geofys. Publikasjoner, Vol. 17, 17pp.

Charney, J.G., R. Fjørtoft, and J. von Neumann, 1950: Numerical Integration of the Barotropic Vorticity Equations, Tellus, Vol. 2, 237-254.

Charney, J.G., 1955: The Use of the Primitive Equations of Motion in Numerical Prediction, Tellus, Vol. 7, 22-26.

Charney, J.G., 1962: Integration of the Primitive and Balance Equations, Proc. Intern. Sym. Numerical Weather Prediction, Tokyo, 131-152.

Eliassen, A., 1949: The Quasi-static Equations of Motion With Pressure as Independent Variable, Geofys. Publikasjoner, Vol. 17, No. 3, 44p.

Endlich, R.M., 1971: Direct Separation of Two-Dimensional Vector Fields into Irrotational and Solenoidal Parts, I., Mathematical Analysis and Applications, Vol. 33, 328-334.

Haltiner, G.J., 1971: Numerical Weather Prediction, John Wiley and Sons, Inc., 317pp.

References (continued)

Hawkins, H.F., and S.L. Rosenthal, 1965: On the Computation of Streamfunctions from the Wind Field, Mon. Wea. Rev., Vol. 93, 245-252.

Kasahara, A., and W.M. Washington, 1967: NCAR Global General Circulation Model of the Atmosphere, Mon. Wea. Rev., Vol. 95, 389-402.

Kasahara, A., and W.M. Washington, 1971: General Circulation Experiments with a Six-Layer NCAR Model, Including, Orography, Cloudiness and Surface Temperature Calculations, J. Atmos. Sci., Vol. 28, 657-701.

Kasahara, A., T. Sasamori, and W.M. Washington, 1973: Simulation Experiments with a 12-Layer Stratospheric Global Circulation Model. I. Dynamical Effect of the Earth's Orography and Thermal Influence of Continentality, J. Atmos. Sci., Vol. 30, 1229-1251.

Krueger, A.F., J.S. Winston, and D.A. Haines, 1965: Computations of Atmospheric Energy and its Transformation for the Northern Hemisphere for A Recent Five-Year Period, Mon. Wea. Rev., Vol. 93, 227-238.

Kung, E.C., 1966: Large-Scale Balance of Kinetic Energy in the Atmosphere, Mon. Wea. Rev., Vol. 94, 627-640.

Kung, E.C., 1967: Diurnal and Long-Term Variations of the Kinetic Energy Generation and Dissipation for Five-Year Period, Mon. Wea. Rev., Vol. 95, 593-606.

Kuo, H.L., 1952: Three-Dimensional Disturbances in a Baroclinic Zonal Current, J. Meteor., Vol. 9, 260-278.

Leith, C.E., Numerical Simulation of the Earth's Atmosphere, Methods in Computational Physics, Vol. 4. Academic Press, New York, 1-28.

Lorenz, E.N., 1955: Available Potential Energy and the Maintenance of the General Circulation, Tellus, Vol. 7, 157-167.

Lorenz, E.N., 1960: Energy and Numerical Weather Prediction, Tellus, Vol. 12, 364-373.

Macuso, R.L., 1967: A Numerical Procedure for Computing Fields of Stream Function and Velocity Potential, J. Appl. Met., Vol. 6, 994-1001.

Morel, P., and O. Talagrand, 1974: Dynamic Approach to Meteorological Data Assimilation, Tellus, Vol. 26, 334-343.

References (continued)

Mintz, Y., 1965: Very Long-Term Global Integration of the Primitive Equations of Atmospheric Motion, Proc. of the WMO/IUGG Symp. on the Res. and Development Aspects of Long-Range Forecasting, Boulder, Colo., 1964, WM Technical Note, No. 66, 1965, 141-167.

Oort, A.H., and J.P. Peixoto, 1974: The Annual Cycle of the Energetics of the Atmosphere on a Planetary Scale, J. Geophy. Res., Vol. 79, 2705-2719.

Palmen, E. and W. Newton, 1969: Atmospheric Circulation Systems, Academic Press, New York, 603pp.

Pearce, R.P., 1974: The Design and Interpretation of Diagnostic Studies of Synoptic-Scale Atmospheric System, Quart. J. Roy. Meteor. Soc., Vol. 100, 265-285.

Peixoto, J.P. and A.H. Oort, 1974: The Annual Distribution of Atmospheric Energy on a Planetary Scale, J. Geophy. Res., Vol. 79, 2149-2159.

Pettersen, S. and S.J. Smebye, 1971: On the Development of Extratropical Cyclones, Quart. J. Roy. Meteor. Soc., Vol. 97, 457-482.

Phillips, N.A., 1956: The General Circulation of the Atmosphere: A Numerical Experiment, Quart. J. Roy. Meteor. Soc., Vol. 82, 123-164.

Phillips, N.A., 1958: Geostrophic Errors in Predicting the Appalachian Storm of November 1950, Geophysica (Helsinki), Vol. 6, 389-405.

Phillips, N.A., 1963: Geostrophic Motion, Rev. of Geophy., Vol. 1, 123-176.

Richardson, L.F., 1922: Weather Prediction by Numerical Process, Cambridge University Press, 236pp.

Rossby, C.G., et al., 1939: Relations between Variations in the Intensity of the Zonal Circulation of the Atmosphere and the Displacements of the Semi-Permanent Centers of Action, J. Marine Res. (Sears Foundation), Vol. 2, 38-55.

Saltzman, B., 1970: Large-Scale Atmospheric Energetics in the Wave-Number Domain, Rev. of Geophy. and Space Phy., Vol. 8, 289-302.

Shukla, J. and K.R. Saha, 1974: Computation of Non-Divergent Streamfunction and Irrotational Velocity Potential from the Observed Winds, Mon. Wea. Rev.,Vol. 102, 419-425.

References (continued)

Smagorinsky, J., 1963: General Circulation Experiments with the Primitive Equations: I. The Basic Experiment, Mon. Wea. Rev., Vol. 91, 99-164.

Smagorinsky, J., S. Manabe and J.L. Holloway, Jr., 1965: Numerical Results from a Nine-Level Circulation Model of the Atmosphere, Mon. Wea. Rev., Vol. 93, 727-768.

Smith, P.J., 1973a: Midlatitude Synoptic Scale Systems: Their Kinetic Energy Budgets and Role in the General Circulation, Mon. Wea. Rev., Vol. 101, 757-762.

Shuman, F.G. and J.B. Hovermale, 1968: An Operational Six-Layer Primitive Equation Model, J. Appl. Meteor., Vol. 7, 525-546.

Swarztrauber, P.N., 1974: The Direct Solution of the Discret Poisson Equation on the Surface of a Sphere, J. of Computational Physics, Vol. 15, 46-54.

Thompson, P.D., 1956: A Theory of Large-Scale Disturbances in Nongeostrophic Flow, J. Meteor., 251-261.

Thompson, P.D., 1961: Numerical Weather Analysis and Prediction, The Macmillan Co., 170pp.

Veronis, G., 1956: Partition of Energy between Geostrophic and Non-geostrophic Oceanic Motions, Deep-Sea. Res., Vol. 3, 157-177.

Washington, W.M. and A. Kasahara, 1970: A January Simulation Experiment with the Two-Layer Version of the NCAR Global Circulation Model, Mon. Wea. Rev., Vol. 98, 559-580.

Wellck, R.E., A. Kasahara, W.M. Washington and G. DeSanto (G. Williamson), 1971: The Effect of Horizontal Resolution in a Finite-Difference Model of the General Circulation, Mon. Wea. Rev., Vol. 99, 673-683.

White, R.M. and B. Saltzman, 1956: On Conversion between Potential and Kinetic Energy in the Atmosphere, Tellus, Vol. 8, 357-363.

Wiin-Nielsen, A., 1966: The Contribution of Divergent Wind Components to the Energy Exchange between the Baratropic and Baroclinic Components, Mon. Wea. Rev., Vol. 94, 1-8.

Wiin-Nielsen, A., 1967: On the Annual Variation and Spectral Distribution of Atmospheric Energy, Tellus, Vol. 19, 540-559.

References (concluded)

Wiin-Nielsen, A., 1968: On the Intensity of the General Circulation of the Atmosphere, Rev. of Geophy., Vol. 6, 559-579.

Wiin-Nielsen, A., 1973: Dynamic Meteorology, Part 1, Vol. 1, Compendium of Meteorology, World Meteorological Organization, WMO-No. 364, Geneva, Switzerland, Edited by A. Wiin-Nielsen, 334, Appendix.

Wiin-Nielsen, A., 1974: Unpublished Manuscript

Wipperman, F., 1957: Die Transformation Potentielles and Innerer Energie in die Energie Rotorloser und diejenige Divergenzfreier Bewegungen, Bertr. Phys. Atmos., Vol. 29, 269-275.